Chapter V

Fluid Transport and Metamorphism in the lower crust:
Evidence from Channelized Reaction Zones

INTRODUCTION

Fluid plays a important role in the genesis of magmas and evolution of metamorphism. Fluid compositions of the lower crust has been inferred from thermodynamic calculations from fluid-buffered reactions and direct observations of fluid inclusions. It has been well documented that CO_2-rich fluid inclusions are present in many granulite terranes (Touret 1971). These fluid inclusions are the trapped samples of fluids related to granulite metamorphism. These investigations are mainly concentrated on amphibolite-granulite or charnokite transitions (e.g., Jackson *et al.*, 1989a,b; Edwards & Essene, 1988; Lamb & Valley, 1988) and calcsillicate rocks (e.g., Glassley, 1983; Harley & Santosh, 1995). However, most rocks of granulite terranes do not represent typical compositions of the lower crust, because intermediate compositions of exposed granulite terranes are distinctly different from mafic composition of xenolith derived from the lowermost crust (Rudnick *et al.*, 1988; Bohlen & Mezger, 1989). It is required to study granulite terranes mostly composed of mafic composition to realize the fluid composition of the lower crust. Examples reported are commonly characterized by CO_2-rich fluid inclusions similar to more felsic granulites, *e.g.* in the Furua complex, Tanzania (Coolen, 1982) and in the Fiordland, New Zealand (Bradshaw, 1989). However, Lamb *et al.* (1987) pointed out that CO_2 in the Adirondack granulite terrane was trapped during a post-metamorphic event.

To clarify the fluid composition in the lower crust, the abundant vein-related metasomatic reaction zones developed within the metamorphosed gabbronorites are remarked. Furthermore, spatial distribution of these veins provides a significant

information about transport mechanism of fluid in the lower crust. Within the pyroxene granulite, reaction zones that symmetrically develops both side of the vein predicts the infiltration of external fluid phase derived from the base of crust or mantle. The vein-related metasomatic reaction zones can be classified into five types; 1) no-reaction zone, 2) garnet reaction zone, 3) garnet granulite, 4) scapolite-amphibole reaction zone, and 5) amphibole reaction zone. Garnet granulites in the Jijal complex can be considered as one of these reaction zones developed in the Kohistan mafic granulite, because the large garnet granulite body in the Jijal complex was presumably formed as a result of fluid infiltration. The author will summarize several types of the fluid-rock interaction, and discuss the metasomatic process caused by fluid infiltration in mafic granulite bodies in deep crustal conditions of the Kohistan island arc system.

FIELD OCCURRENCE OF REACTION ZONES

Field investigations of these metasomatic reaction zones were carried out about pyroxene and garnet granulites along the Indus Valley. Pyroxene granulites can be observed as pods in the amphibolite, and garnet granulites are restricted in the Jijal complex adjacent to the KAB. These complexes were suffered from granulite facies metamorphism during early to middle Cretaceous (Jan & Howie, 1980; Bard, 1983). Protoliths of metamorphic rocks are gabbroic intrusives of early Cretaceous age, because preservation of relict igneous textures in pyroxene granulites suggests that two-pyroxene-plagioclase assemblage is the same as that in magmatic stage. The southern Kohistan complex shows $^{40}Ar/^{39}Ar$ hornblende ages of 80 Ma which represent a younger metamorphism (Treloar *et al.*, 1989; Wartho *et al.*, 1996). In Chapter IV, it was interpreted that the deepest part was partially transformed to garnet granulites of the Jijal complex due to magmatic underplating in the crust, then regional hydration occurred. There is little evidence that Kohistan pyroxene granulites resulted from dehydration process of amphibolites. In the southern area of the Kohistan arc, pyroxene granulites are commonly intruded by quartzo-

feldspathic veins between a fraction of a millimeter and several centimeter thick, consisting of plagioclase and quartz with or without garnet or hornblende. Based on mineral assemblages and textures, and for convenience of further description, the occurrences of the reaction zones are divided into five types described below. The reaction zone developed along the vein in amphibolites has not been investigated in this study. Figure 5-1 illustrates the pole to planar structure of variable types of vein.

No-reaction Zone

No-reaction zone type is defined by garnet-bearing pegmatitic vein without reaction zone between the vein and host rocks. The pegmatitic vein is almost always filled with large prismatic plagioclase and quartz and occasionally contains large garnet poikiloblasts. This type of the vein is minor throughout the investigated section. Northern limit of distribution is the northern part of the NKA along the Indus Valley (Fig. 2-1). Similar texture of garnets is preserved in garnet-free areas near Kiru in the SKA. Thickness of the vein ranges from a centimeter to a few tens of centimeters. In most case, garnet grains are concentrated in the centre of vein. Grain size of garnet poikiloblast is rarely up to 5 cm in diameter.

Garnet Reaction Zone

The garnet reaction zone developed in pyroxene granulites can be classified into three types. Type I is defined as garnet reaction zone with gradual boundary to the host rocks developed along quartzo-feldspathic vein. Type II is defined as patchy idiomorphic garnet developed at the margin of quartzo-feldspathic vein. Type III is defined as garnet reaction zone in the host rocks unrelated to quartzo-feldspathic vein. Type I can be observed as a light red-coloured zone with relatively large portions of gray coloured-quartz and white-coloured plagioclase aggregate. It is difficult to clearly distinguish between the host rock and the garnet reaction zone due to the gradual decrease in garnet (Fig. 5-2a). Most of

garnet grain in the reaction zone is not idiomorphic and grain size is less than a few mm in diameter. Thickness of garnet reaction zone is maximum 5 mm and reaction front is generally parallel to fractured plane of quartzo-feldspathic vein. In the type II, idiomorphic garnet occurs along the plagioclase dominant vein and its grain size (1 mm - 1 cm) is much larger than the former type (Fig. 5-2b). Type III can be recognized as red-coloured zone with irregular edge in no association with quartzo-feldspathic vein (Fig. 5-2c). General tendency that volume fraction of garnet decreases toward the host pyroxene granulite is quite similar to type I garnet reaction zone with gradual boundary developed parallel to the quartzo-feldspathic vein.

In the NKA, the garnet reaction zone develops in the host rocks at the margin of quartzo-feldspathic vein, that is type I and II. Northern limit of the garnet reaction zone is near Barasin, at middle part of the NKA along the Indus Valley (Fig. 2-1). The quartzo-feldspathic vein with the type I reaction zone is less than 5 mm thick and generally narrower than the vein with the type II reaction zone (several millimeters to 10 cm thick). In the SKA, type III garnet reaction zone is dominant and occurrence of type I or II is rare. Thickness of the reaction zone widely ranges from a few millimeter to several meters. In the southernmost SKA adjacent to the garnet granulite in the Jijal complex, the width of the reaction zone becomes very thicker. Type III reaction zone gradually change into the garnet granulite mass in the Jijal complex. Garnet in the reaction zone generally shows interstitial between pyroxene and plagioclase. In this study, garnet reaction zones with the gradual boundary are described later in detail.

Garnet granulite

In the Jijal complex, garnet granulites homogeneously develops in comparison with the garnet reaction zone in pyroxene granulites of the SKA. At the boundary between garnet and pyroxene granulites, igneous banding which is early structure, in pyroxene granulites is continuously preserved in garnet granulites. The primary compositional layering is

occasionally preserved in the garnet granulite (Fig. 5-2d). It seems that the garnet-bearing assemblage overprinted the early pyroxene granulite unrelated to the vein formation. However, large garnet poikiloblasts (up to 1 cm) occur as a planar alignment in garnet granulites containing scattered small garnet porphyroblasts. Occurrence of garnet granulites at the boundary between the pyroxene granulite and the garnet granulite looks like a vein (Fig. 3-1c), which extremely resembles nature of the garnet reaction zone classified into the percolating type. Thus, a development of garnet granulites was fundamentally caused by fluid infiltration.

Scapolite-Amphibole Reaction Zone Type

Scapolite-amphibole reaction zone develops in the host pyroxene granulite along garnet-bearing quartzo-feldspathic vein. The scapolite-amphibole reaction zone is mesoscopically defined by the light green to gray coloured altered zone (Fig. 5-2e). This type of the reaction zone is very rare in the KAB. The garnet-bearing quartzo-feldspathic vein with scapolite-amphibole reaction zone cut the vein with the garnet reaction zone and the foliation defined by alignment of pyroxene. Then pre-existing garnet reaction zone is completely overprinted by the scapolite-amphibole reaction zone. This reaction zone selectively develops when the surrounding rock contains relatively large amount of garnet.

Amphibole Reaction Zone Type

Amphibole reaction zone can be recognized as deep green coloured altered zone clearly defined by amphibole including pyroxene and develops symmetrically both side of the hornblende-bearing plagioclase-rich veins in the Chilas complex (Fig. 5-2f). Width of the vein varies from 2 millimeter to over 1 meter. The amphibole reaction zone developed along the vein also have variable thickness and its width is proportional to the thickness of the vein (Fig. 5-3). Width of the vein increases with increasing that of the reaction zone.

However, there is little correlation between the width of the amphibole reaction zone and the hornblende-bearing pegmatite. In weakly hydrated area within pyroxene granulites, the network of subplanar amphibole-bearing zone about 1-3 mm wide develops in no association with distinctive plagioclase-rich vein. Hornblende is generally idiomorphic and large grain size (up to 2 mm) in the plagioclase-rich vein. Plagioclase-rich pegmatite contains coarse-grained hornblende poikiloblast (up to 1 cm in diameter). The pegmatitic vein occasionally cuts the vein with the garnet reaction zone in the KAB. Garnet granulites in the Jijal complex are also cut by plagioclase-rich vein with amphibole reaction zone (Fig. 3-1c). These occurrences indicate that hydration event occurred after garnet formation.

WHOLE-ROCK CHEMICAL ANALYSES

Compositional changes between the garnet reaction zone or the scapolite-amphibole reaction zone and host pyroxene granulites were evaluated by whole-rock analysis of selected rock specimens. For no-reaction zone type, slabs of host rock and vein were separately obtained from the single specimen. For type I garnet reaction zone, the quartzo-feldspathic veins are so narrow that the garnet reaction zone cannot cut as separate section. For type III garnet reaction zone, plates of the garnet reaction zone and host rocks were obtained for each sample sequence from <5 mm thick slab cut vertical to the elongated direction of reaction zone. For the scapolite-amphibole reaction zone type, segments of garnet-bearing vein, reaction zone and host rock was obtained, respectively. The contact between the garnet-bearing vein and scapolite-amphibole reaction zone is excluded, because the interface is impossible to determine precisely due to diffusive boundary. For same reason, the contact between host rocks and the garnet reaction zone or the scapolite-amphibole reaction zone is excluded. In the case of the scapolite-amphibole reaction zone type, thickness of the garnet-bearing vein is over 5 mm. Selected slabs were crushed into cm-sized pieces by hammer. Then the pieces were crushed into coarse powder (<1 mm,

about 100 g) in a WC mortar and ground into fine powder in a chalcedony ball mill. For the major element analyses, dried rock powder of 0.4 g was used. The mixture of sample and anhydrous lithium tetraborate ($Li_2B_4O_7$) was made into glass bead. The sample-flux ratio was 1:10. 15-20 mg LiBr was added for easy removal from the crucible. The mixture was fused in a Pt-Au (95:5) crucible with a microwave furnace specially made for heating the crucible for the XRF glass beads. By melting and agitating for about 6 minutes, a disk which is about 3.5 cm in diameter and 0.15 cm thickness was made and was used for measurement. For the trace element analyses, about 4 g of powdered sample in a disk shape which was enveloped with boric acid at side and bottom was pressed with a hydraulic press and was processed to a pellet of about 4 cm diameter, which was used for measurement. Major and trace elements were determined by XRF analysis, using the Phillips PW-1480 instrument in the Geological Institute, University of Tokyo. JB-1 (rock reference samples from Geological Survey of Japan) were repeatedly analyzed with unknown samples in order to confirm the analyses.

Slices of the host pyroxene granulite and adjacent reaction zone including the vein are analyzed. Compositional changes in various types of the reaction zone are shown in Figure 5-4. In the case of no-reaction zone type, chemical compositions of host rock and garnet-bearing vein are clearly different with each other. FeO, MnO and TiO_2 are rich in the vein and Al_2O_3 and Na_2O are poor in the vein compared with the host rock. Sr and Y of the garnet-bearing vein are more than those of the host rock, whereas Ni, Cr, Zr and Nb are less than those in the host rock. In the garnet reaction zone, compositional changes of major oxides are characterized by clear depletion in Na_2O content. This systematic change is obtained from contact pairs of the pyroxene granulite and garnet granulite at Pattan. Other major and trace elements show no systematic change in the host and reaction zone. For the scapolite-amphibole reaction zone, chemical compositions of the garnet-bearing quartzo-feldspathic vein is also presented. Except for TiO_2 and Sr, MnO and Y increase and Al_2O_3, Na_2O and Zr decrease toward the vein in the reaction zone. The

scapolite-amphibole reaction zone tends to have higher concentrations of K_2O, Ni, Pb and Rb rather than the vein and the host rock. In the case of amphibole reaction zone type, the amphibole reaction zone is poor in Na_2O. Other elements do not show any significant compositional change. In summary, mass transfer between the reaction zone and host rocks is not significant except for Na_2O.

PETROGRAPHY

Modal analyses using the point counting method for selected samples are presented in Figure 5-5. Characteristics of each reaction zone are summarized in Table 5-1. Petrographical consequence of the reaction zone and the vein can be classified into three components in common: (1) host pyroxene granulites; (2) variable reaction zones and (3) a central plagioclase-rich vein. These components are described following section, respectively.

(1) Host rock

The pyroxene granulite is commonly cut by plagioclase-rich veins and replaced by reaction zones. Host pyroxene granulites show generally common features in spite of variable types of the reaction zone. The mineral assemblage of the host pyroxene granulite consists of mainly pink pleochroic hypersthene, Al-rich augite and plagioclase (An_{50-60}) with minor tschermakitic hornblende, quartz, opaque minerals and apatite. Most of rocks have no mineralogical banding such as pyroxene-rich and plagioclase-rich layers. Exsolution lamellae in large pyroxene grain at the core suggesting crystallization at high temperature (up to 1000 °C) are preserved in rocks with cumulate texture. Fe-Ti oxide platelets develop at the core of clinopyroxene, when pyroxene granulites contain poorer ilmenite. Although isolated brown hornblende is presumably primary phase with magmatic origin, occurrence of pyroxene partially replaced by amphiboles suggests that the host rock may be variably hydrated. No dehydration or decarbonization reactions have

been recognized. The opaque oxides consist of ilmenite and Ti-rich magnetite which have exsolved. Deformation was heterogeneous at high temperature and during hydration with increasing water activity or decreasing temperatures. Pyroxene granulite do not contain garnet, scapolite, K-feldspar and biotite. Host rock around the scapolite-amphibole reaction zone is fundamentally same as that around other type of veins. The major difference is existence of garnet and pyrrhotite. Occurrence of garnet is scattered in the host rock, because most of early garnet-bearing veins without scapolite-amphibole reaction zone are folded subparallel to the foliation. Pyrrhotite commonly appears near this type of vein.
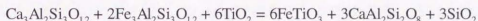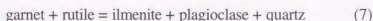
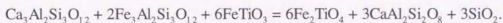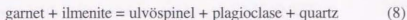## (2) Reaction zones

Garnet reaction zones

The garnet reaction zone is composed of plagioclase, clinopyroxene, quartz, garnet, biotite, K-feldspar, rutile, ilmenite, magnetite and apatite with residual orthopyroxene and hornblende. Within the garnet reaction zone, because volume fraction of clinopyroxene, orthopyroxene and hornblende decreases instead of garnet, it is suggested that the garnet-forming reaction is related to the breakdown of these minerals. Garnet accompanied with quartz and small amount of rutile occurs as corona around ortho- and clinopyroxene and hornblende where these minerals were originally in contact with plagioclase. Idiomorphic garnet cannot be observed in the reaction zone. Width of garnet corona increases from several μm to 500 μm toward the vein. Disappearance of hornblende occurs at further side from the vein or centre of the reaction zone in comparison with total consumption of orthopyroxene. In contrast, clinopyroxene is stable phase throughout the reaction zone and its modal composition in the reaction zone occasionally is larger than that in the host rock. The garnet corona around orthopyroxene contains fine-grained clinopyroxene and vermicular inclusions of quartz (Fig. 5-6c). The breakdown of pyroxene is controlled by series of mineral reactions (3-5) described in Chapter IV. In plagioclase matrix of the

garnet reaction zone, isolated hornblende grains showing interstitial texture commonly occur at the triple junction of plagioclase grain boundary (Fig. 5-6a). These reactions have been used as relatively accurate geobarometry because of large volume changes (e.g. Newton & Perkins, 1982). However, garnet-forming reactions in the pyroxene granulite are locally developed or channelized. Large pyroxene grain with exsolution lamellae situated between the garnet reaction zone and the host rock is replaced by garnet-quartz symplectite only at the garnet reaction zone side (Fig. 5-6d). It indicates that garnet-forming reactions are not due to increasing pressure or isobaric cooling but they are resulted from change of fO_2 and fluid composition.

Magnetite, ilmenite and rutile are present in both of the garnet reaction zone and the host rock. Ilmenite is abundant rather than magnetite. Toward the vein, modal composition of rutile increase with increasing garnet and quartz, and with decreasing plagioclase. This type of rutile is formed by the following reaction of end components written as

$$\text{garnet} + \text{rutile} = \text{ilmenite} + \text{plagioclase} + \text{quartz} \qquad (7)$$
$$Ca_3Al_2Si_3O_{12} + 2Fe_3Al_2Si_3O_{12} + 6TiO_2 = 6FeTiO_3 + 3CaAl_2Si_2O_8 + 3SiO_2$$

(Bohlen & Liotta, 1986). As well as rutile-forming reaction, exsolution textures in magnetite and ilmenite blebs suggesting the breakdown of ulvöspinel component in magnetite may be formed by following reaction (Essene & Bohlen, 1985; Bohlen & Liotta, 1986);

$$\text{garnet} + \text{ilmenite} = \text{ulvöspinel} + \text{plagioclase} + \text{quartz} \qquad (8)$$
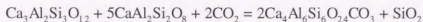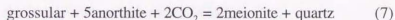$$Ca_3Al_2Si_3O_{12} + 2Fe_3Al_2Si_3O_{12} + 6FeTiO_3 = 6Fe_2TiO_4 + 3CaAl_2Si_2O_8 + 3SiO_2.$$

82

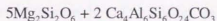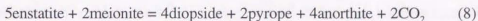These reactions observed in the garnet reaction zone strongly depend on increasing pressure.
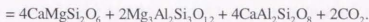
Scapolite-amphibole reaction zone type

The scapolite-amphibole reaction zone consists of scapolite, calcic-amphibole, orthopyroxene, plagioclase, biotite, K-feldspar, quartz, ilmenite, magnetite and apatite. Spatial distribution of reaction zones shows finger-like penetrating into the garnet-bearing vein towards host rocks. Spatial distribution of Al and Mg show the two dimensional mineral distribution of scapolite, clinopyroxene, orthopyroxene and amphibole (Fig. 5-7). At the margin of the garnet-bearing vein, scapolite and calcic-amphibole have a direct contact with each other (Fig. 5-6f), whereas scapolite and calcic-amphibole in the reaction zone form clusters, respectively.

Scapolite formation requires CO_2-buffered reactions, because calcite is never involved throughout the host rock to the vein. The scapolite reaction zone develops with quartz near idiomorphic garnet in the vein. This type of scapolite seems to be formed by following reaction of end components written as

$$\text{grossular} + 5\text{anorthite} + 2CO_2 = 2\text{meionite} + \text{quartz} \qquad (7)$$
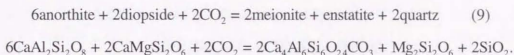$$Ca_3Al_2Si_3O_{12} + 5CaAl_2Si_2O_8 + 2CO_2 = 2Ca_4Al_6Si_6O_{24}CO_3 + SiO_2$$

(Moecher & Essene, 1990; 1991). Although orthopyroxene is stable phase in the scapolite reaction zone, clinopyroxene is never coexistent with scapolite (Fig. 5-6e). It suggests that clinopyroxene is not reaction product but reactant phase due to the scapolite forming reaction together with expense of pre-existing garnet as follow:
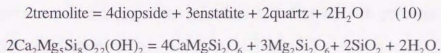
$$5\text{enstatite} + 2\text{meionite} = 4\text{diopside} + 2\text{pyrope} + 4\text{anorthite} + 2CO_2 \qquad (8)$$
$$5Mg_2Si_2O_6 + 2\,Ca_4Al_6Si_6O_{24}CO_3$$

$$= 4CaMgSi_2O_6 + 2Mg_3Al_2Si_3O_{12} + 4CaAl_2Si_2O_8 + 2CO_2.$$

If calcic scapolite is formed by reaction without garnet, then the scapolite-forming reaction is

$$6anorthite + 2diopside + 2CO_2 = 2meionite + enstatite + 2quartz \quad (9)$$
$$6CaAl_2Si_2O_8 + 2CaMgSi_2O_6 + 2CO_2 = 2Ca_4Al_6Si_6O_{24}CO_3 + Mg_2Si_2O_6 + 2SiO_2.$$

However, distribution of scapolite is restricted in adjacent zone of garnet clusters in the vein. The scapolite-forming reaction may derived from breakdown of the grossular component in garnet, suggesting reaction (7). Reaction (7) is thought to be the most important reaction, because of occurrence of scapolite coexisting with interstitial quartz and of decrease of orthopyroxene in the scapolite reaction zone.

Calcic-amphibole occurs interstitial between plagioclase grains, and it is continuous to the garnet-bearing vein. In domains of calcic-amphibole, pyroxene surrounded by plagioclase disappears. The fact that quartz in the domain is more than that in host rock is consistent with reaction products of quartz. The calcic-amphibole-forming reaction is controlled by the breakdown of pyroxenes as follow;

$$2tremolite = 4diopside + 3enstatite + 2quartz + 2H_2O \quad (10)$$
$$2Ca_2Mg_5Si_8O_{22}(OH)_2 = 4CaMgSi_2O_6 + 3Mg_2Si_2O_6 + 2SiO_2 + 2H_2O.$$

The amphibole-reaction zone surrounded by randomly oriented Ti-rich biotite and very small amount of K-feldspar seem to represent front of fluid infiltration. It is consistent with concentration of K based on whole-rock chemical analysis.

Iron-titanium oxides commonly occur in host rocks and reaction zone. Ilmenite shows extensive, broad, unaltered, exsolution lamellae of hematite (Fig. 5-6h). They are

84

characterized by well developed hematite exsolution lamellae in ilmenite. Moreover, some magnetite grains have exsolution lamellae of ilmenite. This texture has been interpreted as subsolidus oxidation of the ulvöspinel component in magnetite to form ilmenite by the reaction:

$$6\text{ulvöspinel} + O_2 = 2\text{magnetite} + 6\text{ilmenite} \qquad (11)$$
$$6Fe_2TiO_4 + O_2 = 2Fe_3O_4 + 6FeTiO_3.$$
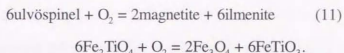
Many authors used this reaction to determine the temperature and oxygen fugacity of magnetite-ilmenite pairs (e.g. Buddington & Lindsley, 1964; Bohlen & Essene, 1976).

Host pyroxene granulites adjacent to the reaction zone contains phyrrhotite and pyrite with chalcopyrite lamellae and blebs, whereas reaction zone never involves sulphides. Pyrite and pyrrhotite are commonly rimmed by thin (5-10 μm) magnetite films along plagioclase grain boundaries (Fig. 5-6h). The textural associations of pyrrhotite, pyrite and magnetite suggest arrested oxidation corresponding to the reaction:

$$6\text{pyrrhotite} + 2O_2 = 3\text{pyrite} + \text{magnetite} \qquad (12)$$
$$6FeS + 2O_2 = 3FeS_2 + Fe_3O_4.$$
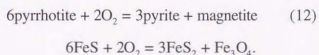
This texture is common in pyroxene granulites including Mg-rich pyroxene with high Mg/Fe whole rock chemistry.

Amphibole reaction zone type

Pyroxene is partially replaced by hornblende and quartz aggregates. Clinopyroxene is commonly altered to fine colourless actinolite laths with quartz blebs clouded with magnetite dust changing to the brownish-greenish hornblende. Whereas orthopyroxene is replaced by aggregates of colourless cummingtonite laths with quartz blebs changing to

the hornblende toward plagioclase grains. While actinolite-hornblende transition is optically gradational, cummingtonite-hornblende contacts are sharp. Brown hornblende seems to form near interstitial Fe-Ti oxide. The textures represent that hornblende associated with quartz are produced by hydration reaction of pyroxenes and plagioclase.

Garnet granulite

The plagioclase-bearing garnet granulite in the Jijal complex is composed of high Al_2O_3 clinopyroxene, garnet, plagioclase, amphibole, ilmenite, rutile, magnetite, ilmenite and apatite. Equidimensional 1-2 mm sized grains of plagioclase show a good granoblastic texture. Clinopyroxene has rounded with long axes of about 1 mm. Quartz forms irregular polycrystalline aggregates which consist of polygonal grains. Rutile often occurs as solid inclusion in garnet poikiloblasts. Garnet also occurs as xenoblastic aggregates (up to 5 mm) or small polygonal grains (c. 500 μm) in the plagioclase matrix. Scapolite occurs with quartz and garnet, and most of scapolite grains are considered to be secondary phase along the grain boundary between garnet and plagioclase. However, a rounded scapolite inclusion in garnet can be rarely observed, suggesting the formation before garnet.

(3) Vein

The dominant constituent in veins is plagioclase (50-60 vol%) and quartz (25-30 vol%). Compositions of plagioclase range from andesine to labradorite. Garnet occurs as cluster at the margin of veins. Modal composition of garnet is about 10 vol%. Garnet is idiomorphic shape and inclusion-free. Plagioclase and quartz are coarse-grained (up to 1 mm) with abundant tiny fluid inclusions (<5μm). Other minor phases (less than 2 vol%) are fluorine-rich apatite, hornblende, biotite, clinopyroxene and ilmenite. In the case of the type I garnet reaction zone, garnet-bearing vein includes less commonly tabular hornblende with platelets of Fe-Ti oxides (Fig. 5-2a). Relict brown hornblende, partly

changed to symplectites of clinopyroxene and garnet provides evidence that hornblende is primary phase. In the case of the scapolite-amphibole reaction zone type, garnet-bearing vein involves garnet, scapolite, brown hornblende, plagioclase (An_{45-55}), quartz and ilmenite. Garnet and scapolite occur as euhedral grains in contact with plagioclase and quartz. In the case of the amphibole reaction zone, quartzo-feldspathic vein is composed of mainly plagioclase (oligoclase to andesine), quartz and large green hornblende with low Ti- and K-contents in comparison with other types of the vein.

MINERAL CHEMISTRY

Compositional variations from host rocks throughout the reaction zone to the vein are described in this section. Mineral compositions were determined using JEOL 733 MKII and JXA 8900L electron microprobes at the University of Tokyo. Standard analytical conditions were 15 kV acceleration voltage, 12 nA beam current, tight beam diameter and 10 s counting times. F and Cl in scapolite, apatite, amphibole and biotite were measured under same condition except for broad beam (5μm) using LiF and sodalite standard. Fe^{3+}-contents in pyroxene and oxide minerals were calculated by stoichiometry. Fe^{3+}-contents in hornblende were estimated by scheme of Robinson *et al.* (1982). Apatite formulae were constructed, assuming that (OH, F, Cl) occupy one of 13 anion sites. SO_3^{2-} and Cl^- in scapolite formulae were calculated assuming 25O. As for exsolved grains such as pyroxenes and Fe-Ti oxides, parts of single phases were carefully measured. Representative mineral compositions are shown in Tables 5-2 to 5-8, and compositional variations of minerals vertical to elongation of the vein are shown in Figures 5-9 to 5-14.

No-Reaction Type

There are no compositional variations of host rocks toward the vein. Plagioclase and quartz clusters in the quartzofeldspathic vein are directly contact with host pyroxene granulite. Idiomorphic garnet is characterized by no compositional zoning as shown in

Figure 5-8a and inclusion-free. The no-reaction zone type generally occurs in the NKA and garnet composition is characterized by higher mole fraction of pyrope component (up to 30 mol%) and lower mole fraction of grossular component (less than 20 mol%) compared with the SKA and Jijal complex.

Garnet Reaction Zone Type

Garnet occurs along the grain boundary between pyroxene or hornblende and plagioclase (Fig. 5-6c). X_{Sps} is very low and decrease toward centre of the vein. In the case of the type II, $Mg/(Mg+Fe^{2+})$ ratio increases from 0.25 to 0.37 toward the vein, and X_{Alm} and X_{Pyr} show reverse patterns toward centre of the vein, respectively. However, $[Mg/(Mg+Fe^{2+})]$ in the type I reaction zone is little variation.

Orthopyroxene is hyperthene. $Mg/(Mg+Fe^{2+})$ in the reaction zone slightly increases from 0.53 to 0.65 toward the vein. Ferric/ferrous ratio slightly decreases from 0.08 to nearly zero in the reaction zone toward the vein. CaO and MnO in orthopyroxene are uniformly low and typically decrease from 0.7 to 0.5 wt% and from 0.78 to 0.25 wt% toward the vein, respectively. Al_2O_3-contents of orthopyroxene tend to decrease toward the vein from 2.7 wt % in the host rock to 2.0 wt% in the reaction zone. Compositional zoning of Al_2O_3 in orthopyroxene shows normal zoning suggesting Al_2O_3-decrease toward the margin of grain as well as granoblastic grains of orthopyroxene in surrounding pyroxene granulites of the NKA.

Clinopyroxene coexisting with orthopyroxene is from salite to augite with $X_{Mg} = 0.23$-0.35 and $Fe^{3+} = 0$-0.2. In the reaction zone, X_{Mg} generally decreases and Fe^{3+}-contents increase toward the vein as well as orthopyroxene. Ferric/ferrous ratio slightly decreases from 0.08 to nearly zero in the reaction zone toward the vein. MnO-contents in clinopyroxene are uniformly low but distinctly decreases from 0.38 to 0.06 wt% toward

the vein. Ti- and Na-contents does not vary toward the vein. For the type I reaction zone, Al_2O_3-contents of clinopyroxene tends to decrease toward the vein from 4.1 wt % in the host rock to 3.0 wt% in the reaction zone. Compositional zoning of Al_2O_3-contents in clinopyroxene shows normal zoning suggesting Al_2O_3 in decrease toward the margin of grains. For the type II reaction zone, Al-contents in clinopyroxene mantled by garnet and quartz symplectite do not vary toward the vein. Whereas Al-contents in small clinopyroxene with garnet and quartz surrounding orthopyroxene are lower than those in large clinopyroxene. Al-poor clinopyroxene can be considered as a new phase.

Plagioclase is the most abundant mineral in the reaction zone. In the case of type I, An-contents in plagioclase show compositional variations in the reaction zone from the host pyroxene granulite to the veins. An-contents in the vein are higher than those in the reaction zone and the host rocks. On the other hand, in the case of the type II, An-contents show no variation.

Amphibole is magnesio-tschermakitic hornblende in the sense of Leake (1978). Hornblende disappears in the reaction zone apart from the vein or centre of the reaction zone except for relict brown hornblende. In the reaction zone, X_{Mg} systematically decreases from 0.52 to 0.63 toward the vein. To the vein, Fe^{3+}-contents in hornblende decrease from 0.68 to 0.21. Ferric/ferrous ratio also decrease from 0.28 to 0.11 toward the vein. Al-contents generally decrease to the vein. Na- and Mn-contents slightly decrease to the vein. In the type II, contents of K^+ ion abruptly increase from 0.27 to 0.47 to the centre of the reaction zone. Contents of Ti^{4+} ion show a modest increase from 0.14 to 0.36 to the vein. F- and Cl-contents in anion site show no systematical variation.

Fe-Ti oxides are mostly ilmenite and small amount of rutile only in the reaction zone. Magnetite is rare in the reaction zone. Ti-contents in ilmenite generally increase toward the vein (Fig. 5-11).

Scapolite-Amphibole Reaction Zone Type

Plagioclase is dominant and slightly decrease in An-contents from 0.50-0.47 to 0.48-0.45 in the transition from the host pyroxene granulite to the vein.

Scapolite in the garnet-bearing vein is unzoned and consistent in composition between the reaction zone and the vein. EqAn (equivalent to anorthite) values (Evans *et al.*, 1969) calculated on the basis of Si:Al ratios after normalization of Al+Si to 12 cations are in the range 60-63. Scapolite compositions calculated from Na, Ca and K cation proportions are higher in apparent EqAn (EqAn*(Ca/Ca+Na+K) = 73-75). K-contents are very low (less than 0.2 wt%). Anion site of scapolite is sulfate-rich typical of mafic granulite with $SO_4/(SO_4+CO_3+Cl) = 0.42-0.50$ (e.g. Lovering & White, 1969; Edwards *et al.*, 1979; Jones *et al.*, 1983; Stolz, 1987; Moecher & Essene, 1991). Cl content is very low below the level of detection limit (< 0.1 wt%) in all samples.

Orthopyroxene in the reaction zone and host rock is hyperthene. Orthopyroxene does not contact with hornblende in the reaction zone. X_{Mg} slightly increases from 0.57 to 0.59 toward the vein. Ferric/total iron ratio slightly decreases in the reaction zone toward the vein. Fe^{2+}-contents of orthopyroxene in contact with scapolite are slightly higher. Minor components such as CaO- and MnO-contents in orthopyroxene are uniformly low, typically 0.7 and 0.5 wt%, respectively and show no systematic change toward the vein. Al_2O_3-contents of orthopyroxene core decrease toward the vein from 2.7 wt % in the host rock to 2.4 wt% in the reaction zone. Compositional zoning of Al-contents in

orthopyroxene shows normal zoning as well as that in the surrounding pyroxene granulites of the NKA.

Clinopyroxene coexisting with orthopyroxene ranges from salite to augite with X_{Mg} = 0.65-0.75 and Fe^{3+} = 0.13-0.3. Clinopyroxene never coexists with scapolite and hornblende in the reaction zone. X_{Mg} and Fe^{3+}-contents are not significant change to the vein, but these values vary for each individual grains. Compositional zoning of Al-contents in clinopyroxene shows normal zoning suggesting Al in decrease toward the margin of grain in similar to that in the surrounding pyroxene granulites with granoblastic texture of the NKA. Al-contents of clinopyroxene show no variation toward the vein.

Amphibole shows cluster and interstitial shape between plagioclase grain boundary. X_{Mg} systematically does not change toward the vein, although X_{Mg} widely ranges from 0.36-0.46. To the vein, Fe^{3+}-contents in hornblende within the amphibole reaction zone tend to decrease from 0.6 to 0.2 in cations calculated by Robinson et al. (1982). Ferric/ferrous ratio also decreases toward the vein. Ca-, Na- and K-contents show no significant variations; and Ti-contents shows a slight increase from 0.18 to 0.26 toward the vein.

Iron-titanium oxides are mostly ilmenite and secondary magnetite in pyroxene. Ilmenite shows extensive, broad, unaltered, exsolution lamellae of hematite (Fig. 5-6h). The hematite lamellae consitute nearly 60 volume per cent in all grains and show both primary and secondary hematite exsolution which may be interpreted from phase relations on the $FeTiO_3$-Fe_2O_3 join (Haggerty, 1991). Hematite and ilmenite form a continuous solid solution above 700 °C. Hematite-ilmenite solvus at lower temperatures lead to two sets of exsolution lamellae, when the grain pass through the solvus during cooling. However, because both sets of hematite and ilmenite exsolution lamellae in all of the grains are observed, these grains must be unaffected by retrograde alteration during cooling.

Especial care was taken to obtain consistent bulk compositions of exsolved hemo-ilmenite grains. Individual hemo-ilmenite grains analyses were averaged to obtain a composite whole. Averaged composition of ilmenite is 20 mol% hematite component.

Biotite occurs as anhedral patch around the amphibole aggregate. Differences in composition of biotite in the reaction zone was not detected. $Mg/(Mg+Fe^{2+})$ ratio shows constant value of 0.54-0.56 with high Ti contents (>5 wt%).

Apatite is F-rich and very small amount (<0.1 vol%) in the reaction zone. Anion site is mainly occupied by F as well as the apatite in the surrounding pyroxene granulite. Sulfate contents in this type of the reaction zone are very small around 0.3 wt%, but sulfate contents are much larger than those of other reaction zones and host pyroxene granulites.

Garnet granulite

Garnet is typical of almandine-pyrope-grossular series in composition. Grossular component is clearly higher than pyroxene granulites in the KAB. Chemical compositional profiles across garnet porphyroblasts are shown in Fig. 5-8b. Garnet porphyroblasts are strongly zoned from the core to the margin. The grossular component increases from the core to the margin. The increase of grossular component toward the rim indicates whether pressure increase, or cooling for the assemblage of garnet-clinopyroxene-plagioclase-quartz (*e.g.* Newton & Perkins, 1982).

Clinopyroxene is characterized by high total Al-contents (>0.25 p.f.u). Increase in Al-contents toward the rim suggests that CaTs and Jd components significantly increase toward the rim as well as those in clinopyroxene from the pyroxene granulites in the KAB. Na-contents in clinopyroxene increase southward in garnet granulites in the Jijal complex. Jadeite content in clinopyroxene from the southernmost Jijal garnet granulite is over 0.15.

Plagioclase generally shows lower An content (An_{30-40}) than pyroxene granulites. Compositional zoning shows higher anorthite content in the core.

Scapolite locally occurs in garnet granulites. EqAn values are in the range 57-60. These values is slightly smaller than those in scapolite of pyroxene granulites in the KAB. K-contents are very low (less than 0.2 wt%). Scapolite is sulfate-rich with $SO_4/(SO_4+CO_3+Cl) = 0.28$-$0.52$. In the scapolite dominant rocks, scapolite contains higher sulfate-contents (up to 0.5). Cl-contents are very low under the detection limit (< 0.1 wt%) in all samples.

Amphibole reaction zone

Amphibole partly replaces orthopyroxene and clinopyroxene and forms a corona texture. Figure 5-17 shows compositional change of amphiboles through actinolite grain to plagioclase grain. With increasing with Al_2O_3- and FeO-contents, MgO- and SiO_2-contents decrease in hornblende away from actinolite grain. Cummingtonite surrounding orthopyroxene contains very small CaO-contents less than 0.3 wt% and total Al_2O_3-contents less than 0.2 wt%. Al- and Na-contents in cummingtonite suddenly increase near the plagioclase grain. In both actinolite to hornblende and cummingtonite to hornblende, $Mg/(Mg+Fe^{2+})$ ratio gradually increases toward the plagioclase grain.

Plagioclase is generally labradorite in host pyroxene granulites. Core compositions of plagioclase in the reaction zone are in good agreement with those in unaltered pyroxene granulites. Plagioclase which contacts with hornblende is more affected by the alteration, and are continuously zoned from the core (An_{60}) to the rim (An_{40-50}).

FLUID INCLUSIONS

93

The fluid inclusions was investigated in the quartzo-feldspathic vein and the garnet reaction zone. Plagioclase, quartz and garnet contain small fluid inclusions (<2 μm). Both carbonic and aqueous varieties are recognized. Within veins, CO_2-dominant fluid inclusions are most abundant in quartz, but also occur in garnet and plagioclase. They range from <1 μm to ~10 μm in diameter, with most <5 μm. They are single phase and show characteristic high relief and high internal reflectance. In quartz, they show locally well developed negative shapes and occur commonly along sharply-defined healed fractures. Some clusters show an obvious planar arrangement, and others are isolated. In garnet, they form tubular, wormy inclusions locally of dendritic aspect, concentrated along healed fractures. In plagioclase, a lesser amount of fluid inclusions can be observed. Aqueous fluid inclusions show comparatively low relief, low internal reflectance and have generally rounded or vermicular shapes, with a bubble usually visible at room temperature. They are typically less than 5 μm in diameter, and form distinct trails, often with an orientation perpendicular to the elongation direction of quartz. Mixing with carbonic inclusions has not been observed, although both types occur in single quartz grains. The abundant aqueous fluid inclusions in partially retrograde assemblages are consistent with later influx of aqueous fluids accompanying retrograde metamorphism.

In most of fluid inclusions, no phase transitions could be observed on cooling stage experiments to -180 °C by microthermometry using Linkham gas-flow heating/cooling stage at the Osaka City University. The apparent lack of phase change is probably caused by a combination of small inclusion size, irregular cavity walls and the dark colour of the inclusions, which prevent observation of small CO_2 crystals and/or minor amounts of liquid nitrogen and hydrocarbon forming on cooling. Raman spectroscopy and FT-IR analysis were carried out to determine chemical composition of fluid inclusions. Laser Raman microspectroscopy is non-destructive method that has the potential to obtain direct molecular structural information of materials. In principle, it can be used to analyze solid, liquid and gaseous inclusions *in situ*. Fluid inclusions have been analyzed with a

94

multichannel laser-Raman microprobe in the laboratory of Earth and Planetary Sciences, Tokyo Institute of Technology. An objective with a $100 \times$ magnification was used. The laser wavelength was 514.53 nm of green line of Ar^+ laser. The power of radiation at the laser source was 800 mW. The integration time was 3 seconds and the number of integrated spectra 2. Furthermore fluid composition was also measured by FT-IR at the Department of Geosciences, Osaka City University.

Raman microprobe analyses of selected fluid inclusions in the quartzo-feldspathic veins are given in Figure 5-18. Processing of the Raman data was carried out using following peak positions and relative Raman cross-sections (σ) for the volatile components at 1 bar; CO_2 $\Delta v = 1388$ cm^{-1}, $\sigma = 1.5$, N_2 $\Delta v = 2311$ cm^{-1}, $\sigma = 1.0$ and CH_4 $\Delta v = 2917$ cm^{-1}, $\sigma = 7.57$, (Dubessy *et al.*, 1989). The accuracy of quantitative Raman spectroscopy of high-pressure gas mixtures is still a matter of discussion as physical properties on the laser Raman photometry are not all exactly known (Pasteris *et al.*, 1988; 1990). Therefore, analytical results represent qualitative amount of gas species in the fluid inclusions.

Raman spectra of scattered fluid inclusions in quartz in garnet-bearing quartz-feldspathic veins show intensively sharp peak at 1390 cm^{-1} suggesting presence of carbon dioxide, whereas fluid inclusion in skeletal shaped garnet in the garnet reaction zone have broad peak around 3620 cm^{-1} of Raman shift suggesting presence of H_2O. Some carbonic fluid inclusions also have small sharp peak at 2333 cm^{-1} corresponding to the peak position of nitrogen, and in rare cases, they have broad peak around 2920-2930 cm^{-1} presumably corresponding to the peak position of hydrocarbon. Nitrogen and methane are the most common species in carbonic fluid inclusions (e.g. Touret, 1981; Hall & Bodnar, 1990; Andersen *et al.*, 1995). In most of cases, Raman spectra of carbonic fluid inclusion have no evidence of the broad peak around 3620 cm^{-1}. Fluid inclusions in garnet generally are aqueous rather than carbonic compared with those in quartz. The presence of carbonic

inclusions in quartz is also confirmed by FT-IR analysis using 50 μm beam diameter (Fig. 5-19). Consequently, carbonic fluid inclusions with small amounts of nitrogen and hydrocarbon always exist in quartz and garnet. These scattered isolated fluid inclusion in quartz may represent early generation of fluid which was trapped during early stage of vein formation, and which is unrelated to the later aqueous fluid inclusions.

Fluid composition cannot estimate using the microthermometric analysis because of extensive small size of fluid inclusions including nitrogen and hydrocarbon which have lower melting temperature. Furthermore, Raman data is not quantitative due to absence of the accurate standard of gas species. Thus presence or absence of each kind of volatile phase can be discussed.

DISCUSSION

The distribution of fluid in the lower crust of the Kohistan arc can be considered based on distribution of the reaction zones. Furthermore the garnet granulite is also product related to fluid infiltration. The garnet reaction zone in pyroxene granulites develops along only the quartzo-feldspathic vein. In contrast, garnet granulite in the Jijal complex is relatively homogeneous segment as the garnet-bearing phase. These reaction textures are very similar with each other to those in the garnet reaction zone developed in pyroxene granulites. If garnet granulites are formed by infiltration mechanism of the same fluid, different styles of garnet distribution between garnet granulite and pyroxene granulite do not only suggest the difference of *P-T* condition but also they are controlled by the difference of other factors. On the other hand, the distribution of scapolite is characterized by channelized or localized patterns throughout the granulite facies rocks. Figure 5-20 shows schematic fluid distribution of the lower crustal section in the Kohistan arc during the metamorphism. In following section, origin of several types of the reaction zone will be considered based on phase petrology and causes of variable nature of metasomatic reaction zone will be discussed.

Origin of garnet in the mafic lower crust

The garnet reaction zone along the vein in the mafic granulite terrane has been reported by a few previous workers. Bradshaw (1989b) reported garnet-bearing quartzo-feldspathic veins in pyroxene granulites in the Early Cretaceous Fiordland terrane of New Zealand. He attributed the formation of these veins to dehydration of the host rock triggered by infiltration of carbonic fluids. Metasomatism accompanied dehydration, as shown by increases in K, Na, Si, Ba and Sr and decreases in Ca, Fe, Mg, Ti and Y in the garnet reaction zone relative to the two-pyroxene granulite. On the other hand, Pattison (1991) reported garnet-bearing veins and patches including tonalitic leucosome in the Grenville Province, Canada. He pointed out that the formation of the veins is caused by channelized dehydration, while the tonalitic leucosome suggests local internally-derived anatexis. In the Kohistan vein, the occurrence is similar to that of Fiordland complex. The depletion of Na_2O in the garnet reaction zone is attributed to direct loss of Na^+ to the infiltrating fluid during hornblende breakdown. It is unlikely to result from removal of partial melts from the garnet reaction zone, because K^+ has remained constant; K^+ is more incompatible than Na and thus would be expected to be more readily partitioned into a melt phase. Na^+ may have been dissolved as NaCl in an expelled aqueous fluid, with Cl and H_2O also derived from hornblende breakdown. The absence of systematic variation in plagioclase composition between the host rock and the garnet reaction zone suggests that hornblende is the main source of Na.

Phase relations

Predicted phase relations provide important insights into the nature and controls of garnet-forming reaction in the reaction zone. A closed system can be modeled by the end-member reactions in the garnet reaction zone, and then garnet and clinopyroxene can be considered as product assemblages. Assuming that a_{H_2O} is constant, garnet-forming

97

reaction can be triggered by decrease in temperature at constant pressure (arrow 1 in Fig. 5-21a). Hornblende within the reaction zone firstly disappears toward rim of the vein or centre of the reaction zone with increasing the modal composition of garnet. Water is mobile components controlling the appearance of hornblende. Predicted reaction sequences in T-a_{H_2O} space for the two-stage development of the garnet reaction zone are illustrated as an arrow 2 in Figure 5-21a. Quartz is treated as an excess component in the system. The topology of the system requires that hydration reactions lie on opposite sides of the [tr] reaction: enstatite + anorthite = pyrope + diopside. The positive dP/dT of this univariant reaction, with enstatite + anorthite lying on the high-T low-P side, indicates that dehydration must have occurred at the time of decrease in T and/or increase in P (Fig. 5-21b). With increasing a_{H_2O}, hydration of the host pyroxene granulite would first occur via [py], then [di] reaction occurs. The formation of pyrope + tremolite via [di] reaction is largely precluded by earlier disappearance of orthopyroxene via [py]: enstatite + diopside + anorthite + H_2O = tremolite. With increasing a_{H_2O}, replacement of tremolite by garnet would first occur via [en]. Thus decrease of modal composition of hornblende toward the centre of the reaction zone or the vein should correspond decrease of a_{H_2O}.

In the reaction system, location of these reactions in P-T space can be considered using diagram of Bradshaw (1989b) (Fig. 5-21b). As required by the topology of the system, [hbl] lies on the low P and high T side of inferred conditions of garnet and clinopyroxene-bearing assemblages in the reaction zone. In most pyroxene granulites, the garnet-forming reaction [en] did not occur, as indicated by widespread occurrence of hornblende-bearing and garnet-free assemblages in the host rock. The restricted development of the garnet reaction zone can be explained by local conditions of reduced a_{H_2O}, which caused invariant point and all dehydration reactions to shift lower T and P along the low T extension of [hbl]; this extension corresponds to the reaction in no

98

association with H_2O. Lowered a_{H_2O} could facilitate the dehydration of hornblende to form the garnet granulite at low T and P conditions.

Garnet granulites in the Jijal complex homogeneously develop instead of garnet reaction zones in the KAB. In the estimated peak metamorphic conditions of garnet granulites, garnet + clinopyroxene assemblage is enough stable even if a_{H_2O} is nearly equal unity. Garnet granulites in the Kohistan arc therefore can be widely developed under high T conditions (up to 800 ˚C). Thus the formation of garnet granulites in the Jijal complex does not need the low a_{H_2O}. The fact that garnet granulite reaction zones in the Fiordland complex are restricted only along quartzo-feldspathic veins indicates that the garnet-forming reaction could not regionally occur under lower temperature (c. 700 ˚C) rather than the Jijal garnet granulite. Origin of channelized garnet reaction zone may be triggered by infiltration of carbonic fluids. In fact, carbonic fluid inclusion occurring in the vein adjacent to the garnet reaction zone is characteristic.

Physical conditions inferred from compositional variation

For the type III reaction zone, compositional variations of ferro-magnesian minerals in the reaction zone from the host rock to the vein can be apparently observed, as for especially Fe/Mg exchange. Figure 5-22 shows distribution coefficient (K_D) of iron to magnesium among each mafic minerals. The K_D (Fe/Mg) values are unrelated to the distance from the centre of the reaction zone. Constant K_D value presumably represents local re-equilibrium after the garnet formation, because Fe/Mg interdiffusion is relatively faster than other chemical species under high T granulite facies condition. The K_D directly shows degree of the progressive garnet-forming reaction. On the other hand, absence of compositional change of plagioclase across the reaction zone leads to a change of equilibrium coefficient of reactions (5). Difference of estimated pressure condition between the edge and centre of the reaction zone based on variable methods of garnet-clinopyroxene-plagioclase-quartz geobarometer is 200-300 MPa at almost the same temperature condition (Table 5-9). If the

estimated pressure conditions are correct, dP/dx, where x is distance, is 30-50 MPa/mm in the reaction zone from the vein to host rock. At constant temperature, one possible explanation is that the chemical compositions at the edge of the reaction zone adjacent to the host rock recorded lithostatic pressure, whereas those at centre of the reaction zone recorded fluid pressure. Thus equilibrium in high pressure was caused by overpressure due to locally large amounts of fluid influx. An alternative possibility is that plagioclase does not accomplish local re-equilibrium after garnet formation, since the plagioclase substitution ($CaAlNa_{-1}Si_{-1}$) is very slow because of charge-coupled cross site exchange. Although X_{Mg} in garnet increases from pyroxene to plagioclase, estimated pressure from centre of garnet corona undoubtedly increases toward centre of the reaction zone. Assuming that Darcy's law is valid, permiability can be estimated by pressure gradient, dP/dx:

$$q_f = -\left(\frac{K}{\mu_f}\right)\left(\frac{dP}{dz}\right) \qquad (13)$$

where μ_f is the fluid viscosity, (dP_f/dz) is the fluid pressure gradient, and K is the permiability of rocks. For the conditions of interest, both viscosity and fluid pressure gradient are constant ($\mu_f = 1.5 \cdot 10^{-3}$ g·cm^{-1}·s^{-1}, and $(dP_f/dz) = 300$-500 MPa·cm^{-1}). Thus, any valiability of the fluid fluxes from eqn. (13) is due to permiability. Permiability is proportional to a power of porosity:

$$K = \omega \phi^n \qquad (14)$$

where ω and n are material-dependent constants that are approximately independent for low values of porosity (<1%). The exponent n, varies between 3 and 6, and increases with increasing content of nonequidimensional grains in a rock. The constant ω, may vary

100

over orders of magnitude and is dependent grain size, shape distribution, and wetting properties. For a fluid flux rate (q_f) of 10^{-11} to 10^{-12} m·s^{-1} (Walther & Orville, 1982), then permiability of rock around the type III garnet reaction zone is 10^{-24} to 10^{-25} m^2. Laboratory experiments and in-situ well tests (Brace, 1980) suggested that rock permiabilities range from 10^{-17} m^2 to 10^{-23} m^2. However, these values were generally determined at room temperature and low confining pressure. Etheridge *et al.* (1984) estimated higher permiability ranging from 10^{-15} m^2 to 10^{-18} m^2 at hydraulic fracturing condition. Thompson & Connoly (1990) estimated that lower crustal permiabilities are 4.6×10^{-20} m^2 for driving pressure gradient with fluids at lithostatic pressure when Darcian fluid flow occurs throughout porous lower crust. These previous estimations of rock permiabilty shows clearly higher value than that from this study. Because fluid flux rate derive from an average metamorphic fluid released by devolatilisation reactions in the metamorphic pile, which contains 5 wt% volatiles, the value (q_0) of 10^{-11} to 10^{-12} m·s^{-1} is unknown wherher is valid or not. If permiability at rocks around type III garnet reaction zone is 10^{-20} m^2, fluid flux rate is over 10^{-7} m·s^{-1}. However, this fluid flux rate cannot be satisfied by fluid released by devolatilisation. Thus it is concluded that lower crust consisting of pyroxene granulites is characterized by low permiability under granulite facies condition. The low rock permiability may lead to no accomplishment of porous media flow derived from large dihedral angle between solid and fluid phase and development of hydrofracturing (vein formation).

On the other hand, for the type I reaction zone, only garnet has no variation of X_{Mg} in the reaction zone. The K_D values between pyroxene and hornblende are constant, whereas those between garnet and pyroxene or hornblende decrease toward the vein. Thus, estimated temperature using garnet-clinopyroxene geothermometer decreases toward the vein, whereas calculated pressure inferred from garnet-clinopyroxene-plagioclase-quartz geobarometers has little variation due to no compositional variation of An-contents in plagioclase and grossular component in garnet. If estimated temperature is

correct, cold fluid would pass through the host pyroxene granulites. It is unrealistic interpretation. Absence of compositional variation in garnet probably reflects difference of diffusion rate between garnet and other ferro-magnesian minerals.

Formation Model of Garnet Reaction Zone

Evolution of garnet reaction zone is required for two processes; fracturing of rock and percolating of fluid. Figure 5-23 illustrates summary and formation model of the garnet reaction zone. In the case of fracturing, widespread fracturing filled with plagioclase and quartz in host pyroxene granulites formed joint-like networks. The high fluid pressure in the stressed rocks is easy to make hydrofracturing. Crack formed by hydrofracturing should be instantaneously filled with the fluid. If the crack filled with fluid influx has lower $f\mathrm{H_2O}$ than host rock, gradient of water fugacity ($f\mathrm{H_2O}$) would be formed around the crack. If dihedral angle between $\mathrm{H_2O}$ and surrounding minerals is less than $60°$ which is equivalent to the critical value of percolative fluid flow (Watson & Brenan, 1986), $\mathrm{H_2O}$ migrates percolatively toward the crack. Thus hornblende breakdown reaction is triggered by locally lowered $f\mathrm{H_2O}$ along the fracture due to decrease in $f\mathrm{H_2O}$. If dihedral angle between $\mathrm{H_2O}$ and surrounding minerals is more than $60°$, transport of $\mathrm{H_2O}$ should be controlled by the diffusional process. In this case, there is no need for infiltration of low $f\mathrm{H_2O}$ fluid from the fracture to the garnet reaction zone. In fact, this model is in good agreement with the results from fluid inclusion studies; garnet in the reaction zone contains aqueous fluid inclusion, whereas quartz in the vein involves carbonic fluid inclusion. The aqueous fluid inclusions in garnet are probably derived from hornblende breakdown reaction. Furthermore, pressure conditions at the boundary between the reaction zone and the vein, inferred from geobarometry, tends to be somewhat lower than that at the reaction front. These observations are required for not infiltration of low $f\mathrm{H_2O}$ fluid in the reaction zone but removement of $\mathrm{H_2O}$ from the reaction zone.

In the case of percolating model without presence of the clearly defined quartzo-feldspathic vein, pressure difference between the edge and the centre of the reaction zone is remarkably larger than that of the fracturing model. This result might not reflect difference of lithostatic pressure but difference of fluid pressure. In described earlier, if so, minerals at the centre of the vein recorded the over fluid pressure being larger than the lithostatic pressure. If the fluid had low $f\mathrm{H_2O}$, dehydration of hornblende would start at centre of the reaction zone due to locally lowered $f\mathrm{H_2O}$. The volume decrease accompanying the garnet-forming reaction provided open space at the reaction front, further enhancing fluid circulation related to infiltration toward the host rock along the fluid channels. Even if dihedral angle between the fluid and mineral exceeds 60°, substantial influx of fluid is able to be immediately filled with the open space. This process might enhance advancement of breakdown of hornblende, repeatedly. Moreover, coupling of both disappearance of hornblende and decrease in water activity would lead to breakdown of orthopyroxene. Low $f\mathrm{H_2O}$ fluids infiltrating along a given channel would become progressively enriched in $\mathrm{H_2O}$ as a consequence of hornblende breakdown, such that reactions in which hornblende replaces pyroxene would eventually occur at the infiltrating front; dehydration would occur only after water-rich fluids were flushed from a given area. Water released from hornblende breakdown should migrate outward, presumably upwards driven by buoyancy (Nakashima, 1995).

Origin of scapolite in the lower crust

Stability of scapolite

Scapolite can be chemically represented as a solid solution of four end-members: marialite, $Na_3Al_3Si_9O_{24}\cdot NaCl$; a hypothetical end-member $Na_3Al_3Si_9O_{24}\cdot CaCO_3$; meionite, $Ca_3Al_6Si_6O_{24}\cdot CaCO_3$; and sulfate meionite, $Ca_3Al_6Si_6O_{24}\cdot CaSO_4$. Almost all of analyze from natural scapolite range from 30 to 80 mol% meionite (Evans *et al.*, 1969). These intermediate compositions do not lie on a simple binary join between meionite and

marialite, and the anion site can be filled with CO_3 at $Ca/(Ca+Na)=0.75$. Newton & Goldsmith (1975) have determined the stability relations of the end member scapolites marialite, meionite and sulfate meionite. In the system $Ab-An-CaCO_3$ at 1200 °C and 1.5 GPa, a large range of scapolite solid solutions can exist. Carbonate scapolite coexists with plagioclase from An_{100} to An_{33}. In the system $Ab-An-CaSO_4$ at the same condition, the sulfate scapolite can coexists with Ab-richer plagioclase. Pure carbonate meionite is unstable at moderate to low temperature (Orville, 1975) and can be produced in the reaction $3An + CaCO_3 \Rightarrow$ meionite over 800 °C in the Na-free system (Moecher & Essene, 1990). Stability field of scapolite has been considered with calcite. The high pressure breakdown of meionite to grossular, kyanite, quartz and calcite occurs over 2 GPa. Pure sulfate meionite is stable at high pressure field in the reaction $3An +$ anhydrite $\Rightarrow$ meionite.

Thus sulfate-rich meionite could only be expected to exist under rather deep-seated and high-temperature conditions. Newton & Goldsmith (1975) found that the scapolite becomes more sodic relative to the plagioclase with decreasing temperature, and proposed the geothermometer based on the experimentally determined Na/Ca distribution between Cl-free scapolite and plagioclase. However, the pair of scapolite and plagioclase in the Kohistan arc provides over 1300 °C which is much larger than metamorphic temperatures (around 800 °C) obtained by the two-pyroxenes thermometry. This result probably indicates the effect of pressure in removing Ca from plagioclase into garnet and pyroxene or absence of equilibrium between scapolite and plagioclase.

Phase equilibria for scapolite in the system $CaO-MgO-Al_2O_3-SiO_2-CO_2-H_2O$ (CMASCH) has not been considered. The important reactions of $T-X_{CO_2}$ equilibria in the CMASCH system are calculated using thermodynamic set of Holland & Powell (1990) for pure meionite among the pyrope-grossular-enstatite-diopsode-tremolite-scapolite-clinozoisite-anorthite-quartz assemblage. In the vein-related scapolite reaction zone, figure 5-24 shows $T-X_{CO_2}$ diagram at 600 MPa. Because scapolite coexists with hornblende,

both of scapolite and tremolite in the end member reactions are stable over wide range of X_{CO_2}. However, the reaction, calcite + plagioclase = meionite occur, tremolite cannot coexist with pure meionite in any X_{CO_2}. On the other hand, the absence of tremolite in the garnet granulite at 1200 MPa suggests that stability field of scapolite is restricted in high X_{CO_2} .at low temperature condition or low X_{CO_2} .at high temperature condition.

CO₂ activity in the lower crust

The a_{CO_2} in high-grade metamorphism is insensitive to direct thermodynamic calculation from mineral equilibria, because CO_2-bearing phases are relatively uncommon in high-grade silicate lithologies compared to hydrous phases. However, scapolite have been considered as a common assemblage in the high-grade gneiss terranes and a powerful monitor to evaluation of a_{CO_2}. In the case of vein-related scapolite reaction zone, the mineralogical differences between the reaction zone and the host pyroxene granulite are appearance of scapolite, biotite and hornblende in the host rock near veins at the consumption of orthopyroxene, clinopyroxene and plagioclase. Reaction (9) suggesting scapolite-forming reaction occurs at high pressure (up to 2.0 GPa). In contrast, reaction (7) suggesting breakdown of garnet occurs under granulite facies condition at reasonable depth of the lower crust. In fact, the vein-related reaction zone without garnet in pyroxene granulites is never observed. Therefore, it might be expected that garnet already formed in the host pyroxene granulite before scapolite formation. Moecher & Essene (1991) directly calculated a_{CO_2} using reaction (7) from rocks in high grade gneiss terranes and xenoliths. Scapolite, the activity model of Baker & Newton (1996) is used, provides somewhat smaller a_{CO_2} than that of other models (Oterdoom & Gunter, 1983; Moecher & Essene, 1990; 1991). The scapolite-bearing reaction zone in the pyroxene granulite yield $a_{CO_2} >$ 0.88 at 750-850 ˚C and 0.8 GPa, whereas the scapolite-bearing garnet granulite yield $0.56 < a_{CO_2} < 0.89$ at 750-850 ˚C and 1.2-1.5 GPa. These results suggesting $a_{CO_2} >$

0.45 are in good agreement with the calculated a_{CO_2} of the mafic granulites and xenoliths (Moecher & Essene, 1991). When scapolite inclusion in garnet is in equilibrium with core of garnet and plagioclase, calculated a_{CO_2} of core composition is higher than that of rim composition. Assuming the fluid composition of binary H_2O-CO_2, X_{CO_2} is over 0.6 (Fig. 5-25). Relatively high a_{CO_2} should be required for the scapolite forming reaction of the Kohistan granulites.

Oxidation states and origin of sulfate-rich scapolite

Opaque minerals, sulphides and graphite are important minerals to understand the role of volatiles in formation of the various reaction zones developed in the lower crust of the Kohistan arc. Most of pyroxene granulites usually contains significant amount of hemo-ilmenite and small amount of magnetite. Chemical composition of these minerals can provide information of redox state during formation of reaction zones. Oxygen fugacity (fO_2) can be estimated from oxidation reactions involving oxide and silicate minerals. Carmichael (1991) showed that alkaline basalts record very high primary oxidation states, suggesting that important constituent of volatile is H_2O, CO_2 and SO_2. Scapolite-forming reactions may correlate with these redox state. Scapolite contains significant amount of sulfate ion in the anion site. In addition, pyroxene granulites including scapolite reaction zone in the NKA, contains sulphide, especially pyrrhotite. These results allow calculation of sulfur fugacity. Redox state of metamorphic fluids in the Kohistan arc was monitored by analysis of oxygen and sulfur fugacities between the reaction zone and the host rock.

High-sulfur scapolite is important constituent of xenoliths in basaltic or kimberitic lava and breccias (e.g. Jones *et al.*, 1983) and of mafic granulites and anorthosites (e.g. Blattner and Black, 1980; Coolen, 1982; Austrheim & Griffin, 1985). In general, sulfate content in scapolite in mafic granulites is much higher than that in calc-silicate gneisses and anorthosites (Moecher & Essene, 1991). Sulfate-rich scapolite in the lower crust is generally considered to be metamorphic or metasomatic origin (Lovering & White, 1964;

Okrusch et al., 1979), formed by a complex reaction involving a relatively CO_2-rich fluid phase, calcic-plagioclase and accessory sulfides. The vein-related scapolite seems to develop within the pyrhotite-rich pyroxene granulites. The primary sulfides in the host pyroxene granulite is apparently oxidized by fluid composition with high oxygen fugacity and released sulfate anion incorporate into scapolite. Occurrence of scapolite developed along the vein and consumption of primary garnet and sulfide reveals that these scapolite are secondary phase originated by fluid infiltration with high oxygen fugacity. Sulfate in scapolite is probably derived from reaction with sulfides or other forms of reduced sulfur from the mantle. It is likely that oxidation takes place by a ferrous-ferric equilibrium with deep crustal minerals, and with no transfer of oxygen or need for other oxidizing agents. A simplified reaction between silicate minerals, sulfides and oxides would be (Goldsmith, 1975):

$$S^{2-} \text{ (in sulfide)} + 4Fe_2O_3 \text{ (in magnetite)} = SO_4^{2-} \text{ (in scapolite)} + 8FeO \text{ (in silicate)}.$$
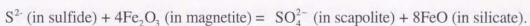
This reaction should lead to reduction in hematite component of magnetite and decrease in X_{Mg} in silicate minerals. Although compositional variation vertical to the vein is not supported by the above reaction, ferrous iron content of orthopyroxene in contact with scapolite is slightly higher.

Self-consistent temperature/oxygen fugacity mesurements based on clinopyroxene-orthopyroxene-ilmenite-quartz were calculated by using QUIlF program of Andersen *et al.* (1993). Compairing with T-fO_2 condition of scapolite-amphibole reaction zone between the host pyroxene granulites and the garnet reaction zone, they were calculated only from the samples in the NKA at the same pressure condition of 800 MPa. Clinopyroxene coexisting other minerals was choosen from adjacent area to scapolite reaction zone. In the case of garnet reaction zone, orthopyroxene, which is the nearest to the vein within the reaction zone, coexisting with clinopyroxene and ilmenite were selected as an equilibrium

set of each mineral. In the host pyroxene granulites, arbitrary pairs were selected. The T-fO_2 pairs are plotted in figure 5-26. It suggests that garnet-forming reaction occurred under reduced and lower temperature condition in comparison with surrounding pyroxene granulites, and scapolite-forming reaction occurred at higher fO_2 and T condition. The results from garnet reaction zone are in good agreement with decerease in Fe^{3+}/Fe_{total} in each minerals toward the vein. CO_2-rich fluid confirmed by fluid inclusion study is still stable, because the reduced conditions are located above equilibrium of invariant reaction of graphite + O_2 = CO_2. Pair from scapolite-amphibole reaction zone shows higher T and fO_2 condition. The result from scapolite reaction zone is plotted on reaction curve of pyrite + magnetite = pyrrhotite + O_2. Pyrrhotite in the host pyroxene granulites adjacent to the reaction zone is rimmed by magnetite and small amount of pyrite. It indicates that fO_2 elevated at the time of crystallization of scapolite. Crystalliazation of scapolite also requires the presence of SO_2 in metamorphic fluids. Plotting the values of fO_2 and fS_2 on the equilibrium diagrm of the system Fe-Si-O-H-S, it can be seen that the stability of sulfate-rich scapolite requires fO_2 significantly higher than that coexisting with pyrrhotite. The lack of sulphide in the reaction zone also suggests that sulfate ion in scapolite is formed by pyrrhotite breakdown at higher fO_2. Thus, scapolite-forming reaction in the NKA is presumably triggered by oxydizing metamorphic fluid.

The garnet granulite in the Jijal complex shows compositional banding, characterized by clinopyroxene + garnet-rich and plagioclase-rich layers. Scapolite occurs in plagioclase-rich layers and some scapolite totally substitutes instead of plagioclase. Metasomatic production of sulfate-rich scapolite would require an environment with a relatively high fO_2 and presumably fH_2O. In fact, vein-related scapolite in the NKA coexists with hornblende in the reaction zone adjacent to the garnet-bearing quartzo-feldspathic vein. Layered scapolite-bearing garnet-clinopyroxene-plagioclase xenoliths from Delegate, Australia, were interpreted as cumulates from basaltic magmas (Irving, 1974), although it was not specifically argued that the scapolite was of igneous origin.

Strong evidence for the existence of igneous scapolite is provided by its occurrence as phenocrysts in latite dome from Arizona (Goff & Eddy, 1979), as megacrysts in tephra from the Enval-Volvic volcanic line, France (Boivin & Cumus, 1981), and as inclusions in garnet from McBride, Australia (Stoltz, 1987), with apatite, amphibole, clinopyroxene and Fe-Ti oxides. The garnet granulites in the Kohistan arc underwent an event of elevated pressure. If all scapolite is a primary phase derived from basaltic magma, it must be present prior to formation of garnet porphyroblast. Some garnet porphyroblasts certainly contain scapolite inclusions in garnet granulites of the Jijal complex. However, there is no textural evidence for such a occurrence of sulfate-bearing scapolite mantled by sulphides or phyrrhotite rimmed by magnetite. These facts might indicate that the infiltrated fluid initially includes the significant amounts of sulfate ion. It has been recognized the presence of amphibole, anhydrite and sulfate-rich apatite at some subduction-related island arc such as Pinatubo volcano, Philippine. It indicates that sulfate-bearing fluid or melt with high oxygen fugacity from the depth pass through the lower crust. Therefore sulfate-bearing fluid should react with plagioclase and garnet in the lower crust and sulfate-rich scapolite may behave as sulfate reservoir. The existence of sulfate-rich scapolite in the lower crust of the Kohistan arc is good evidence for the sulfate-rich fluid in the lower crust.

Fluid in the mafic lower crust

Origin of the CO_2-rich fluids

Petrological characteristics and fluid inclusion study of the vein-related reaction zone is required for the infiltration of CO_2-rich fluid or fluid characterized by low water activity. From this study, the source of the fluid cannot be clarified. Dominant CO_2 source at deep crustal levels may be derived from decarbonization of relatively thin layers of carbonate rocks (Glassley, 1983). No marble, calk-silicate rocks as possible sources of CO_2 are found nearby in the lower crust of the Kohistan arc. Carbonate-bearing lithologies such as

marbles are noticeably absent from compilations of xenolith lithologies (Rudnick & Taylor, 1987; Griffin & O'Reilly, 1987). A juvenile source of CO_2 was inferred from the -6 ‰ ^{13}C carbon isotope composition obtained from scapolite in a plagioclase-rich vein at the Fiordland complex (Blattner & Black 1980). The carbon isotope composition ($\delta^{13}C$) of CO_2 extracted from scapolite in granulite facies orthogneisses and mafic granulites (-8.2 to -1.2 ‰) are consistent with crystallization of the scapolite from a mafic melt or generation of CO_2 from mafic melts emplaced in the lower crust or upper mantle (Moecher *et al.*, 1994). These values are relatively lighter than the values from the calc-silicate and mafic granulites derived from a supracrustal rock. If scapolite studied here assumes relatively lighter values of $\delta^{13}C$, principal source of CO_2 is dominantly derived from mafic magma. Then, the scapolite forming reaction from the Kohistan arc may be triggered by infiltration of CO_2-rich fluid originated from juvenile mantle during prograde metamorphism. Carbon isotope studies need to evaluate the source of carbon in scapolite from granulites in the Kohistan arc.

Fluid transport mechanism affecting pressure inferred from vein distribution

There are many studies suggesting that hydrofracturing is a possible mechanism for metamorphic fluid transport. Studies on veins formed by the crack-seal mechanism (Fisher & Blantley, 1992) suggest episodic fluid flow by hydrofracturing. Experimental studies of dihedral angle Θ in fluid-saturated porous rock (Watson & Brenan, 1987; Holness, 1992) suggest that interconnected fluid networks essential to permeable flow may not develop. Metamorphic fluid in the lower crust inferred from channelized distribution of metasomatic zone may be transported not by steady permeable flow but by transient hydrofracturing. The restricted development of scapolite and garnet in the relict pyroxene granulite of the KAB can be explained by migration of carbonic fluid lowered a_{H_2O} along the channelways. A fluid-saturated lower crust with hydrostatic pore fluid

pressure as for low a_{H_2O} fluid is only supported by the occurrence of homogeneously developed garnet granulites in the Jijal complex. The movement of a small fluid fraction through a matrix of crystal is only possible if the fluid fills a connected network of pores. Then it is likely that the system will be in both chemical and textural equilibrium. However, a whole system of the pyroxene granulites in the KAB did not reach the complete equilibrium. Because the fluid network of porous media strongly depends on the dihedral angle, the channelized distribution of the reaction zone reflects that effective dihedral angle Θ_{eff} between low a_{H_2O} fluid and solid phase in the mafic granulite is over 60° under granulite facies conditions at the moderate crustal depth (0.5-1.0 GPa). In fact, Watson & Brenan (1987) reported that Θ between quartz and fluid increases with increasing fraction of CO_2 to H_2O in a binary fluid. Channelized fluid migration is presumably controlled by crack propagation accompanied with hydrofracturing caused by the local excess pore fluid pressure. However, because the garnet reaction zone in the SKA is no relation to crack formation, a large amounts of fluid influx to form a connected network of pores in matrix of crystals should be required for the formation of the garnet reaction zone. It might take place the increasing pressure at centre of the reaction zone.

On the other hand, homogeneously developed garnet granulites in the Jijal complex should be formed as a result of percolative fluid flow. Based on experimentally determined wetting characteristics of fluids, Watson & Brenan (1987) pointed out that aqueous fluids are likely to form an interconnected network along grain boundaries in the continental crust. Holness (1992) found that the wetting properties between H_2O and quartz is strongly dependent on pressure at 800 °C. The dihedral angle decreases less than 60° over 800 MPa. Thus, occurrence of garnet granulite in the Jijal complex, which underwent higher pressure metamorphism, suggests decrease in the dihedral angle due to the increasing pressure. The fact that substantial quartz is produced by the garnet-forming reaction facilitates a regional dehydration in the rock system at above the critical pressure

111

of dihedral angle. For fluids close to pure CO_2, the dihedral angle remains constant over $60°$ in the pressure range of 100-1500 MPa (Holness, 1992). These observations indicate that newly generated water due to dehydration of hydrous minerals in quartz matrix is selectively flushed outward and then residual fluid composition would enrich CO_2. Furthermore, enrichment of CO_2 would introduce an increase in activity of carbon dioxide and then produce scapolite. Largely developed scapolite may behave as a significant CO_2 reservoir in deep crust over 1.0 GPa.

CONCLUSIONS

1. Occurrence of garnet in the Kohistan arc is relatively homogeneous at the higher pressure area in the Jijal complex, whereas it is channelized along the quartzo-feldspathic vein at the lower pressure area in the Kamila amphibolite belt.

2. The garnet reaction zone developed within pyroxene granulites is triggered by channelized infiltration of fluid with low water activity. Breakdown of hornblende due to decrease in water activity leads to formation of garnet. Compositional change of minerals in the garnet reaction zone toward the vein is gradual and related to the modal composition of garnet.

3. Scapolite-forming reaction occurs in the pyroxene granulites along the garnet-bearing quartzo-feldspathic vein in the Kamila amphibolite belt, whereas it occurs throughout the rock mass in the Jijal garnet granulite. Scapolite with quartz is formed by consumption of garnet and calcic-plagioclase. Activity of carbon dioxide estimated from scapolite equilibria shows higher value over 0.5.

4. Scapolite of the Kohistan arc is metasomatic in origin related to the fluid infiltration after intrusion of gabbroic magma. Abundance of sulfate-rich scapolite in garnet granulite reflects existence of sulfate reservoir in the lowermost crust of the Kohistan arc, whereas restricted occurrence of sulfate-rich scapolite in pyroxene granulites represents channelized infiltration of oxidizing fluid accompanying breakdown of sulphides.

5. Fluid composition is characterized by enrichment of CO_2 and reduced water activity based on phase petrology and fluid inclusion study. Transport mechanism of fluid changes at the boundary between the garnet granulite and pyroxene granulite, probably derived from pressure difference.

Table. 5-1. A summary of several types of reaction zone in the Kohistan pyroxene granulites

Sample No.	TYPE	VEIN	Reaction Zone	HOST
A1	Hbl reaction zone	Undefined	Uralitization Opx-Cum-Qtz-Hbl-Pl Cpx-Act-Qtz-Hbl-Pl Total Width: 1 cm	Opx-Cpx-Pl-Qtz-Ilm±Hbl±Bt
UO1	Scp-Hbl reaction zone	Grt-Pl-Scp-Qtz±Ap±Zr Euhedral: Grt, Pl, Scp Pl: antiperthitic Grt inclusion-free Total Width: 5 mm	Scp-Hbl-Bt-Kf-Pl-Qtz-Ap Interstitial: Hbl, Bt Pl: Ilm, Mt inclusion expence of Cpx-Opx Width: 9 mm	Opx-Cpx-Pl-Qtz-Ilm±Hbl Ilm is pseudomophed by Hbl Pl: Ilm, Mt inclusion
U3	No reaction	Grt-Pl-Qtz-Ap Euhedral: Grt, Pl Pl: mesoperthitic Grt inclusion-free Total Width: 6 mm	Grt-Hbl-Cpx-Ilm-Qtz-Ap Grt rimmed by Hbl Qtz inclusion in Grt Width: <1 mm	Hbl-Opx-Cpx-Pl-Qtz-Ilm Brownish Hbl Pl: Ilm, Mt inclusion
D8	Grt reaction zone Type I	Cpx-Opx-Pl-Qtz-Ap Pl: mesoperthitic Total Width: <2 mm	Grt-Cpx-Pl-Kf-Qtz-Hbl-Bt-Ilm-Ap Interstitial: Hbl, Bt Pl: Ilm, Mt inclusion Grt: Cpx, Hbl, Bt, Ilm, Qtz inclusion Width: <4 mm	Opx-Cpx-Pl-Qtz-Ilm±Hbl Interstitial: Hbl Pl: Ilm, Mt inclusion
CH2	Grt reaction zone Type I	Grt-Pl-Qtz-Hbl-Bt(-Ilm)-Ap Euhedral: Grt, Pl Interstitial: Hbl, Bt Total Width: 2 mm	Grt-Hbl-Bt-Cpx-Pl-Kf-Qtz-Ap Grt: Cpx, Hbl, Bt, Ilm, Qtz inclusion Pl: inclusion-free Width: 2-3 mm	Opx-Cpx-Pl-Qtz-Ilm±Hbl±Bt Ilm is pseudomophed by Hbl Pl: Ilm, Mt inclusion
PL2	Grt reaction zone Type III	Undefined	Grt-Cpx-Pl-Qtz-Bt-Hbl-Kf-Ilm-Rt-Ap Hbl is rimmed by Cpx Pl: Cpx, Ilm, Mt inclusion Grt: Cpx, Opx, Hbl, Bt, Ilm, Qtz inclusion Total Width: 1cm	Opx-Cpx-Pl-Qtz-Ilm±Hbl Pl: inclusion-free
P5	Grt reaction zone Type III	Undefined	Grt-Cpx-Pl-Qtz-Bt-Rt-Ilm-Ap-Cc Grt: Cpx, Opx, Bt, Rt, Qtz inclusion Pl: inclusion-free Uralitization Total Width: 8 mm	Opx-Cpx-Pl-Qtz-Ilm±Hbl±Bt Pl: inclusion-free

Table 5-2. Representative chemical compositions of pyroxene in the garnet reaction zone

	D8							PL2						
	Vein-related type							Garnet granulite type						
	opx			cpx				opx			cpx			
	Host	RZ(E)	RZ(C)	Host	RZ(E)	RZ(C)	P	Host	RZ(E)	RZ(C)	Host	RZ(E)	RZ(C)	P
SiO_2	50.06	50.35	51.40	50.29	49.80	50.42	51.49	49.57	49.97	51.15	48.67	49.64	51.67	51.78
Al_2O_3	2.53	2.40	2.42	3.79	4.15	4.03	2.95	3.24	3.04	2.56	4.74	4.97	3.33	2.77
TiO_2	0.08	0.11	0.05	0.38	0.42	0.44	0.23	0.01	0.02	0.10	0.36	0.35	0.41	0.36
FeO^*	28.56	27.87	24.74	13.23	11.06	9.84	8.46	29.13	26.11	24.39	14.61	10.96	7.37	7.71
MnO	0.63	0.67	0.26	0.38	0.33	0.14	0.01	0.87	0.44	0.22	0.44	0.71	0.07	0.04
MgO	17.53	17.88	20.52	11.54	11.15	12.52	13.06	17.03	18.89	20.52	10.58	10.80	13.33	13.62
CaO	0.53	0.59	0.47	20.05	21.54	21.02	22.28	0.56	0.46	0.46	20.55	21.65	22.77	22.75
Na_2O	0.06	0.00	0.02	0.72	0.69	0.68	0.60	0.01	0.01	0.02	0.68	0.86	0.82	0.65
K_2O	0.01	0.00	0.01	0.00	0.00	0.02	0.01	0.03	0.02	0.00	0.00	0.00	0.00	0.02
Cr_2O_3	0.00	0.04	0.00	0.00	0.02	0.10	0.06	0.00	0.08	0.00	0.04	0.00	0.02	0.09
Total	99.98	99.91	99.88	100.37	99.17	99.21	99.15	100.44	99.02	99.41	100.64	99.95	99.79	99.78
$O=6^{\dagger\dagger}$														
Si	1.919	1.928	1.934	1.889	1.887	1.895	1.929	1.897	1.912	1.932	1.833	1.864	1.914	1.921
Al	0.114	0.108	0.107	0.168	0.185	0.179	0.130	0.146	0.137	0.114	0.210	0.220	0.145	0.121
Ti	0.002	0.003	0.001	0.011	0.012	0.012	0.007	0.000	0.000	0.003	0.010	0.010	0.011	0.010
$Fe^{3+}{}^{\dagger\dagger\dagger}$	0.048	0.028	0.024	0.086	0.067	0.055	0.041	0.061	0.037	0.019	0.153	0.095	0.062	0.063
$Fe^{2+}{}^{\dagger\dagger\dagger}$	0.868	0.865	0.754	0.330	0.283	0.254	0.224	0.871	0.799	0.751	0.307	0.249	0.166	0.177
Mn	0.021	0.022	0.008	0.012	0.011	0.004	0.000	0.028	0.014	0.007	0.014	0.023	0.002	0.001
Mg	1.002	1.021	1.151	0.646	0.630	0.702	0.729	0.971	1.078	1.155	0.594	0.605	0.736	0.753
Ca	0.022	0.024	0.019	0.807	0.874	0.846	0.894	0.023	0.019	0.018	0.829	0.871	0.904	0.904
Na	0.004	0.000	0.001	0.052	0.051	0.049	0.043	0.001	0.001	0.001	0.049	0.063	0.059	0.047
K	0.000	0.000	0.001	0.000	0.000	0.001	0.000	0.001	0.001	0.000	0.000	0.000	0.000	0.001
Cr	0.000	0.001	0.000	0.000	0.000	0.003	0.002	0.000	0.002	0.000	0.001	0.000	0.001	0.002
total	4.000	4.000	4.000	4.000	4.000	4.000	4.000	4.000	4.000	4.000	4.000	4.000	4.000	4.000
$Mg\#^*$	0.536	0.541	0.604	0.662	0.690	0.734	0.765	0.527	0.574	0.606	0.659	0.708	0.816	0.810
Fe^{3+}/Fe_{total}	0.052	0.031	0.031	0.206	0.192	0.178	0.155	0.065	0.044	0.025	0.332	0.275	0.273	0.261

RZ(E): edge of the reaction zone, RZ(C): center of the reaction zone, P: productant clinopyroxene occurring around orthopyroxene grain.

*: FeO was calculated as total iron

††: Cation was calculated based on 6-oxygens

†††: Fe^{2+} and Fe^{3+} were calculated based on garnet stoichiometry

*: $Mg\#=Mg/(Mg+Fe^{2+})$ in atomic

Table 5-3. Representative chemical composition of hornblende in the reaction zone

| | Garnet reaction zone D8 | | | Garnet reaction zone PL2 | | | Scapolite reaction zone UO1 | | | No reaction zone U3 | |
| | Vein-related type | | | Garnet granulite type | | | | | | | |
	Host	RZ	Vein	Host	RZ(E)	RZ(C)	RZ(E)	RZ(C)	Vein	H(F)	H(N)
SiO_2	41.32	40.73	40.20	40.43	39.96	41.56	41.22	40.85	41.29	42.06	41.99
Al_2O_3	13.30	13.97	14.25	15.33	13.86	12.63	13.30	13.12	12.58	13.01	13.10
TiO_2	2.75	1.91	2.26	1.25	3.13	3.27	2.07	2.17	2.06	2.23	2.45
MgO	10.32	9.66	8.67	8.49	10.07	11.93	9.87	9.78	10.16	15.10	14.58
$FeO^†$	14.40	16.15	17.56	17.16	13.81	12.21	16.30	16.74	15.40	0.18	0.13
MnO	0.04	0.07	0.13	0.20	0.12	0.00	0.13	0.21	0.20	10.06	10.33
CaO	10.97	11.40	11.40	11.41	11.47	11.77	11.45	11.52	11.36	11.73	11.81
Na_2O	1.44	1.17	1.23	1.22	1.16	1.07	1.19	1.34	1.28	1.51	1.31
K_2O	2.03	2.09	1.98	1.44	2.06	2.48	1.99	1.94	1.80	1.75	1.84
NiO	0.10	0.03	0.00	0.00	0.00	0.08	0.00	0.00	0.00	0.02	0.02
Cr_2O_3	0.01	0.05	0.03	0.00	0.00	0.00	0.00	0.02	0.00	0.01	0.02
Cl	0.10	0.09	0.11	0.00	0.00	0.00	0.00	0.00	0.00	0.06	0.12
	-0.03	-0.02	-0.03	0.00	0.00	0.00	0.00	0.00	0.00	-0.01	-0.03
F	0.14	0.28	0.00	0.00	0.00	0.00	0.00	0.00	0.00	0.00	0.08
	-0.06	-0.12	0.00	0.00	0.00	0.00	0.00	0.00	0.00	0.00	-0.04
Total	96.75	97.30	97.83	96.93	95.64	97.00	97.52	97.69	96.12	97.70	97.72
$O=23^{††}$											
Si	6.203	6.111	6.046	6.069	6.089	6.212	6.166	6.125	6.252	6.295	6.274
Al^{iv}	1.797	1.889	1.954	1.931	1.911	1.788	1.834	1.875	1.748	1.705	1.726
Al_{total}	2.354	2.470	2.527	2.713	2.490	2.226	2.345	2.319	2.246	2.296	2.308
Al^{vi}	0.556	0.581	0.572	0.782	0.579	0.439	0.511	0.444	0.497	0.590	0.582
Ti	0.311	0.215	0.255	0.141	0.358	0.368	0.233	0.245	0.235	0.251	0.275
$Fe^{3+†††}$	0.283	0.467	0.454	0.567	0.127	0.061	0.462	0.479	0.373	0.079	0.081
Cr	0.001	0.005	0.004	0.000	0.000	0.000	0.000	0.000	0.000	0.001	0.003
Mg	2.308	2.160	1.944	1.898	2.287	2.657	2.200	2.185	2.293	2.244	2.300
$Fe^{2+†††}$	1.524	1.560	1.754	1.587	1.633	1.466	1.577	1.620	1.577	1.810	1.741
Mn	0.005	0.008	0.016	0.025	0.015	0.000	0.016	0.027	0.026	0.023	0.017
Ni	0.012	0.003	0.000	0.000	0.000	0.009	0.000	0.000	0.000	0.002	0.002
Sum FM	13.000	13.000	13.000	13.000	13.000	13.000	13.000	13.000	13.000	13.000	13.000
Ca	1.764	1.833	1.837	1.836	1.873	1.886	1.835	1.851	1.843	1.881	1.891
Na(M4)	0.236	0.167	0.163	0.164	0.127	0.114	0.165	0.149	0.157	0.119	0.109
Na_{total}	0.420	0.339	0.359	0.354	0.343	0.309	0.345	0.390	0.376	0.438	0.378
Na(A)	0.184	0.173	0.196	0.190	0.216	0.195	0.180	0.240	0.219	0.319	0.269
K	0.388	0.399	0.380	0.276	0.400	0.472	0.380	0.371	0.348	0.334	0.351
Sum(A)	0.572	0.572	0.576	0.466	0.615	0.667	0.560	0.611	0.566	0.653	0.620
OH	1.907	1.847	1.973	2.000	2.000	2.000	2.000	2.000	2.000	1.985	1.931
Cl	0.026	0.022	0.027	0.000	0.000	0.000	0.000	0.000	0.000	0.015	0.031
F	0.067	0.131	0.000	0.000	0.000	0.000	0.000	0.000	0.000	0.000	0.039
$Mg\#^{††††}$	0.602	0.581	0.526	0.545	0.583	0.644	0.773	0.772	0.809	0.554	0.569
Fe^{3+}/Fe_{total}	0.157	0.230	0.206	0.263	0.072	0.04	0.418	0.426	0.407	0.042	0.044

RZ(E): edge of the reaction zone, RZ(C): center of the reaction zone, H(F): Further side from the vein in the host rock, H(N): Near side of the vein in the host rock.

† : FeO* was calculated as total iron

†† : Cation was calculated based on 23-oxygens

††† : Fe^{2+} and Fe^{3+} were calculated based on Robinson et al. (1982)

†††† : $Mg\#=Mg/(Mg+Fe^{2+})$ in atomic

116

Table 5-4. Representative mineral compositions of garnet in the garnet reaction zone

	D8 Vein-related type garnet		PL2 Garnet granulite type garnet	
	RZ(E)	RZ(C)	RZ(E)	RZ(C)
SiO_2	38.79	38.69	38.18	38.67
Al_2O_3	21.07	21.52	20.51	20.80
TiO_2	0.01	0.03	0.26	0.21
$FeO^{\dagger}$	25.40	25.38	25.84	24.53
MnO	0.85	0.71	1.15	0.63
MgO	6.91	6.89	4.60	6.44
CaO	6.94	6.97	8.67	8.71
Na_2O	0.01	0.02	0.04	0.04
Cr_2O_3	0.00	0.00	0.02	0.03
Total	99.98	100.20	99.28	100.05
$O=12^{\dagger\dagger}$				
Si	3.003	2.985	3.013	2.992
Al	1.922	1.957	1.907	1.897
Ti	0.001	0.002	0.015	0.012
$Fe^{3+\,\dagger\dagger\dagger}$	0.074	0.072	0.042	0.099
$Fe^{2+\,\dagger\dagger\dagger}$	1.570	1.566	1.664	1.488
Mn	0.056	0.046	0.077	0.041
Mg	0.798	0.793	0.541	0.743
Ca	0.575	0.576	0.733	0.722
Na	0.002	0.003	0.007	0.005
Cr	0.000	0.000	0.001	0.002
total	8.000	8.000	8.000	8.000
X_{Alm}	0.524	0.525	0.552	0.497
X_{Pyr}	0.266	0.266	0.180	0.248
X_{Gro}	0.192	0.193	0.243	0.241
X_{Sps}	0.019	0.015	0.025	0.014

RZ(E): edge of the reaction zone,
RZ(C): center of the reaction zone.
$\dagger$: FeO was calculated as total iron
$\dagger\dagger$: Cation was calculated based on 6-oxygens
$\dagger\dagger\dagger$: Fe^{3+} and Fe^{2+} were calculated based
on garnet stoichiometry

Table 5-5. Representative chemical compositions of scapolite in the Kohistan granulites

	Reaction zone		Garnet granulite				
Sample no.	UO1		1609		KU85		
					core	rim	inclusion
SiO$_2$	46.33	46.17	46.56	47.59	46.10	46.48	46.31
Al$_2$O$_3$	26.61	26.43	25.74	26.60	26.16	26.06	26.04
FeO†	0.11	0.10	0.05	0.07	0.13	0.05	0.19
CaO	17.38	17.47	16.74	17.08	17.18	16.90	17.40
Na$_2$O	3.26	3.18	3.79	3.96	3.36	3.65	3.35
K$_2$O	0.13	0.13	0.02	0.05	0.03	0.03	0.04
Cl	0.03	0.03	0.00	0.02	0.00	0.02	0.01
	-0.01	-0.01	0.00	0.00	0.00	-0.01	0.00
SO$_3$	4.39	3.73	4.79	4.35	2.56	3.04	2.80
Total	98.69	97.66	98.06	100.18	95.52	96.22	96.13
O=25††							
Si	6.719	6.787	6.773	6.802	6.919	6.910	6.901
Al	4.548	4.578	4.413	4.480	4.627	4.567	4.574
Fe	0.013	0.013	0.006	0.009	0.017	0.006	0.024
Ca	2.700	2.752	2.609	2.616	2.763	2.693	2.779
Na	0.916	0.905	1.093	1.098	0.978	1.051	0.967
K	0.025	0.024	0.004	0.009	0.005	0.007	0.008
Cl	0.007	0.006	0.000	0.004	0.000	0.006	0.002
S	0.478	0.411	0.523	0.467	0.288	0.339	0.313
Total	15.468	15.577	15.470	15.626	15.597	15.578	15.567
EqAn(ME)	0.61	0.61	0.58	0.59	0.60	0.59	0.59
EqAn	0.74	0.75	0.70	0.70	0.74	0.72	0.74
a$_{Me}$(OG)	0.23	0.25	0.28	0.31	0.43	0.39	0.41
a$_{Me}$(NB)	0.03	0.03	0.02	0.02	0.04	0.03	0.04
X$_{Al}$	0.40	0.40	0.39	0.40	0.40	0.40	0.40

EqAn(ME) is calculated from (Al-3)/3 based on Moecher and Essene (1990).

EqAn = Ca/(Ca+Na+K).

a(OG): activity model of Oterdoom & Gunter (1983). a(NG): activity model of Newton & Baker (1996).

† : FeO was calculated as total iron

†† : Cation was calculated based on 25-oxygens

Table 5-6. Representative chemical compositions of apatite in the pyroxene granulites

	UO1	D8	U3	P5		CH2	PL2
				core	rim		
SiO_2	0.30	0.19	0.09	0.13	0.25	0.20	0.22
Al_2O_3	0.00	0.00	0.00	0.00	0.00	0.00	0.00
TiO_2	0.00	0.05	0.05	0.04	0.00	0.00	0.03
FeO^+	0.14	0.09	0.18	0.02	0.09	0.15	0.14
MnO	0.01	0.01	0.04	0.12	0.00	0.05	0.03
MgO	0.05	0.01	0.00	0.00	0.00	0.05	0.03
CaO	55.73	55.11	55.64	56.57	56.39	56.24	55.68
Na_2O	0.03	0.06	0.03	0.00	0.05	0.09	0.07
$K2O$	0.00	0.03	0.00	0.03	0.01	0.00	0.02
Cr_2O_3	0.06	0.00	0.00	0.00	0.00	0.00	0.07
P_2O_5	41.30	41.12	41.61	41.82	40.96	41.29	41.53
NiO	0.02	0.00	0.07	0.00	0.09	0.00	0.00
V_2O_3	0.00	0.00	0.03	0.00	0.05	0.00	0.00
Cl	0.25	0.52	0.85	0.73	0.66	0.75	0.17
	-0.06	-0.12	-0.19	-0.16	-0.15	-0.17	-0.04
F	3.08	2.58	2.67	1.90	2.02	2.24	2.39
	-1.30	-1.09	-1.12	-0.80	-0.85	-0.94	-1.01
SO_3	0.28	0.02	0.00	0.02	0.00	0.00	0.03
Total	99.88	98.59	99.94	100.42	99.58	99.94	99.36
$O=13^{++}$							
Si	0.026	0.017	0.008	0.012	0.022	0.017	0.019
Al	0.000	0.000	0.000	0.000	0.000	0.000	0.000
Ti	0.000	0.004	0.004	0.002	0.000	0.000	0.002
Fe	0.010	0.006	0.013	0.001	0.007	0.011	0.010
Mn	0.001	0.001	0.003	0.009	0.000	0.004	0.002
Mg	0.006	0.001	0.000	0.000	0.000	0.006	0.004
Ca	5.222	5.230	5.228	5.266	5.311	5.280	5.225
Na	0.006	0.010	0.005	0.000	0.009	0.015	0.012
K	0.000	0.003	0.000	0.004	0.002	0.000	0.002
Cr	0.004	0.000	0.000	0.000	0.000	0.000	0.005
P	3.058	3.084	3.089	3.076	3.048	3.063	3.079
Ni	0.001	0.000	0.005	0.000	0.006	0.000	0.000
V	0.000	0.000	0.002	0.000	0.004	0.000	0.000
Total	8.333	8.356	8.356	8.369	8.409	8.396	8.359
Cl	0.037	0.078	0.126	0.107	0.099	0.111	0.024
F	0.852	0.722	0.740	0.521	0.562	0.620	0.663
S	0.018	0.002	0.000	0.001	0.000	0.000	0.002
OH	0.093	0.199	0.135	0.370	0.339	0.270	0.311

$^+$: FeO was calculated as total iron
$^{++}$: Cation was calculated based on 13-oxygens

Table 5-7. Representative chemical compositions of
biotite in the pyroxene granulites

	UO1	D8		CH2	
		core	rim	core	rim
SiO_2	36.83	37.13	37.08	37.58	36.50
Al_2O_3	15.17	14.68	14.70	15.18	14.88
TiO_2	4.86	5.92	6.10	6.50	6.06
FeO^*	16.88	15.61	16.18	15.31	15.25
MnO	0.07	0.02	0.00	0.04	0.03
MgO	12.27	11.91	12.41	13.73	13.21
CaO	0.03	0.14	0.00	0.08	0.41
Na_2O	0.01	0.07	0.01	0.06	0.07
K_2O	9.50	9.48	9.62	9.68	7.46
Cr_2O_3	0.00	0.00	0.09	0.00	0.04
NiO	0.00	0.07	0.01	0.01	0.01
V_2O_3	0.08	0.36	0.27	0.02	0.12
Cl	0.04	0.07	0.06	0.18	0.04
	-0.01	-0.02	-0.01	-0.04	-0.01
F	0.06	0.00	0.12	0.00	0.00
	-0.02	0.00	-0.05	0.00	0.00
SO_3	0.15	0.14	0.07	0.06	0.08
Total	95.92	95.57	96.66	98.38	94.14
O=11"					
Si	2.760	2.778	2.754	2.727	2.740
Al	1.340	1.295	1.287	1.299	1.316
Ti	0.274	0.333	0.341	0.355	0.342
Fe	1.057	0.977	1.005	0.929	0.957
Mn	0.004	0.001	0.000	0.002	0.002
Mg	1.371	1.329	1.374	1.486	1.479
Ca	0.003	0.011	0.000	0.006	0.033
Na	0.001	0.009	0.001	0.006	0.010
K	0.908	0.905	0.912	0.896	0.715
Cr	0.000	0.000	0.005	0.000	0.002
Ni	0.000	0.004	0.001	0.000	0.000
V	0.005	0.022	0.016	0.001	0.007
Cl	0.005	0.009	0.007	0.021	0.005
F	0.013	0.000	0.028	0.000	0.000
S	0.009	0.008	0.004	0.003	0.005
Total	7.749	7.680	7.734	7.733	7.613
Mg#†††	0.56	0.58	0.58	0.62	0.61
a_{en}	0.17	0.19	0.18	0.22	0.22

* : FeO* was calculated as total iron
†† : Cation was calculated based on 11-oxygens
††† : Mg#=Mg/(Mg+Fe^{2+}) in atomic

Table 5.x Representative compositions of Fe-Ti oxides from the Kohistan pyroxene granulites

	UO1				BR4		D8				D11				PL2				PL4			
	ilm	Ex-ilm	Ex-mt	Inti-mt	ilm	mt	ilm	mt	inti-mt	inti-mt	ilm	Ex-ilm	Ex-mt	Inti-mt	ilm	mt	Ex-mt	Inti-mt	mt	Ex-ilm	Ex-mt	Inti-mt
SiO_2	0.04	nd	0.02	0.01	0.00	0.00	0.01	0.10	0.00	0.12	nd	nd	nd	0.00	0.00	0.00	0.03	0.06	0.05	0.08	0.06	
Al_2O_3	0.10	nd	0.07	0.04	0.01	0.20	0.01	0.19	0.02	0.06	nd	nd	0.02	0.01	0.02	0.16	0.02	0.01	0.02	0.47	0.29	
TiO_2	47.66	49.34	19.78	31.61	49.80	18.75	49.72	0.54	48.16	19.65	48.15	48.55	17.73	30.06	46.71	0.23	48.46	18.68	50.70	0.15	20.37	
Cr_2O_3	0.04	0.01	0.02	0.01	0.56	0.80	0.66	0.64	0.53	0.46	0.02	0.01	0.15	0.10	1.03	2.41	0.06	0.09	0.00	0.42	0.25	
V_2O_3	0.43	0.34	0.77	0.60	0.037	0.30	0.00	0.09	0.00	0.05	0.37	0.34	0.81	0.62	0.12	0.501	0.58	1.00	0.53	1.14	0.09	
Fe_2O_3[†]	9.52	6.16	29.23	20.00	5.25	31.12	5.14	66.26	7.30	30.87	7.96	6.29	31.94	21.68	10.56	64.63	7.01	31.41	3.66	65.81	40.95	
FeO[†]	41.15	43.15	48.95	46.63	43.95	48.41	42.89	31.54	41.52	48.93	42.11	42.49	46.49	44.89	41.76	31.66	42.96	48.06	44.29	31.19	36.43	
MnO	0.28	0.25	0.09	0.15	0.16	0.06	0.41	0.00	0.44	0.42	0.38	0.43	0.12	0.25	0.05	0.00	0.54	0.44	1.24	nd	0.49	
MgO	0.83	0.55	0.10	0.28	0.36	0.07	0.77	0.07	0.66	0.25	0.46	0.41	0.81	0.65	0.11	0.00	0.07	0.00	0.07	0.03	0.05	
Total	100.05	99.80	99.03	99.33	100.13	99.72	99.59	99.42	98.63	100.81	99.45	98.54	97.34	98.25	100.35	99.69	99.72	99.84	100.55	99.27	99.78	
cation[*]	2	2	3	3	2	3	2	3	2	3	2	2	3	3	2	3	3	3	2	3	3	3
Si	0.001	0.000	0.001	0.001	0.000	0.000	0.000	0.004	0.000	0.004	0.000	0.000	0.000	0.000	0.000	0.001	0.002	0.001	0.003	0.002		
Al	0.003	0.000	0.003	0.002	0.000	0.009	0.001	0.009	0.000	0.003	0.000	0.000	0.001	0.000	0.011	0.007	0.001	0.005	0.001	0.021	0.013	
Ti	0.902	0.938	0.567	0.904	0.941	0.531	0.941	0.016	0.922	0.550	0.920	0.936	0.517	0.866	0.882	0.007	0.925	0.531	0.959	0.004	0.585	
Cr	0.001	0.000	0.001	0.001	0.018	0.038	0.021	0.000	0.017	0.022	0.001	0.001	0.008	0.005	0.033	0.117	0.002	0.004	0.000	0.021	0.012	
V	0.009	0.007	0.023	0.018	0.001	0.009	0.000	0.004	0.000	0.001	0.008	0.007	0.025	0.019	0.002	0.018	0.012	0.030	0.011	0.035	0.027	
Fe^{3+}	0.180	0.117	0.838	0.572	0.099	0.882	0.097	1.918	0.140	0.865	0.152	0.121	0.932	0.625	0.200	1.845	0.134	0.894	0.069	1.909	1.177	
Fe^{2+}	0.866	0.912	1.559	1.482	0.923	1.524	0.902	1.015	0.884	1.524	0.894	0.910	1.508	1.439	0.877	1.005	0.912	1.519	0.931	1.005	1.164	
Mn	0.006	0.005	0.003	0.005	0.003	0.002	0.009	0.032	0.010	0.013	0.008	0.009	0.004	0.008	0.001	0.000	0.012	0.014	0.026	0.000	0.016	
Mg	0.031	0.021	0.006	0.016	0.014	0.004	0.029	0.003	0.025	0.014	0.017	0.016	0.005	0.037	0.004	0.000	0.003	0.000	0.003	0.002	0.003	
X_{ilm}	0.907	0.940			0.949		0.950		0.928		0.923	0.938			0.898			0.932			0.965	
X_{usp}			0.581	0.763		0.561		0.016	0.563				0.533	0.750		0.008	0.552		0.005	0.506		

Inti-mt: reconstructed magnetite composition including exsolved ilmenite. Ex-mt: exsolved part of magnetite. Ex-ilm: exsolved ilmenite in magnetite. Inti-ilm: ilmenite with initial composition
[†] FeO and Fe_2O_3 were calculated from stoichiometry
[*] ilmenite and magnetite formulae were normalized to 2 and 3 cations, respectively.

Table 5-9. Results from thermobarometry in the garnet reaction between center and edge

Sample No.		ref P[†]	T(K)	T(EG)	T(A)	T(PN)	T(G)	ref T[††]	$P(M_{Fe})$	$P(M_{Mg})$	P(E)	P(PN)
				Grt-Cpx					Grt-Cpx-Pl-Qtz			
Vein-related type												
D8	center	800	701	760	641	618	799	750	1102	912	865	824
	edge	800	731	784	672	657	818	750	1065	950	894	853
Garnet granulite type												
PL2	center	1000	787	814	720	737	797	750	1229	1125	1035	995
	edge	1000	748	806	710	735	837	750	814	720	737	779

Temperature in °C, Pressure in MPa. Garnet-clinopyroxene geothermometer from T(K): Krogh (1988); T(EG): Ellis & Green (1979); T(A): Ai (1994); T(PN): Pattison & Newton (1988); T(G): Ganguly et al. (1996). Garnet-clinopyroxene-plagioclase-quartz geobarometer from P(M): Moecher et al. (1988); P(E): Eckert et al. (1991) and P(PN): Perkins & Newton (1981). Fe and Mg gives the results for the Fe- and Mg-endmember reactions modeled by Moecher et al. (1988).

[†]Reference pressure to calculate temperature. [††]Reference temperature to calculate pressure.
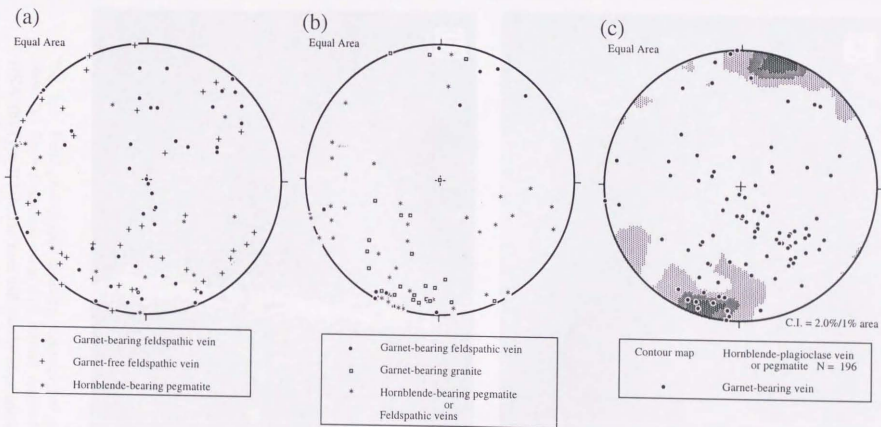
Fig. 5-1. Equal-area lower hemisphere stereographic projections of pole to the fractured plane of the various type of veins in the Kamila amphibolite belt. (d) Regional variations from Pattan to Kiru; (e) from Kiru to Dasu; (f) from Dasu to Lutar.

Fig. 5-2. Field photographs showing occurrence of garnet reaction zone. (a) Type I reaction zone with diffuse reaction front in the NKA. (b) Type II reaction zone with patchy idiomophic garnet at the margin of the leucocratic vein in the NKA.

124
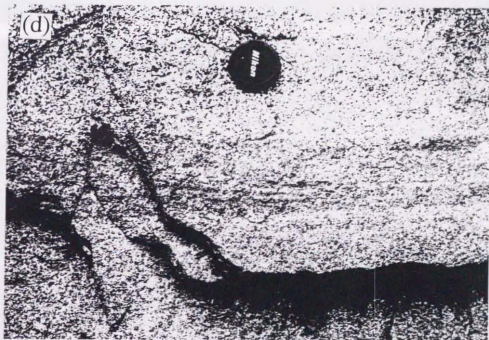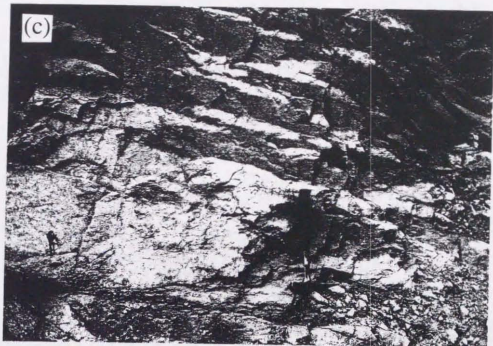
Fig. 5-2. (continued). Field photographs showing occurrence of garnet reaction zone. (c) Type III reaction zone occurring unrelated to the quartzo-feldspathic vein in the SKA. Light coloured area is garnet reaction zone and dark area corresponds to the pyroxene granulites. (d) Well-preserved igneous banding in the garnet granulite of the Jijal complex. Note that the garnet reaction zone is not affected by the compositional banding.
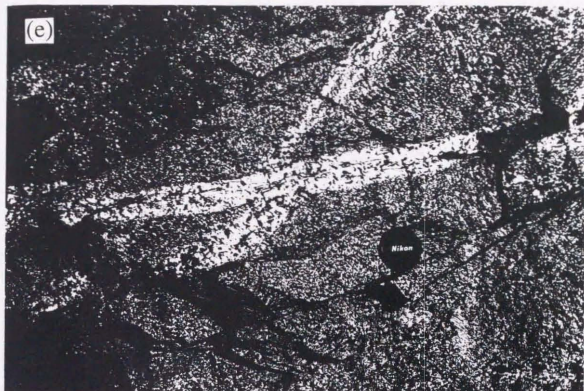
Fig. 5-2. (continued.) Field photographs showing occurrence of inter-realtionships among various types of reaction zone. (e) Quartzo-feldspathic vein with amphibole reaction zone cut quartzo-feldspathic vein with type II garnet reaction zone. (f) Field phtograph showing occurrence of scapolite-amphibole reaction zone related to the quartzo-feldspathic vein. Coarse-grained dark domain consists of hornblende and scapolite.

126
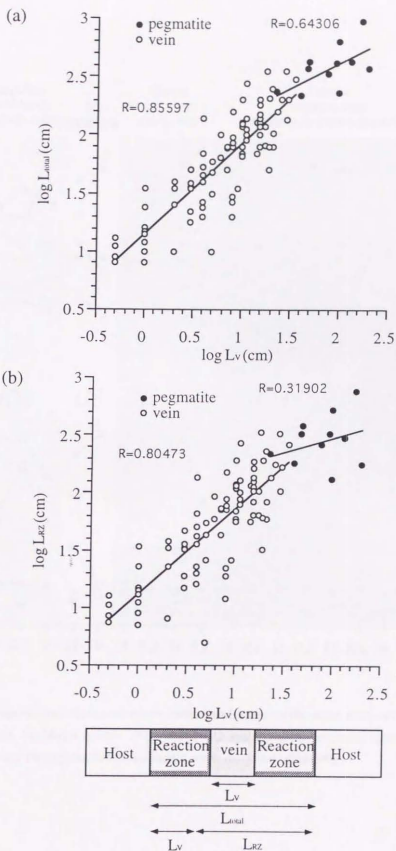
Fig. 5-3. Geometrical relationship between the amphibole reaction zone and the quartzo-feldspathic vein. (a) Log total width of reaction zone including vein vs. log width of vein. (b) Log total width of reaction zone vs. log width of vein. Note that linear correlation between them except for the pegmatite pair.
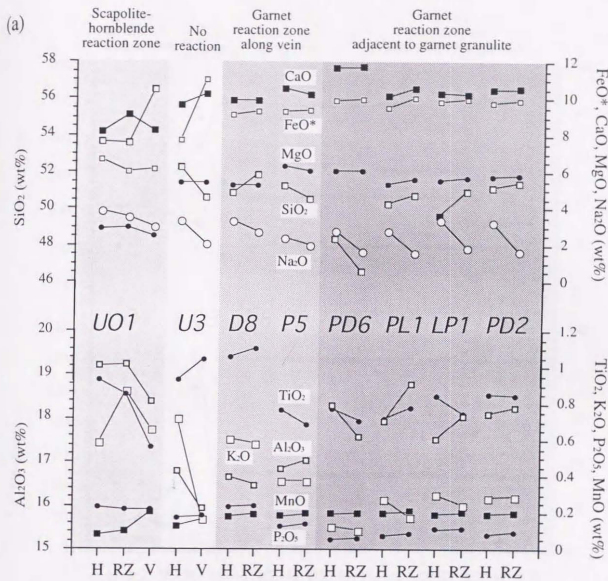
Fig. 5-4. Compositional change of whole rock chemistry from the close pairs of several types of reaction zone. (a) Major oxides. Note that Na₂O systematically decrease toward the vein, whereas K₂O vary throughout the metasomatic zone. (b) Minor elements.

Fig. 5-4. (continued)

129
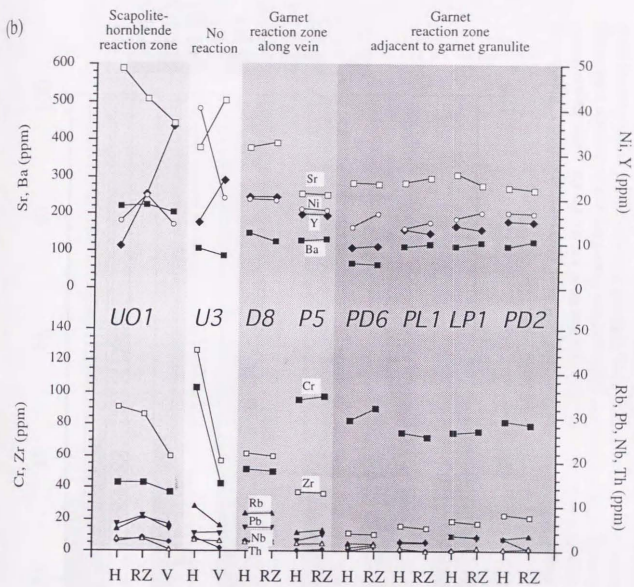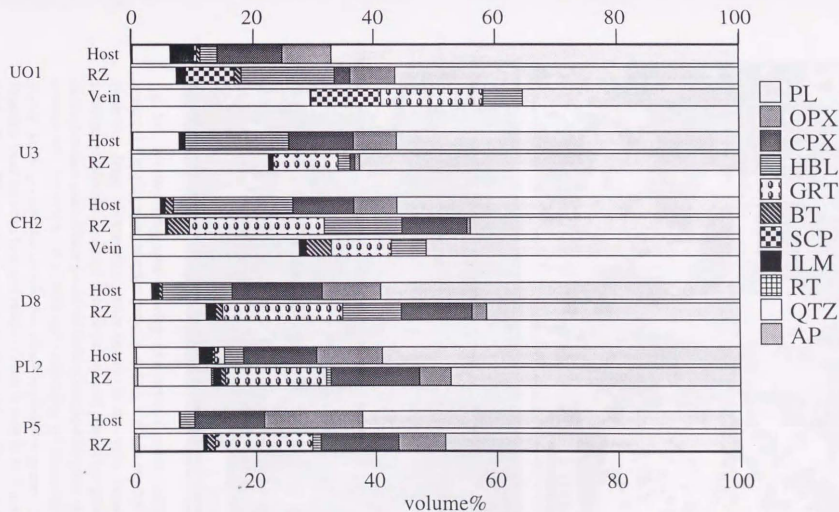
Fig. 5-5. Modal compositional change between the reaction zone and host pyroxene granulite. Plagioclase, orthopyroxene and clinopyroxene decrease toward the vein or the reaction zone except for the scapolite-amphibole reaction zone (UO1), whereas modal composition of garnet and quartz increase toward the vein or reaction zone in any case. UO1; scapolite-amphibole reaction zone, U3; no reaction zone, CH2 and D8; vein-related garnet reaction zone, PL2 and P5; garnet granulite type reaction zone. In the case of D8, reaction zone is not distinguished from vein.
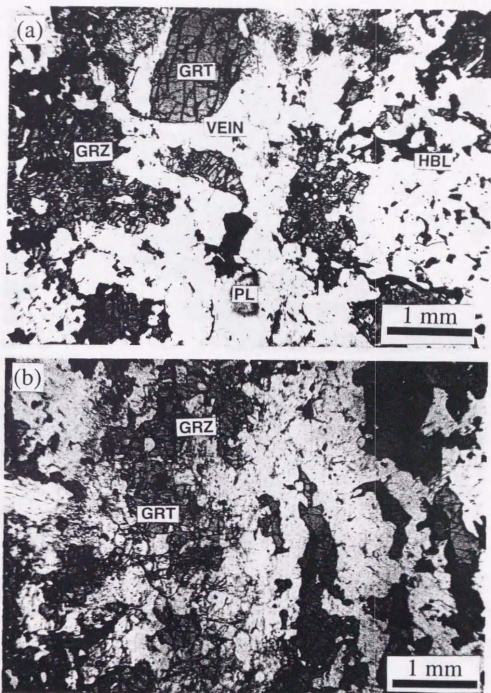
Fig. 5-6. Micro-photographs showing occurrence of garnet reaction zone. (a) Type I garnet reaction zone in sample CH2 in the NKA. Note that large idiomorphic garnet occurs in the vein. Brown-coloured hornblende develops at triple junction of plagioclase grains in the reaction zone. Plane polarized light. Quartzo-feldapthic vein corresponds the center of photograph, consisting of idiomorphic garnet, large plagioclase grains and relict hornblende grains. (b) Reaction front between host and reaction zone in sample PL2 in the SKA. Type III garnet reaction zone unrelated to the quartzo-feldspathic vein. Plane polarized light.
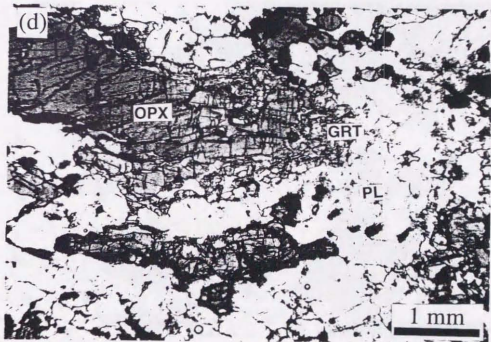
Fig. 5-6. (continued). (c) Typical reaction texture in the garnet reaction zone in sample PL2, plane polarized light. Orthopyroxene grains rimmed by garnet, clinopyroxene and quartz symplectite. (d) Orthopyroxene grain located between the host and the type II garnet reaction zone in sample P5, plane polarized light. Large orthopyroxene grain is enclosed by garnet-quartz symplectite at only right side. Right hand side corresponds to center of the reaction zone.
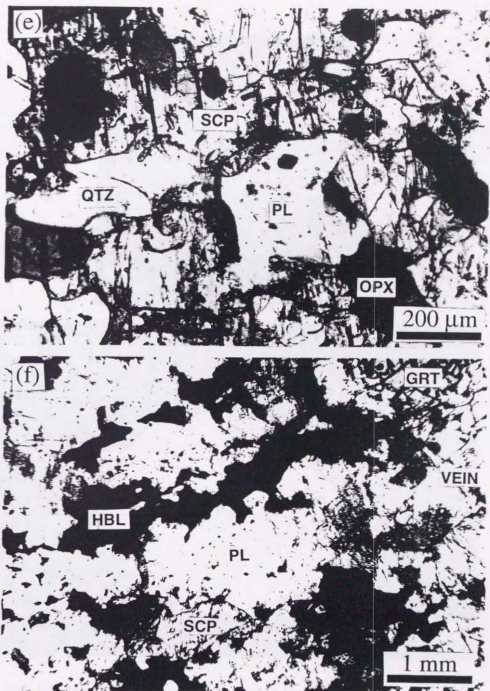
Fig. 5-6. (continued.) Micro-photographs showing occurrence of scapolite-amphibole reaction zone. (e) Scapolite coexisting with orthopyroxene, plagioclase and quartz in the reaction zone in sample UO1, plane polarized light. Width of field of view is 1 mm. (f) Hornblende occurring vertical to the vein along the grain boundaries of plagioclase in sample UO1, plane polarized light. Width of field of view is 5 mm.
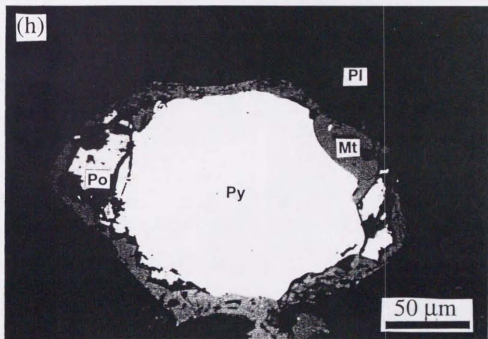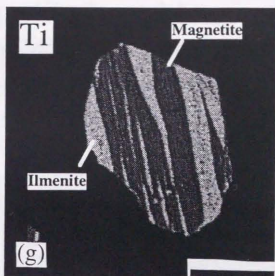
Fig. 5-6. (continued). (g) Element image map of typical hematite-rich hemo-ilmenite grain that shows extensive primary and second generation hematite exsolution lamellae in the sacpolite-amphibole reaction zone. Dark regions are hematite. Light regions are ilmenite. Bar is 100 μm. (h) Microphotograph of a remaining relict pyrrhotite (Po) and pyrite (py) grain in sample BR6 with a reaction rim of magnetite (Mt) and accessory chalcopyrite (Cp).

UO1 Scapolite-hornblende reaction zone
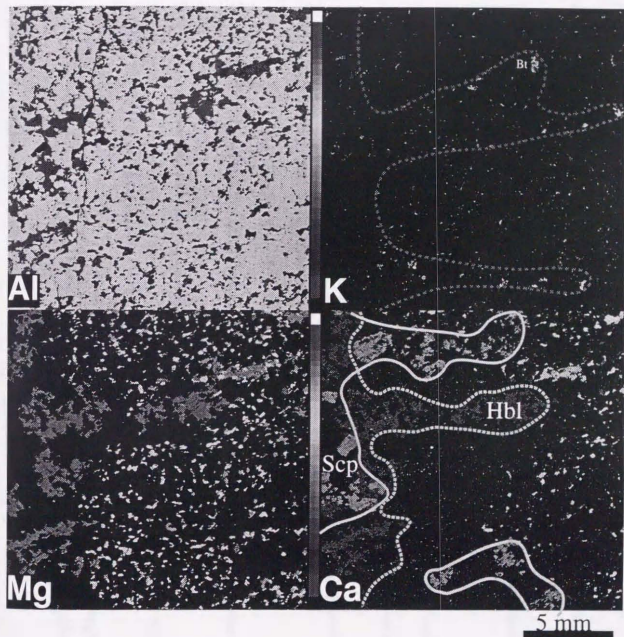
Fig. 5-7. Compositional map of the scapolite-amphibole reaction zone. Left edge of the map is equivalent to a boundary between the reaction zone and the garnet-bearing quartzo-feldspathic vein. Note that the amphibole distribution from a elemental map of Mg and the scapolite distribution from a elemental map of Ca. Amphibole distribution is characterized by connective ocuurrence along the plagioclase grain boundaries, whereas scapolite distribution is isolated in the reaction zone.
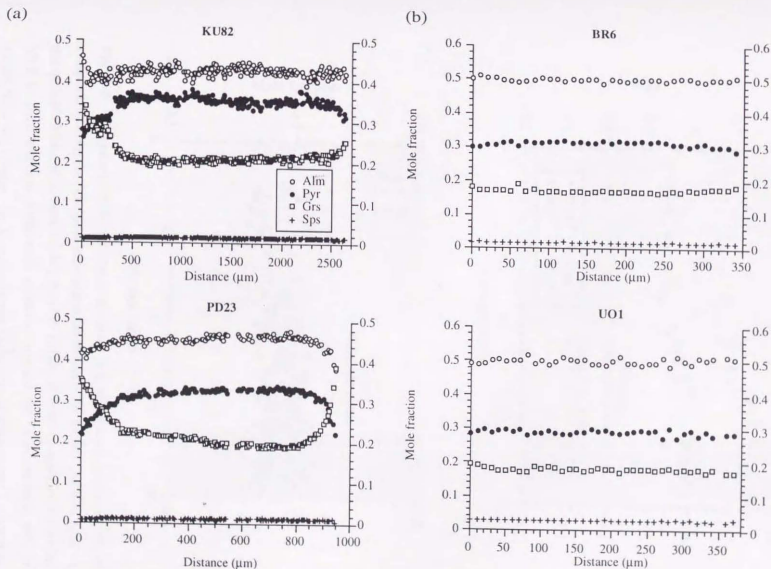
Fig. 5-8. Compositional zoning profiles of garnet from the Kohistan granulite. (a) Garnet from the garnet granulite in the Jijal complex. (b) Garnet in the reaction zone from the relict pyroxene granulites in the Kamila amphibolite belt. Garnet is obtained in the quartzo-feldspathic vein adjacent to the scapolite-amphibole reaction zone from Sample No. UO1.
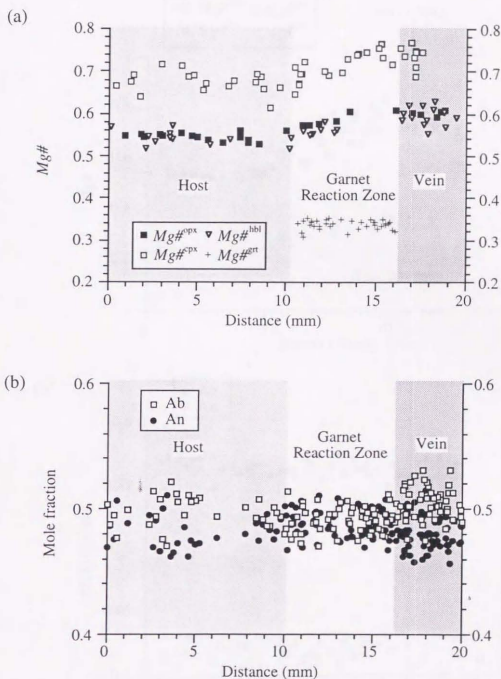
Fig. 5-9. Compositional variations of minerals in type I garnet reaction zone in sample D8, from the host pyroxene granulite through the garnet reaction zone to the quartzo-feldspathic vein. (a) Mg number (Mg#) in ferro-magnesian minerals. Mg# in pyroxene and hornblende increases toward the vein, whereas that in garnet does not change. (b) Compositional variations of plagioclase. Anorthite content in plagioclase within the vein shows slightly lower value than that within the host and the reaction zone.

137
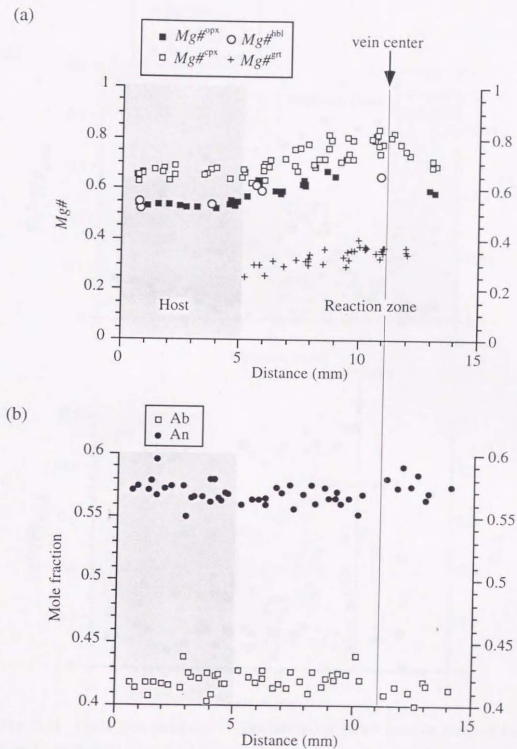
Fig. 5-10. Compositional variations of minerals in type III reaction zone in sample PL2 in the SKA, from the host pyroxene granulite to the center of the garnet reaction zone. (a) Mg number (Mg#) in ferro-magnesian minerals. Mg# in all minerals including garnet increases toward center of the reaction zone. (b) Compositional variations of plagioclase. Anorthite content in plagioclase does not vary throughout the garnet reaction zone.
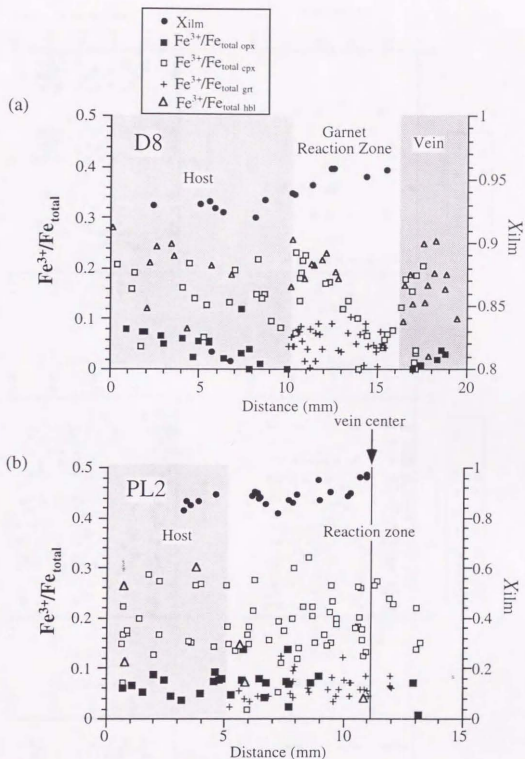
Fig. 5-11. Ferric iron variations of minerals in the garnet reaction zones of the type I and type III. (a) Type I garnet reaction zone in sample D8 in the NKA. The ratio of ferric iron to total iron of pyroxene and hornblende decreases toward the vein, whereas that of garnet does not change. (b) Type III garnet reaction zone in sample PL2 in the SKA. The ratio of ferric iron to total iron of all minerals does not change. In both of the cases, ilmenite component in hematite-ilmenite solid solution increases toward the vein or center of the reaction zone.
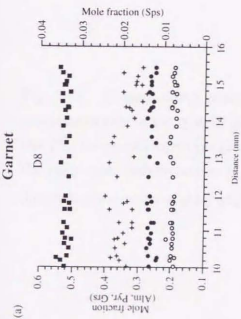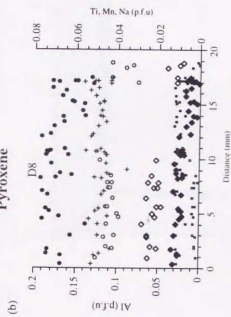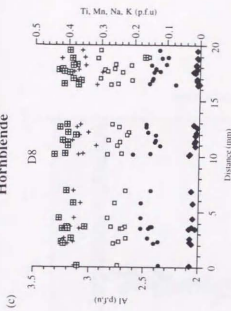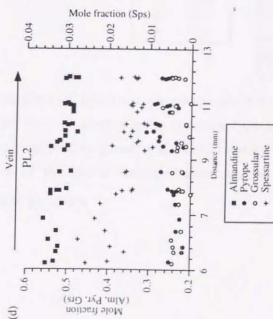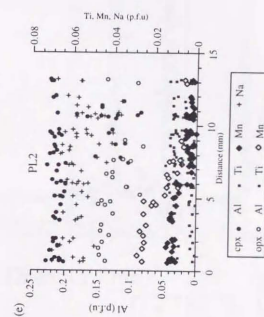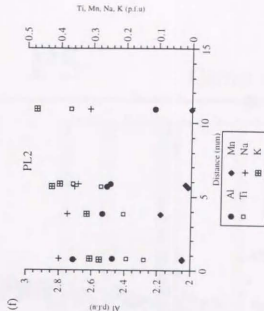
Fig. 5-12. Compositional variation of minerals across the garnet reaction zone of type I (a-c) and type III (d-f). The value of distance showing the location vertical to elongation of the vein is equivalent to those in Figure 5-9 to 5-11. (a) Compositional variation of garnet solid solution in the reaction zone from type I. (b) Minor cation variation in pyroxene from type I. (c) Minor cation variation in hornblende from type I. (d) Compositional variation of garnet solid solution in the reaction zone from type III. (e) Minor cation variation in pyroxene from type III. (f) Minor cation variation in hornblende from Type III.
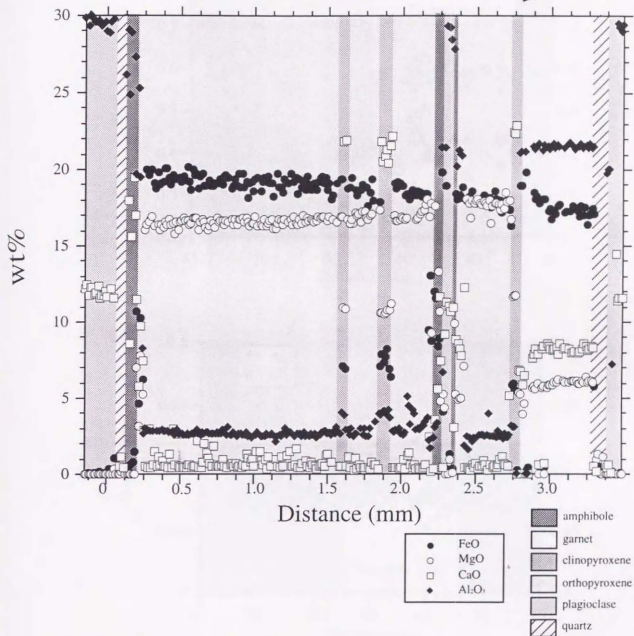
Fig. 5-13. Compositional zoning profiles of pyroxene pseudomorphed by garnet and quartz aggregate in the type III garnet reaction zone. Garnet granulite type from Sample No. P5. Large orthopyroxene grain is replaced by garnet and quartz on only left side. On the right side, orthopyroxene is out of the garnet reaction zone. Arrows indicates a direction of the center of the garnet reaction zone.
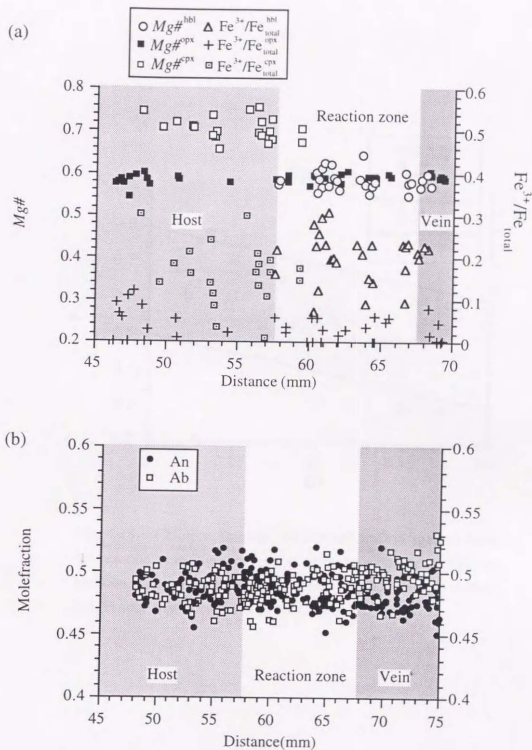
Fig. 5-14. Compositional variations of minerals in a scapolite-amphibole reaction zone from the host pyroxene granulite to the garnet-bearing quartzo-feldspathic vein. (a) Mg# and Fe^{3+}/Fe_{total} variations in two pyroxenes and hornblende. (b) Compositional variations of plagioclase.
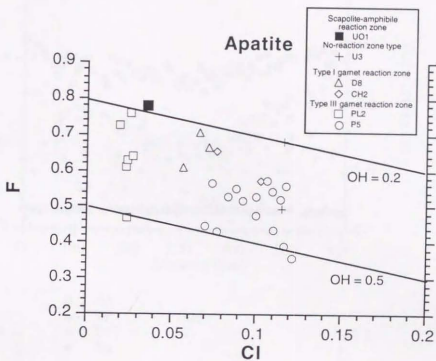
Fig. 5-15. Chlorine, fluorine and inferred H_2O in apatites from the reaction zone. Note that apatite from the scapolite-amphibole reaction zone is F-rich and contains significant amount of sulfate ion. F-poor apatite contains larger Cl- and OH-contents.
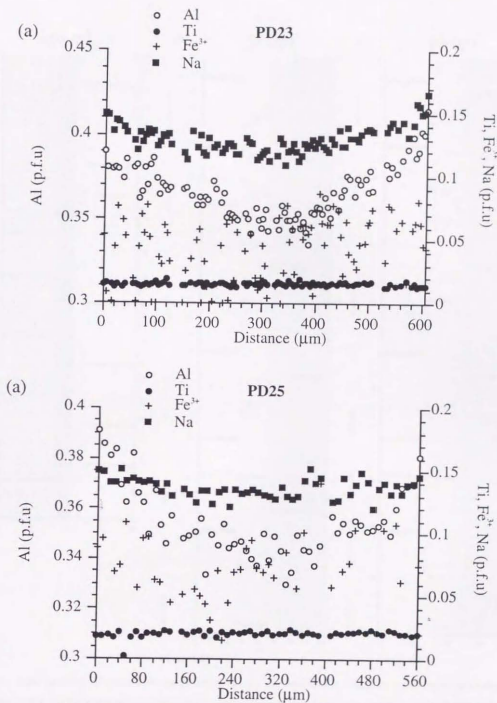
Fig. 5-16. Compositional zoning profiles (Al, Na, Ti &Fe^{3+}) of clinopyroxene from the garnet granulite in the Jijal complex. (a) Zoned garnet in the scapolite-bearing garnet granulite. (b) Zoned garnet in the scapolite-free garnet granulite. Al and Na contents increase toward the margin in similar to that from the SKA.
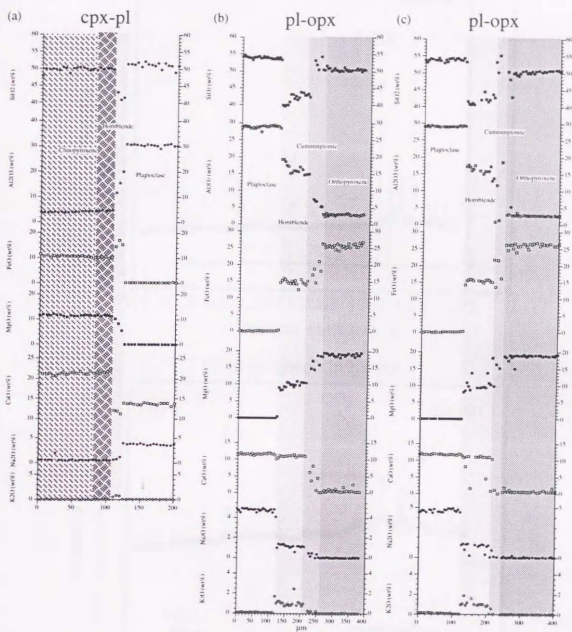
Fig. 5-17. Line profiles of chemical composition across the amphibole reaction zone from pyroxene grain to plagioclase grain. (a) Compositional variation of clinopyroxene to plagioclase. (b) & (c) Compositional variations of orthopyroxene to plagioclase. Crossed line: clinopyroxene; dark shaded area: orthopyroxene, semi-dark shaded area: cummingtonite, light shaded area: hornblende, hatched area: actinolite; no shaded area: plagioclase.
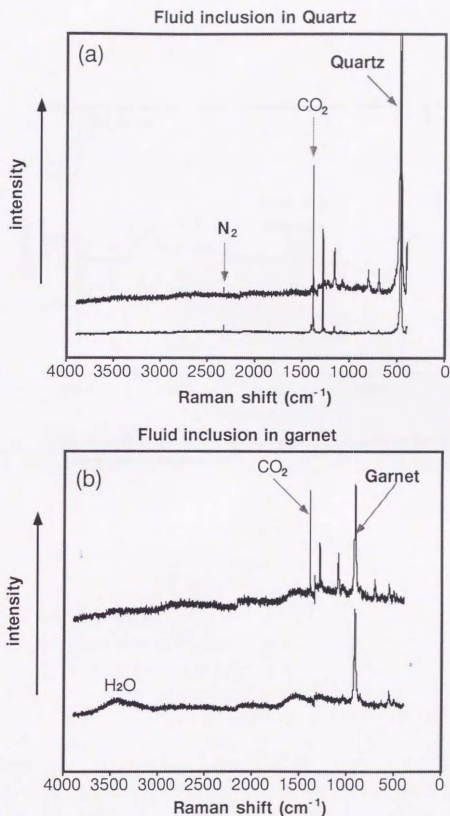
Fig. 5-18. Raman spector analysis of fluid inclusions in type I garnet reaction zone in smple D8 in the NKA. (a) Fluid inclusion in quartz within the quartzo-feldspathic vein. Strong intensity of Raman shift at 1388 cm-1 suggesting presence of CO_2-rich fluid and at 2333 cm-1 suggesting existence of N_2 fluid. (b) Fluid inclusions in garnet within the garnet reaction zone. Same garnet grain contains two types of fluid inclusions; one has broad peak of around 3000 cm-1 indicating H_2O-rich fluid and the other has sharp peak at 1388 cm-1 suggesting presence of CO_2-rich fluid inclusion.
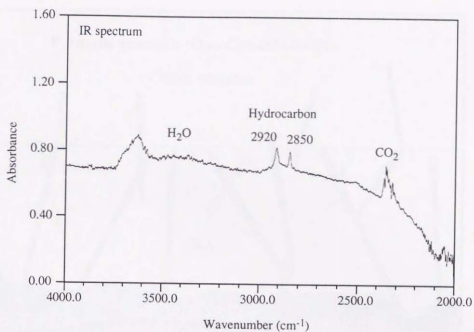
Fig. 5-19. FT-IR specrtrum of fluid inclusions in quartz within the garnet-bearing quartzo-feldspathic vein.
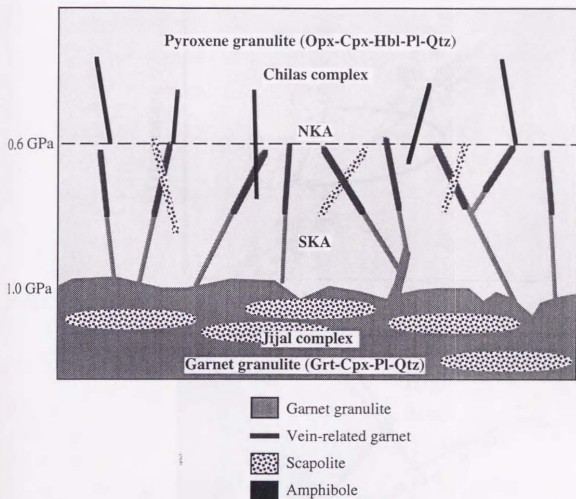
Fig. 5-20. Schematic column of the lower crust of the Kohistan arc, showing developed area of reaction zone and vein distribution caused by fluid infiltration. Homogeneous developed garnet area above nearly 1.0 GPa corresponds to the garnet granulite in the Jijal complex. Large amount of scapolite locally occurs in the Jijal garnet granulite. Distribution of garnet and scapolite is localized in the pyroxene granulites. In the SKA, the garnet reaction zone develops as a vein-like occurrence without the quartzo-feldspathic vein, whereas in the NKA, garnet occurs along the quartzo-feldspathic vein. From the northern part of the NKA to the Chilas complex, garnet and scapolite disappear and amphibole reaction zone developes along the quartzo-feldspathic vein or pegmatites, at the lower pressure condition, presumably less than 0.6 GPa.
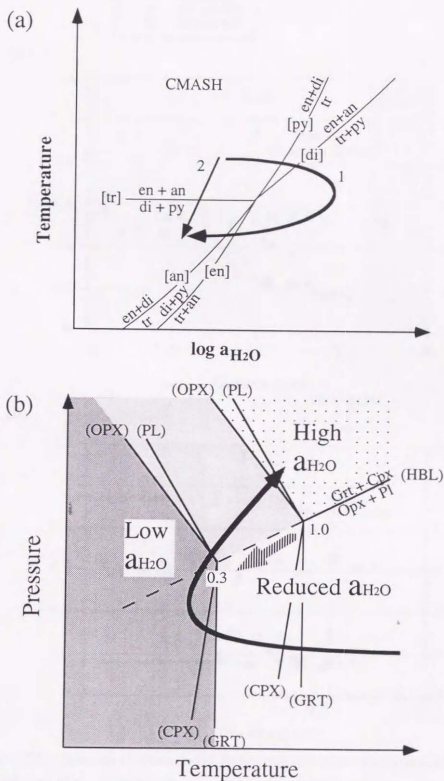
Fig. 5-21. (a) Schematic isobaric T-log aH₂O diagram showing the two stage reaction or one stage reaction sequence in the garnet reaction zone. Arrow 1 indicates that initial hydration accompanied infiltration of high water activity fluid; subsequent dehydration is related to lowering water activity fluid. Arrow 2 representing the direct garnet forming reaction unrelated to fluid infiltration. (b) Pressure-temperature diagram showing phase relations in part of the model garnet granulite closed system proposed by Bradshaw (1989b). Shift of dehydration reaction to lower T is modeled by a decrease in XH₂O from 1.0 to 0.3.
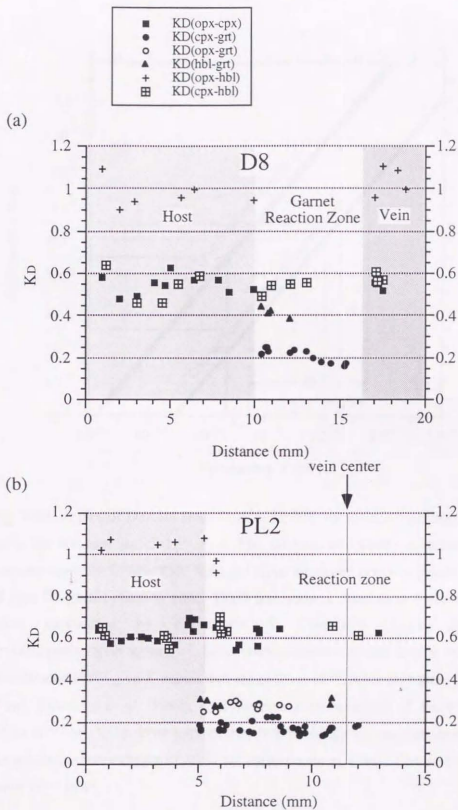
Fig. 5-22. Variation diagram in the garnet reaction zone, showing distribution coefficient (KD) of Fe/Mg among all minerals including large amount of Fe and Mg. (a) Vein-related type. Distribution coefficient is almost similar value across the reaction zone except for that between garnet and other minerals. (b) Garnet granulite type. Distribution coefficient between each minerals is almost similar value across the reaction zone.
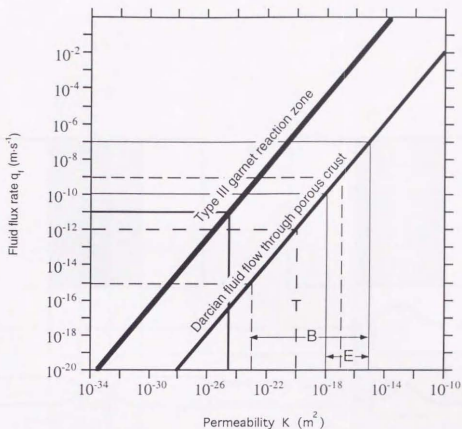
Fig. 5-23. A plot of Darcian fluid-flux, q_f (m·s^{-1}), versus permeability, K (m^2), for constant μ=1.5×10^{-4} Pa·s. The thickest line shows a relation between them for $\partial P/\partial x$=3000 MPa·m^{-1} from estimated pressure gradient of type III garnet reaction zone. Thick line show a relation at a porous crust calculated by Thompson & Connolly (1992) for $\partial P/\partial x=\Delta\rho g$=1.9×10^4 kg·m^{-2}·s^{-2}. Laboratory experiments and in-situ well tests Brace (1980) give K values that range from 10^{-17} m^2 to less than 10^{-23} m^2. Etheridge *et al.* (1984), consider crustal permeability of K=10^{-15} m^2 to 10^{-18} m^2, to be more appropriate. In type III garnet reaction zone, the reference permeability of 10^{-25} m^2 corresponds to a fluid-flux rate of about 10^{-11} m·s^{-1}.
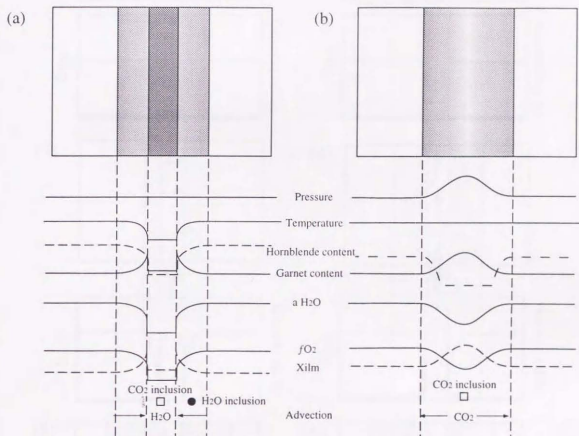
Fig. 5-24. Variations of predicted parameter cross the garnet reaction zone. (a) Type I garnet reaction zone. Estimated pressure and temperature is generally lower at the boundary between the reaction zone and the vein. Modal composition of garnet increases with decreasing that of hornblende and orthopyroxene. Fe-Ti oxides, especially ilmenite show lower values of hematite component near the vein. Fluid inclusion in quartz in the vein is CO_2-rich, whereas that in garnet in the reaction zone is generally characterized by aqueous inclusion. Water migrates into the vein due to difference of water pressure and low water activity fluid does not penetrate into the reaction zone. (b) Type III garnet reaction zone. Estimated pressure shows remarkably higher value at center of the reaction zone, whereas estimated temperature is almost the same condition throughout the reaction zone. Modal composition of garnet increases with decreasing that of hornblende and orthopyroxene. Fe-Ti oxides, especially ilmenite show lower values of hematite component near the vein. Fluid inclusion in quartz and garnet in the reaction zone is CO_2-rich. Fluid transportation into the reaction zone is driven by high fluid pressure compared with surrounding lithostatic pressure. The fluid has low water activity, presumably CO_2-rich.
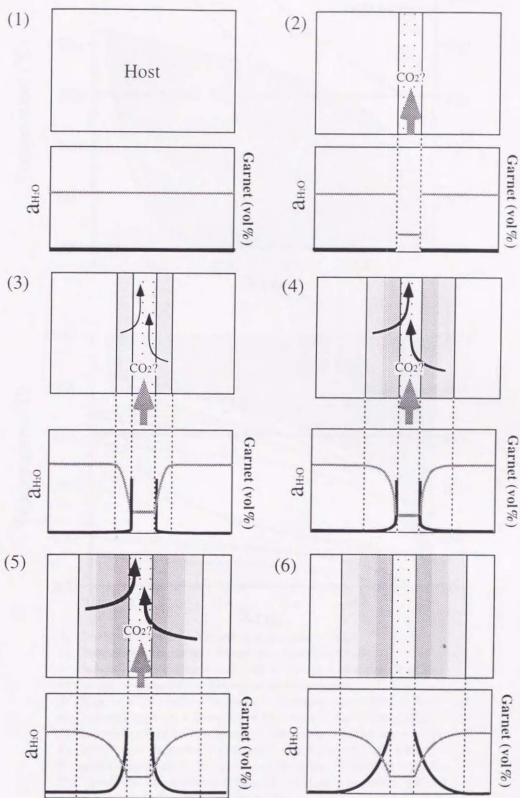
Fig. 5-24. (continued). (c) Formation model of type I garnet reaction zone. Change of garnet modal composition represents water activity gradient from the host rock to the vein. Water migration to the vein is caused by pressure gradient and accompanies with hornblende breakdown and garnet formation. Thick lines indaicate gradient of water activity and solid thick lines represent gradation of modal composition of garnet in the garnet reaction zone.
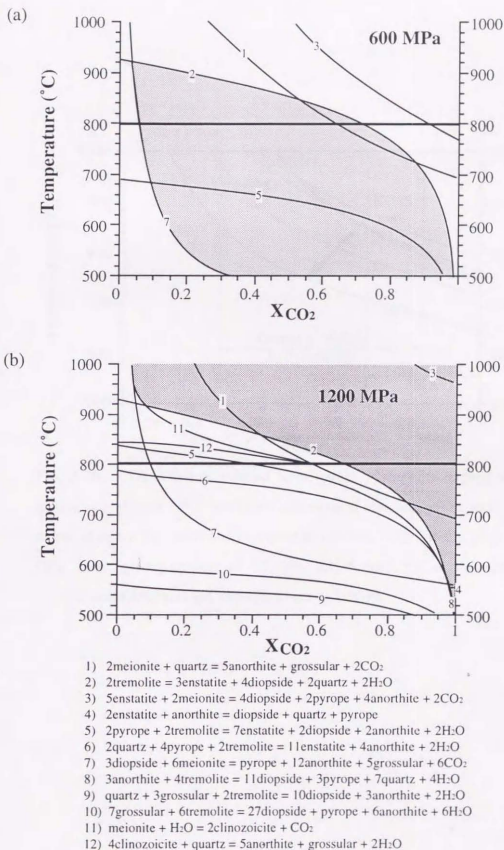
(a)

(b)

1) 2meionite + quartz = 5anorthite + grossular + $2CO_2$
2) 2tremolite = 3enstatite + 4diopside + 2quartz + $2H_2O$
3) 5enstatite + 2meionite = 4diopside + 2pyrope + 4anorthite + $2CO_2$
4) 2enstatite + anorthite = diopside + quartz + pyrope
5) 2pyrope + 2tremolite = 7enstatite + 2diopside + 2anorthite + $2H_2O$
6) 2quartz + 4pyrope + 2tremolite = 11enstatite + 4anorthite + $2H_2O$
7) 3diopside + 6meionite = pyrope + 12anorthite + 5grossular + $6CO_2$
8) 3anorthite + 4tremolite = 11diopside + 3pyrope + 7quartz + $4H_2O$
9) quartz + 3grossular + 2tremolite = 10diopside + 3anorthite + $2H_2O$
10) 7grossular + 6tremolite = 27diopside + pyrope + 6anorthite + $6H_2O$
11) meionite + H_2O = 2clinozoisite + CO_2
12) 4clinozoisite + quartz = 5anorthite + grossular + $2H_2O$

Fig. 5-25. *T-X* CO_2 section calculated at 600 MPa (a) and 1200 MPa (b) for difinitive mineral reactions above described in the scapolite-amphibole reaction zone and in the garnet granulite. Schematic phase relations of CaO-MgO-Al_2O_3-SiO_2 system are calculated from the updated Holland & Powell (1990) data set. Shaded area shows the limited *X* CO_2 stability range of tremolite and meionite assemblage at the given *P-T* conditions.

154
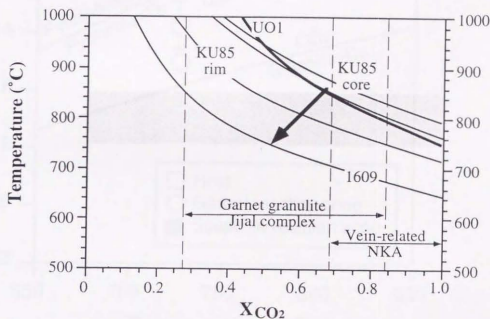
Fig. 5-26. CO₂ activities inferred from garnet + scapolite + plagioclase + quartz assemblages. *P-T* conditions and mineral assemblages of each sample to calculate the CO₂ activities represent as follows; UO1: grt-scp-pl-qtz at 0.6 GPa, 1609: grt-scp-cpx-qtz at 1.2 GPa, KU85 core: grt -scp-cpx-pl-qtz at 1.2GPa, and KU85 rim: grt -scp-cpx-pl-qtz at 1.5GPa.
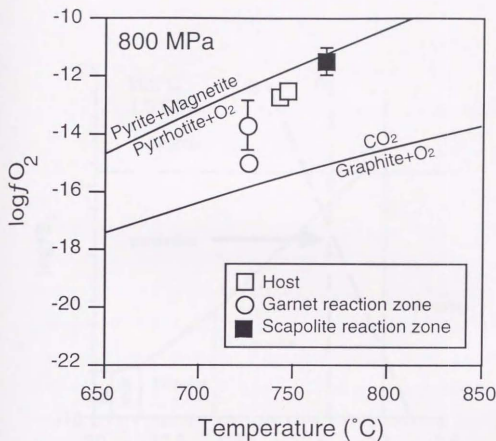
Fig. 5-27. Oxygen fugacity-temperature pairs at 800 MPa from the NKA calculated from the assemblage clinopyroxene-orthopyroxene-ilmenite-quartz using the QUIlF program of Andersen *et al.* (1993). Oxygen fugacity from scapolite-amphibole reaction zone is consitent with pyrite-pyrrhotite-magnetite assemblage of surrounding pyroxene granulites. Oxygen fugacities from garnet reaction zone show slightly lower values than that from other pairs.
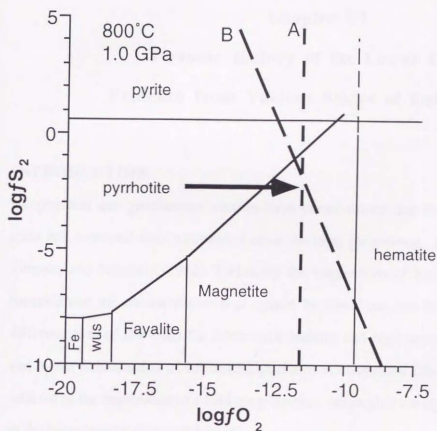
Fig. 5-28. Fe-Si-O-H-S system at 1.0 GPa and 800 °C. Drawn from data of Shi (1992). A. fSO_3 defined by the composition of scapolite from the NKA. B. fO_2 calculated from the assemblage of clinopyroxene-orthopyroxene-hematite-quartz assemblage using QUIIF program of Andersen et al. (1993).

Chapter VI

Tectonic History of the Lower Crust:
Evidence from Various Stages of Deformation

INTRODUCTION

Geophysical and geochemical studies have demonstrated that the extent of continental crust has increased and/or expanded since Archean (Armstrong, 1981, De Paolo, 1983, Turcotte and Schubert, 1982). Following the suggestions of Kay and Kay (1988), the formation of the continental crust is caused by island arc and hot spot volcanisms, by differentiation of the crust for intracrustal melting and high temperature metamorphism and by the delamination of substantial quantities of continental lithosphere. Taylor (1977) referred to the importance of island arc processes, although a variety of processes can lead to the formation of continental crust.

Existence of sandwiched island arcs among the continental crust have been reported at many collisional terrains all over the world, *e.g.* in the Proterozoic Narsajuaq arc, northern Quebec, Canada (Lucas *et al.*, 1992), in the Paleozoic Qinling belt in central China (You *et al.*, 1993), in the Tertiary Peninsular terrane, Alaska (De Bari & Coleman, 1989), and in the Tertiary Hidaka arc in Japan (Toyoshima *et al.*, 1993). Thus, the accretion and the collision of the island arc against the continent played important roles with aspect to an evolution of continental crust. The sandwiched island arcs should be record the several deformation events accompanying with the evolution of the lower crust during accretion and collision. The Kohistan arc is a tilted lower crustal section of a Middle Cretaceous island arc (Tahirkheli *et al.*, 1979, Bard, 1983, Coward *et al.*, 1982, 1986) (Fig. 1-1), and provide significant information to understand the formation of the young island arc at the same situation as Kohistan arc such as the Peninsular terrane,

Alaska and the Hidaka metamorphic belt, Japan in the Tertiary.

Treloar *et al.* (1990) argued that the shear zone in the lower crust of the Kohistan arc can be classified into two different origins: high temperature ductile shear zone depending on crustal thickening and low temperature deformation during exhumation and cooling. However, their conclusion is still insufficient to describe this regional complicated deformation structure, because these structures can be observed as at least five foliated structures by observation of the shear zones such as mineral assemblage, shear sense, *P-T* conditions, and microstructure. High grade deformation, furthermore were subdivided into three types of foliation based on the difference of mineral assemblage forming the foliations and of concentration of pole of foliation. Low temperature deformations are classified into two types based on the difference of orientation of pole to foliation and of kinematic direction. Distributions, magnitudes and microstructures of shear zones or deformation structures within exposed metabasic rocks, especially in the KAB are first described. It is revealed that deformation structures are developed under different metamorphic conditions and tectonic events in the KAB. A tectonic model involving crustal thickening and thinning process is presented.

FOLIATED STRUCTURES

Rocks of the lower crust in the Kohistan arc have been overprinted by various deformation structures. In the KAB, the foliated structures of high grade rocks were subdivided into three phases as follows; (i) pyroxene-bearing penetratively gneissose foliation with subvertical dipping (S1), (ii) hornblende-bearing localized foliation with subhorizontal dipping (S2) and (iii) gneissose foliation with subvertical dipping (S3). In addition, low temperature localized shear zones were classified into two phases by the shear sense and nature as follows; (iv) subhorizontal top-to-the-S sense shear zone (S4) and (v) conjugate set shear zone with subvertical dipping (S5). Table 6-1 summarizes the features of each foliated structure. Figure 6-1 shows the distribution of the each type of

shear zone in the KAB. Distributed pattern about the pole to foliation or shear plane including five types of the shear zone, regionally change northward from NW (Pattan to Kiru) through N (Kiru to Dasu) to S (Dasu to Lutar) (Fig. 6-2). To understand the tectonic history in the lower crust of the Kohistan arc, inter-relationships of these deformation structures will be described in following section.

High grade deformation structures

Homogeneous High-Grade Gneissose Foliation (S1)

Rocks with the highest-grade foliations (S1) are only pyroxene granulite pods in the KAB. S1 is characterized by homogeneous gneissose texture, and it ranges from 10 m to over hundreds of meter as an individual shear zone in the NKA (see Fig. 6-1). Mineral and stretching lineations are not clearly observed; the shape of recrystallized plagioclase aggregates does not represent prolate type (stretching lineation) but flattening shape. Furthermore, the uncertainty of their fabric curvature and drag folds of the feldspathic vein prevents the determination of the shear sense. At the highest strain zone, plagioclase can be observed as a porphyroclast (1-3 mm in a diameter) or as a recrystallized aggregate in the field. Most of these shear zones were hydrated within surrounding undeformed pyroxene granulites.

Anastomosed High-Grade Shear Zones (S2)

The S2 structures are characterized by an anastomosing foliation and well-developed mineral and stretching lineations of hornblende and plagioclase aggregate in the southern part of the SKA from Pattan to Kiru (Fig. 6-1). S2 cuts the early mafic banding and is inhomogeneously distributed in rocks with same bulk chemistry and occur as bands ranging in width from a few centimeter to tens of meters. Shear zones locally forms a network structure (Fig.6-4a). In many cases, pyroxene granulites in the southern part of the SKA are observed as equigranular pods. Initially coarser grained plagioclase within

160

the feldspathic pegmatites remains as a porphyroclast in the shear zones and its grain size gradually becomes bigger toward the equigranular pods.

Mineral lineation of L2 is defined by alignment of hornblende and stretching lineation ribbon-like aggregates of plagioclase, quartz and minor garnet within mylonitic rocks, and it trends towards 45° to 30° and variably dip in the southern part of the SKA (Fig. 6-2a). There are many evidence that flow in the shear zone was non-coaxial and shear sense can be evaluated by deflection of newly formed foliation at the edge of the zone. Drag folds of the feldspathic veins along the shear plane provide evidence for a significant south-west shear movement (Fig. 6-3a). In an equigranular pods, the shear sense criterion is possible to use the feldspathic vein bending towards the surrounding shear zone and shows same sense. Plagioclase porphyroclasts commonly have sigmoidal tails consisting of recrystallized mantle grains suggesting the movement of top-to-the-southwest. In the present position, the relative kinematic sense along on the gently dipping foliation is almost indicative of a top-to-the-SW thrust movement.

Gneissose Foliation in Epidote Amphibolite (D3)

Pyroxene-free gneissose foliation (S3) are not common in the NKA but in the SKA, in especially from Kiru to Dasu (Fig. 6-2). It is characterized by geissosity of EW trend with steep dip to the north, well-developed compositional layering, equigranular pods and north-side-down normal fault sense (Fig. 6-3a). Subvertical foliation (S3) bending the gently dipping S2 foliation (Fig. 6-4b), is remarkably observed at the south of Kiru and the frequency increases northward, and the moving direction is indicative of a top-to-the-northeast normal fault sense. The distribution of S3 foliation is restricted in only the SKA, that is, the northern limit can be just identical to the boundary between the NKA and the SKA. At northern limit of the SKA, although both of S1 and S3 have similar structural trend, high grade gneissose foliation defined by pyroxene and hornblende (S1) could be distinguished from foliation defined by epidote and actinolite (S3).

The mylonitic foliation of S2 is difficult to distinguish from predominantly developed S3 foliation at northern side of Mandraza. They are scarcely confined to equigranular pods with anastomosed nature, because regionally penetrative S3 foliation with a width of hundreds meter scale overprint the anastomosed shear zones with variable trends. The area of the strongest developed S3 foliation is sure to accompany with compositional layering defined by granitic veins and sheets parallel to the S3 foliation. Stretching lineation defined by plagioclase aggregates cannot be so much observed as S2 foliation, but mineral lineation is defined by alignment of hornblende, clinozoisite, actinolite or chlorite developing as a typical structure in the amphibolites. Well-defined mineral lineations trend steeply towards N50°E (Fig. 6-3a). However, near Dasu, mineral and stretching lineations cannot be recognized due to flattening shape of the forming minerals. Buckle folds with vertical fold axis widely develops from Dasu to Kiru and the drag direction indicates W vergence of north side rocks. Because thin granitic veins having thickness less than tens of centimeter forming compositional layering are also folded by the buckling folds, it can be interpreted that the buckling postdates intrusion of granitic sheets.

Low grade shear zones (S4 & S5)

Foliations defined by retrogressive low temperature minerals are classified into two types (S4 & S5) by difference of shear sense and trend (Fig. 6-2). These can be observed as localized nature in amphibolites and granitic rocks. S4 foliation is developed only in the SKA, especially in the vicinity of Kiru (Fig. 6-1). It is characterized by subhorizontal mylonitic foliation with the mineral assemblage of greenschist facies retrogressive metamorphism. Most of them forms the fabric curvature at high angle to the pre-existing foliation (S3) in the SKA, and indicates shear sense of top-to-the-S (Fig. 6-4c). One of subhorizontal ultramylonitic shear zone sharply cut the regional gneissose foliation (S3). It should be interpreted that D4 is later shear zone than D3, In addition, S3 is cut by

micaceous granitic pegmatite near Mandraza, S4 cuts both the S3 foliation and the micaceous pegmatites. Buckling folds dragged S3 foliation are further deflected by S4 foliation.

Mylonitic structure with S5 foliation defined as shear plane develops within the rocks including both of amphibolites and granitic rocks in the KAB. The shear zone can be observed as extensively retrogressive zone. Direct relationship between S4 and S5 can not be recognized. The S5 foliation also cut or deflect the relatively vertical foliation (S3) and the foliated garnet-bearing granitic gneiss or granitic veins parallel to the S3 foliation in addition to even the later pegmatite. Shear planes (S5) are generally SSE-NNW-striking and steeply dipping to the southeast to east. Dominant shear sense is indicative of top-to-the-NW except for the reverse sense (top-to-the-east) at the south of Kamila (Fig. 6-3).

MICROSTRUCTURES

Figure 6-5 shows the regional variation of texture for plagioclase. The microstructure about plagioclase is the key to correlate with the deformation of the studied samples, because plagioclase is the most abundant mineral throughout all the samples except for the samples suffered from retrogression. The mode of deformation about plagioclase can be evaluated by the observation of the thin section and can be classified into four types; (1) a cumulate texture defined by plagioclase laths with well-developed twinning, (2) a granoblastic texture defined by polygonal plagioclase, (3) a dynamically recrystallized ribbon texture or core and mantle texture, and (4) a porphyroclastic texture without dynamically recrystallized grain. In the SKA, it notes that the texture of plagioclase tends to gradually changes from the recrystallized aggregate type to the porphyroclastic type northward, near Kiru. It seems that the deformation style of plagioclase changes from ductile to brittle manner northward (Fig. 6-5). The microstructural features for each type of the shear zone and the protolith will be described below.

Protolith

The protolith consists of coarse-grained pyroxene granulites and amphibolites in relation to granulite to upper amphibolite facies metamorphism. Their mineral assemblage are dominated by plagioclase (An_{40-60}), clinopyroxene, orthopyroxene and tschermakitic hornblende with minor quartz and Fe-Ti oxides (ilmenite+rutile). Pyroxenes and hornblende are euhedral shape and have weak shape preferred orientation depending on igneous flow. Subhedral plagioclase has irregular grain boundary and large grain size with well-developed twinning (up to 5 mm in a diameter) (Fig. 6-6a).

Intensity of retrogression in the undeformed rocks increases northward throughout the KAB independently of distribution of the shear zones (Fig. 2-1). Thus, some pyroxenes are pseudomorphed by tschermakitic hornblende depend on retrogression or the others are totally transformed into hornblende and quartz aggregates. Plagioclase and hornblende are replaced by clinozoisite at their rim during regional retrograde metamorphism due to hydration. In addition, hornblende are totally replaced by actinolite and/or chlorite in the NKA, where highly retrogression regionally occurred under greenschist facies metamorphism.

S1

S1 foliation is only preserved within the pyroxene granulite pods in the KAB. In thin section, the deformation structure is inherently more difficult to distinguish from the intensively developed gneissose foliations due to post-kinematic annealing and grain growth rather than in the field. It has survived within only the zone with strongly foliation. The mineral assemblage within the S1 foliation is composed of clinopyroxene (Mg-rich augite), orthopyroxene (En_{54-64}), brown-coloured hornblende, plagioclase, quartz, ±garnet, ±biotite and Fe-Ti oxides. In the strongly foliated part, modal composition of hornblende increases in comparison with surrounding pyroxene granulites.

Pyroxene behaves as a porphyroclast with or without core and mantle structure

against the matrix grain such as fine-grained hornblende, plagioclase and quartz, and partly recrystallized like core and mantle structure (Fig. 6-6b). Clinopyroxene is likely to dynamically recrystallize in comparison with orthopyroxene, because Burgers vector in the a-direction of clinopyroxene is shorter than that of orthopyroxene. Core of orthopyroxene porphyroclasts show high Al-contents, and rim of porphyroclast and mantle grain have similarly low Al-contents (Fig. 6-7a). Clinopyroxene porphyroclast have high Al- and Ti-contents and preserves distinctive Al-zoning in similar to those of surrounding pyroxene granulites (Fig. 6-7b). The Al-contents simply increase toward the margin of porphyroclast and mantle grains have lower Al-contents than porphyroclast. Chemical composition of hornblende is characterized by high Ti- and K-contents typical of that in the pyroxene granulites (Fig. 6-8).

Most of recrystallized plagioclase grains in lower strained zone has straighter grain boundary and isotropic, polygonal optically strain-free textures depend on post-deformational annealing accompanying with recovery and grain growth (Rutter & Brodie, 1992). Plagioclase behaves plastically at temperature above 500 °C (Tullis, 1990) and granoblastic and well-annealed plagioclase fabrics has been reported from upper amphibolite to granulite facies basic rocks (Ji & Mainprice, 1987). Although strain feature was destroyed by recovery process, compositional difference is observed between porphyroclasts and neoblasts; relatively large plagioclase porphyroclast shows higher An-contents (An_{60-70}) same as that of protolith, than recrystallized grains (An_{45-55}) (Fig. 6-9a-b). An-contents of equigranular recrystallized grains show no variation in the recrystallized aggregate.

As a whole, garnet porphyroblast shows idiomorphic and/or angular shape along the feldspathic vein parallel to S1 foliation. Quartz interstitially occurs as a large strain-free grain in comparison with other minerals. In addition, softer phase Fe-Ti oxide is generally in filled with fracture of hornblende or pyroxene.

Metamorphic temperatures have been estimated from the Fe-Mg exchange reaction

between coexisting garnet and hornblende, following the formulation of Graham and Powell (1984). Metamorphic pressures were calculated using the garnet-hornblende-plagioclase-quartz geobarometer (Kohn and Spear, 1990). Estimated temperature is 655 °C and pressures are between 820-830 MPa. In addition, absence of low grade minerals such as clinozoisite, actinolite and chlorite indicates that development of S1 foliation occurred under up to upper amphibolite facies metamorphic condition.

S2

Within the shear zones with S2 foliation, the mineral assemblage consists of plagioclase (An_{30-50}), green-coloured hornblende, clinozoisite, quartz and Fe-Ti oxides, occasionally garnet. Modal composition of plagioclase tends to be smaller (<40 vol.%) than that of S1 with increasing hornblende and epidote. Mylonitic microstructure shows asymmetric S-C fabric (Lister & Snoke, 1984) suggesting top-to-the-SW.

Pyroxene completely disappears within the fine-grained part of the shear zone, even if the shear zone clearly cuts pyroxene granulite pods. Some green-coloured hornblende occur as a porphyroclast and others are composed of fine-grained matrix (Fig. 6-6c). It indicates that the hornblende has already existed before development of S2 begin. Chemical composition of hornblende forming S2 foliation is similar to that in surrounding undeformed amphibolites, and is characterized by lower K- and Ti-contents and higher Al- and Na-contents in comparison with the hornblende in rocks with the S1 foliation (Fig. 6-8). The plagioclase aggregates are mostly recrystallized during high temperature (up to 500 °C) mylonitization (Tullis, 1990). Plagioclase porphyroclasts show undulatory extinction and subgrain which has low angle misorientation against the host lattice. The An-contents of plagioclase porphyroclast (An_{50}) are nearly same as that of plagioclases in the surrounding equigranular rocks and higher than that of matrix grains (An_{30-40}), as shown in Figure 6-9(c-d). Matrix grains show relatively lower An content than that of S1. These mineral chemistries indicate that regional amphibolite formation occurred at the

same time of development of the S2 foliation. Although white mica occasionally replaces An-rich cores of plagioclase porphyroclast together with small amounts of quartz, epidote and albite, these secondary aggregate does not have deformational features at all. Interstitial to poikilitic clinozoisite occasionally crosscut the S2 foliation. They show no optical intracrystalline strain features such as undoulose/patchy extinction. However, some clinozoisite forms the S2 foliation parallel to the alignment of hornblende. These observations suggest that clinozoisite grew during or after formation of the S2 foliation at lower amphibolite facies.

Estimation of metamorphic conditions during formation of shear zone using the above geothermobarometer (Graham & Powell, 1984; Kohn & Spear, 1991) on adjacent garnet, hornblende and plagioclase rims gives temperatures between 585 ˚C and 650 ˚C, and pressures among 910 and 950 MPa. As described in Chapter IV, these garnet has discontinuous zoning, which indicates pyrope-rich core and grossular-rich rim. In summary, the shear zone formed at higher pressure metamorphic conditions; at least amphibolite facies than that of S1 structure.

S3

The mineral assemblage of amphibolites with S3 structure is composed of hornblende, actinolite, epidote, quartz, ±sphane, ±garnet and Fe-Ti oxides with saussulitized plagioclase and chlorite. S3 foliation is defined by alignment of idiomorphic acicular or platy green-coloured hornblende, pale green or colourless actinolite and pleochroic pink or colourless epidote (Fig. 6-6d).

Calcic-plagioclase within the shear zone completely disappears because of lower grade metamorphic condition compared with S2 foliation, probably lower amphibolite to green schist facies conditions. Blue- to green-coloured hornblende is partly or totally replaced by low-Al_2O_3 (2-3 wt%) actinolite and chlorite within the shear zone in comparison with the protolith. Initially larger tschermakitic hornblende (up to 15 wt%

Al_2O_3) in the matrix of hornblende containing low Al_2O_3, actinolite, chlorite, epidote and quartz behave as a porphyroclast in the shear zone. The S3 foliation is mostly defined by shape preferred orientation of acicular or platy actinolite or pale-coloured hornblende. Intensive mineral lineation with a direction of NW to N dipping sometimes develops. Quartz modaly increases compared with rocks with S2 foliation and forms ribbon by recrystallized aggregates or single grain. Although plagioclase is mostly saussulitized, rarely observed plagioclase grains show no evidence of plastic deformation such as core and mantle structure, subgrain rotation and lattice preferred orientation. Saussulite preserves the rounded shape in the matrix of actinolite, epidote and quartz (Fig. 6-6d). This observation suggests that alteration of plagioclase post-dates development of S3 foliation and plagioclase behave as a porphyroclast during formation of the S3 foliation. This evidence indicates that S3 developed below the brittle-ductile transition of plagioclase (<550 °C); lower amphibolite to green schist facies. White-coloured compositional banding is almost formed by strong preferred orientation of acicular or platy epidote. Epidote is higher pistasite component than that in rocks with S2 foliation (Fe_2O_3 over 15 wt%). Enrichment of pistasite component in epidote presumably represents that formation of S3 foliation occurred under lower metamorphic condition than that of S2 foliation. Epidote has shape preferred orientation parallel to the S3 foliation defined by alignment of amphibole.

S4 & 5

S4 and S5 foliations commonly have S-C fabric with shear plane defined by shape preferred orientation of quartz ribbon and alignment of fine-grained actinolite and chlorite (Fig. 6-6e). Absence of hornblende and plagioclase in these types indicates that they are totally replaced by retrogressive mineral assemblage suggesting greenschist facies metamorphism such as actinolite, chlorite, epidote, muscovite, quartz and minor albite. In the granitic mylonites, epidote behave as a porphyroclast in the matrix of fine-grained

168

chlorite, actinolite, quartz and muscovite and is occasionally micro-boudinaged or fractured and besides, in some case, rotated after the fracturing depending on non-coaxial flow. Ribbon like quartz aggregates forms the principal load-bearing framework.

TECTONIC IMPLICATION

In the SKA, the main deformation phases are classified by Treloar *et al.* (1990) into two categories; high temperature ductile deformation occurred during the main crustal thickening and imbrication of the island arc, and low temperature cataclastic deformation occurred during exhumation and cooling with collision between the Asian plate and Kohistan arc due to the ^{40}Ar-^{39}Ar cooling age of hornblende.

Assuming that the higher grade deformation occurs older during the exhumation of the southern Kohistan arc, S1 foliation, which is characterized by penetrative deformation with granoblastic texture suggesting high temperature ductile manner, should be considered as the earliest deformation texture, called as D1. Most of the dynamically recrystallized texture shows the effects of static recovery and grain growth. It indicates that high grade metamorphism has continued after the main deformation event. For this reason, the D1 structure could be recognized as an intra-arc shear zone during the main granulite facies metamorphic stage during the gabbroic intrusion at the lower crust. Moreover, strain feature of D1 represents the flattening type. Metamorphic *P-T* path suggests that the lower crust of the Kohistan arc experienced the crustal thickening due to magmatic accretion at middle crustal depth. Therefore, D1 might be accommodated with the crustal thickening due to the magma loading when the Kohistan arc was an intra-oceanic island arc.

Structure deflected by S2 foliation developed under upper amphibolite facies metamorphism suggests top-to-the-SW thrust sense. If higher grade deformation occurs earlier stage, deformational phase forming S2 foliation, hereafter called D2 occurred after D1. Compared with D1 structure, the observation of microstructure in D2 indicates that

169

hornblende occurs as a porphyroclast, whilst some clinozoisites occur as a porphyroblast after the formation. It indicates that D2 terminated during main hydration following lower amphibolite facies static metamorphism. Occurrence of the anastomosed shear zone or the strain localization is generally observed in typical high grade terrains such as Grenville Province, Canada (Davidson, 1984), Fiordland complex, New Zealand (Bradshaw, 1989), Coastal Cordillera, northern Chile (Lucassen & Franz, 1996) and Ivrea-Verbano zone, Italy (Schmid *et al.*, 1987). Rutter & Brodie (1985; 1992) suggested that the localized deformation develops during the exhumation of the high grade rocks. The anastomosed shear zone commonly develops within amphibolites and pyroxene granulites, especially at area adjacent to the garnet granulite in the Jijal complex. The garnet granulite mass could behave as rheologically stronger phase depending on large amount of garnet (up to 30% in modal composition) than amphibolites or pyroxene granulites.

Gneissose structure with S3 foliation widely accompanies with uncertain aged-granitic sheets or veins parallel to the S3 foliation. Because subvertical foliation (S3) bends the gently dipping S2 foliation and consists of lower temperature assemblage, it can be interpreted that a deformation phase forming S3 foliation, hereafter called D3, postdates development of D2. Minimum age of this deformation is given by a K-Ar muscovite age of 66 Ma from a hornblende-bearing granitic pegmatite that cross-cuts the S3 foliation (Treloar *et al.*, 1989). The NE normal fault shear sense predicted by D3 structure suggests that this deformation event was likely to be active in extensional stress field at least in the SKA. The extensional environment might be invoked that the subduction rate at the back-arc basin in association with collision between the Asian plate and Kohistan island arc is faster than that of the Tethys oceanic plate at fore-arc. This event may lead to tectonic erosion of the high pressure rocks and crustal thinning. The exposed lower crustal section in the Kohistan arc is too thick to compare with realistic expected thickness of the lower crust, because the width is about 100 km at the longest traverse in spite of the observation that is generally subvertical dipping throughout the

section. The fact requires that the crustal thinning process might occur at the lower crust in the Kohistan arc during the back arc collision. Crustal thinning can be explained by regional scale normal faults at an extensional field. D3 shear zone, suggesting the NE normal fault sense widely develops in a width of 20 km in the central of the KAB. Although S3 forms steeply dip to the north, it is possible to interpret more gently dipping at the back-arc collision stage. Thus, the lower crustal section should experience NS compression during the Main Himalayan collision and the regional steeply dipping structure has been formed especially at the D3 shear zone. The regional anticlinal fold has probably developed in the Chilas complex at the same time (Coward *et al.*, 1987). Consequently, D3 should accommodates the exhumation of the garnet granulites due to the movement of normal fault. According to Zeitler (1985), ^{40}Ar-^{39}Ar biotite and hornblende cooling ages (85.8 ± 0.6 Ma - 73.3 ± 0.8 Ma) show rapid cooling path during the back-arc collision stage and the zircon fission-track cooling ages in southern Kohistan arc is younger northward. Development of buckling fold dragging D3 structure postdates intrusion of granitic sheets and is prior to development of S4 and S5 foliation.

In S4 and S5 structures, it is difficult to speculate the formation age under greenschist facies metamorphism because of absence of geochronologic data. Because these deformation structures cut the all fabric of D1-D3, these deformations occurs after development of S1-S3, called as D4 and D5, respectively. It can be interpreted that these deformation events occurred after the back-arc collision depending on structural relations cut muscovite-bearing pegmatite which has younger age than hornblende cooling age. In addition, the southern Kohistan has kept since minimum 14.1 ± 1.2 Ma among 200 and 300 °C after the back-arc collision (Zeitler, 1985). Quartz had maintained a plastic manner as load framework. Shear zone with S4 foliation indicating top-to-the-south shear sense, probably developed during the Andean type margin stage or Main Himalayan collision stage. Shear zone with S5 foliation indicating mainly top-to-the-NW, acted during the rapid uplift of the Nanga Parbat-Haramosh massif (NPHM) (Zeitler, 1985, Zeitler *et al.*,

171

1989, George *et al.*, 1995). Structural studies suggest that the movement of shear zone at margin of the NPHM shows northwestward directing thrusting of Indian crustal rocks over the Kohistan arc (Butler & Prior 1988). This movement extremely corresponds to the moving direction of D5.

CONCLUSIONS

A tectonic evolutional model in the lower crust of the Kohistan arc on the basis of the predicted deformation events, is illustrated in figure 6-10. The variable deformations developed and superimposed at long-time range under the several tectonic environments as follows; (1) D1 event occurred as an intra-arc deformation and was accommodated by crustal thickening process. (2) D2 structure is characterized by the anastomosed occurrence, SW thrust sense under upper amphibolite facies, and the compressional movement could enhanced the crustal thickening, presumably after formation of garnet granulites in the Jijal complex. (3) D3 structure shows movement of top-to-the-NW normal fault sense under lower amphibolite facies. Development of the movement could be promoted by crustal thinning process with the exhumation of high pressure rocks. (4) D4 is characterized by subhorizontal top-to-the-S movement under greenschist facies and resulted from the crustal shortening owing to the Andean type margin or Indian collision. (5) D5 structure shows retrogressive narrow shear zone suggesting top-to-the-NW thrust sense and is related to the thrusting of the NPHM after the Himalayan collision.

Table 6-1. A summary of deformational phase of metabasic rocks in the Kamila amphibolite belt

	Metamorphic grade Mineral assemblage	Distribution	Width Shear plane	Lineation Shear sense	Occurrence
High grade					
S1	Granulite facies to upper amphibolite facies opx-cpx-hbl-pl-qtz±grt	NKA	10-500 m EW strike steeply dip	None	parvasively homogeneous gneissose texture
S2	Upper amphibolite facies hbl-epi-pl-qtz±grt	Kiru-Pattan	5 cm-10 m mainly NW-SE gently dip	Top to the SW thrust gently dip	anastomosed inhomogeneous mylonitic texture
S3	Lower amphibolite facies (hbl)-act-epi±pl-qtz±chl±grt	Pattan-Dasu	Seveal km EW strike steeply dip	Top to the NE normal fault steeply dip	gneissose texture deflect S2
Low grade					
S4	Greenschist facies act-chl-epi-mus-qtz±grt	Mandraza-Kiru	Several cm subhorizontal	Top to the S thrust	mylonitic texture deflect/cut S3
S5	Greenschist facies (act)-chl-epi-mus-qtz±grt	Lutar-Mandraza	Several cm-m NNW-SSE steeply dip	Top to the W (E) thrust steeply dip	mylonitic texture deflect/cut S3 deflect/cut S4?

Abbreviation; px:pyroxene, hbl: hornblende, act:actinolite, pl: plagioclase, epi: epidote, chl: chlorite, qtz: quartz, grt: garnet, mus: muscovite

Table 6-2. A summary of chemical characteristics and texture of minerals in each deformation strucrure

	S1	S2	S3	S4 & S5
pyroxene	porphyroclastic			
amphibole	brown prismatic	blue-green tabular	actinolite acicular	
plagioclase	An50 granoblastic	An30-40	saussulite porphyroclastic	
epidote		clinozoisite porphyroblast	pistacite-rich acicular	porphyroclastic
chrolite				acicular
quartz	annealed texture		fine-grained aggregate	
White mica				acicular

Shape preferred orientation

174
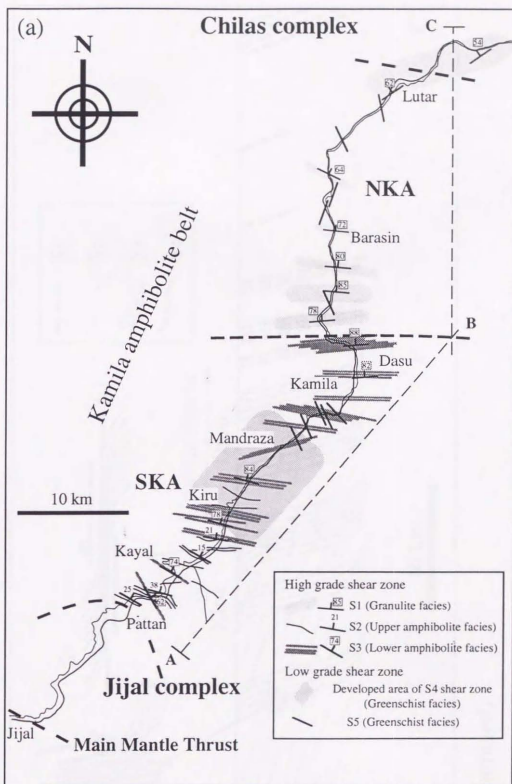
Fig. 6-1. Spatial distribution map of the five types of foliations defined by mineral alignment along the Indus Valley route. (a) A map to show the locations and typical trend of foliation. (b) Simplified cross section (A-C), vertical to the main striking of foliation through the Kamila amphibolite belt.

Fig. 6-1. (continued)

176

177
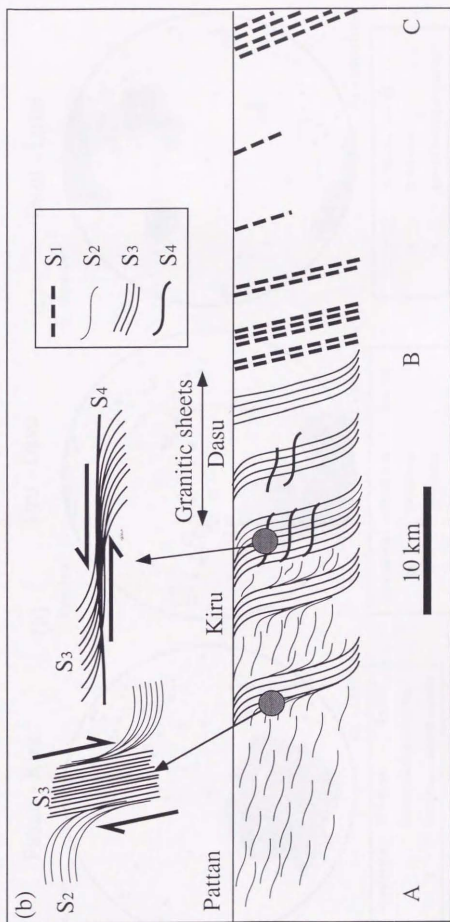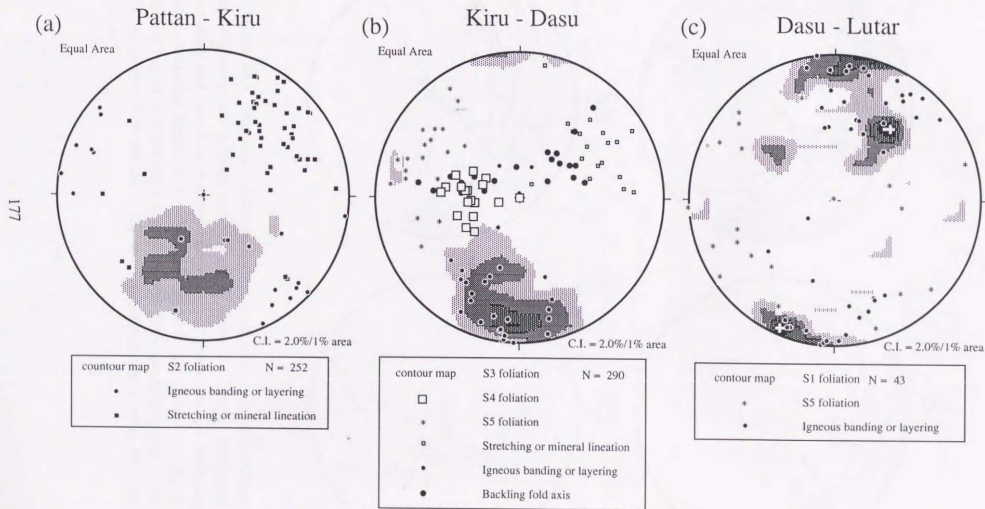
Fig. 6-2. Equal-area lower hemisphere stereographic projections of pole to the shear plane and mineral and stretching lineation in the Kamila amphibolite belt. (a) Regional variations from Pattan to Kiru; (b) from Kiru to Dasu; (c) from Dasu to Lutar.
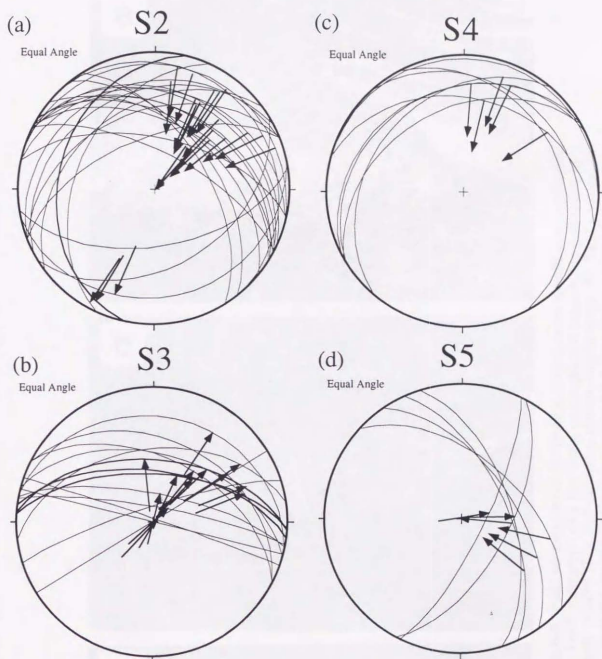
Fig. 6-3. Equal-area lower hemisphere stereographic projections of pole of shear-plane or mineral alignment are depicted with movement directions (arrow) interpreted from fabric curvature and stretching or mineral lineations. (a) Anastomosed shear zone with S2 foliation, indicating mainly north side up SW thrust sense; (b) subvertical gneissose foliation (S3) indicating north side down NE normal fault sense; (c) retrogressive shear zone, S4, suggesting S thrust sense; (d) low temperature shear zone, S5, indicating conjugate set.

178
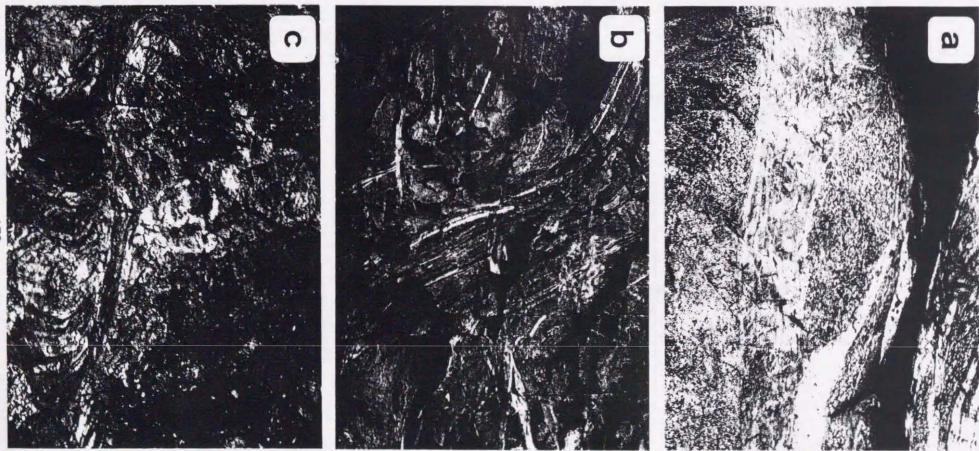
Fig. 6-4. Field photographs of deformed structures in the Kamila amphibplite belt.
(a) Field photograph of a low strain coarse-grained amphibolite pod rimed by a
highly foliated (S2), fine-grained mylonitic amphibolites. (b) Field photographs
showing that steeply dipping S3 foliation bend the relatively gentle dipping shear
zone (S2). (c) Field photograph of subhorizontal low temperature shear zone (S4)
cutting the steeply dipping gneissose foliation (S3).
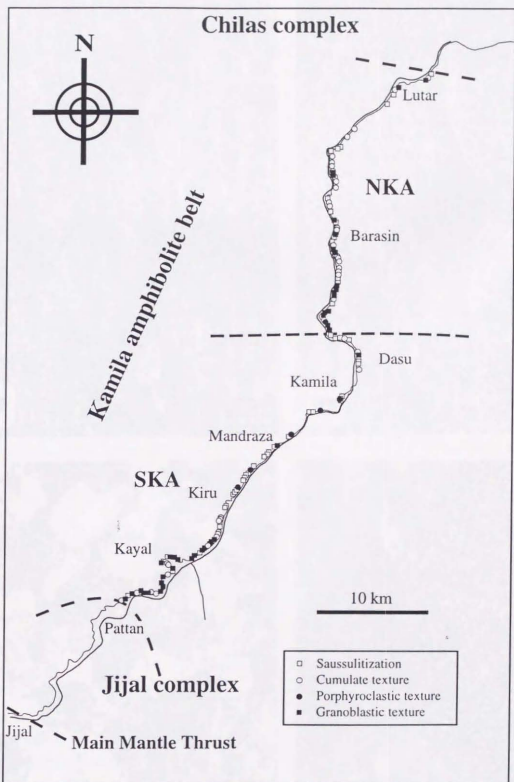
Fig. 6-5. Distribution of deformational texture about plagioclase in the Kamila amphibolite belt. Note that deformational texture changes from granoblastic to porphyroclastic texture northward near Kiru and cumulate texture is well-preserved in the NKA.
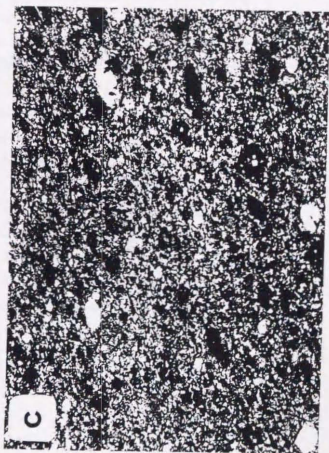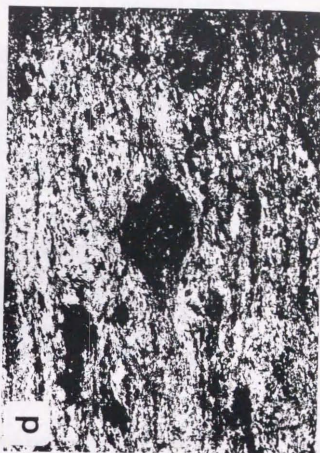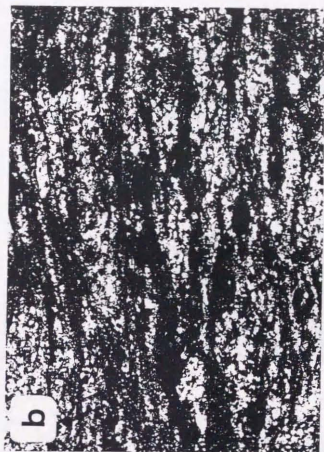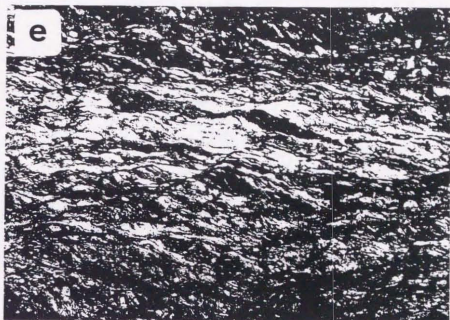
Fig. 6-6. Microphotographs showing typical microstructure of these shear zones. (a) Note that a granoblastic texture with euhedral pyroxene porphyroblasts and interstitial to subhedral plagioclase in the undeformed pyroxene granulites. (b) Microphotograph of a high temperature gneissose foliation (S1) showing clinopyroxene, orthopyroxene and hornblende porphyroclasts and dynamic recrystallized plagioclase aggregates. (c) Microstructure of localized high temperature shear zone with S2 foliation indicating plagioclase and hornblende porphyroclasts and optically strain-free clinozoicite porphyroblasts in fine grained-plagioclase and hornblende matrix. (d) Microphotograph of the deformed amphibolites with gneissose foliation (S3). Note that saussuritized plagioclase behave as a porphyroclast and the alignment of acicular and platy clinozoicite and hornblende porphyroblast defines foliation. (e) Microphotograph of a low temperature basic mylonite (S5) suggesting S-C fabric defined by quartz ribbon and alignment of chlorite. Clinozoicite porphyroclasts occur within fine grained chlorite-actinolite-epidote-quartz matrix and are partialy micro-boudinaged.
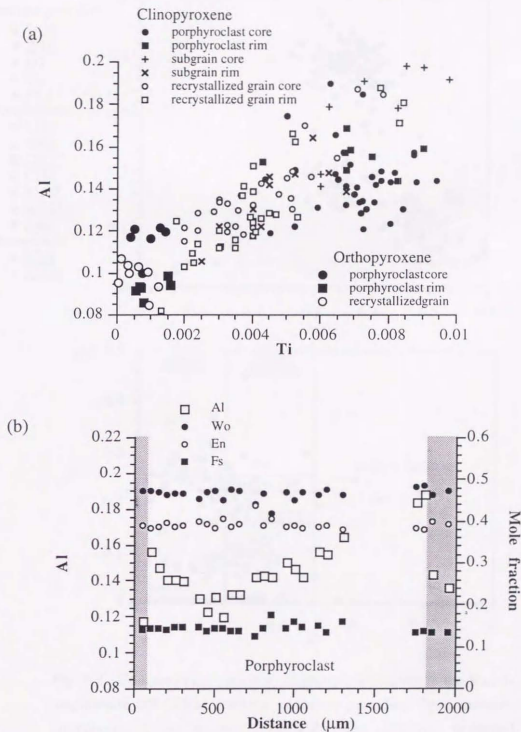
Fig. 6-7. Compositional change of pyroxene forming S1 foliation. (a) Al vs. Ti in pyroxene for analysed sample 1406 with core and mantle structure. (b) Compositional zoning of clinopyroxene porphyroclast surrounded by fine-grained mantle clinopyroxene from the same sample. Shaded area represents the composition of mantle grains.
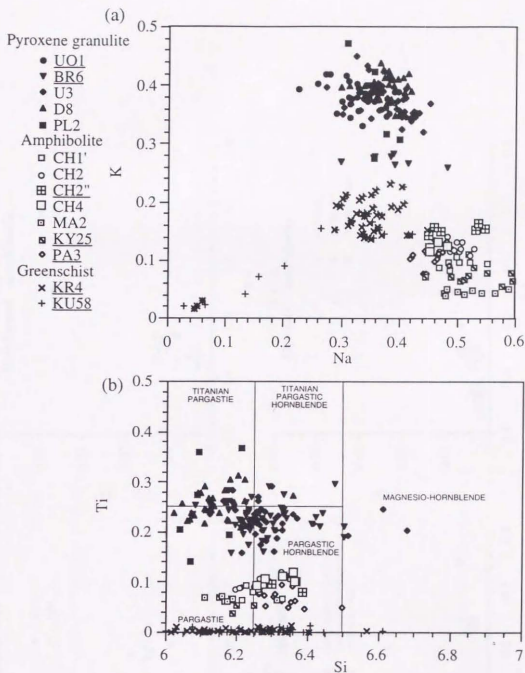
Fig. 6-8. Compositional variation diagram of amphibole in the Kamila amphibolite belt. Close markers: pyroxene granulite, Open markers: amphibolite, Cross: epidote amphibolite, and underline: deformed sample. (a) Na vs. K in amphibole. (b) Ti vs. Si in amphibole from nomenclature of Leake (1978).
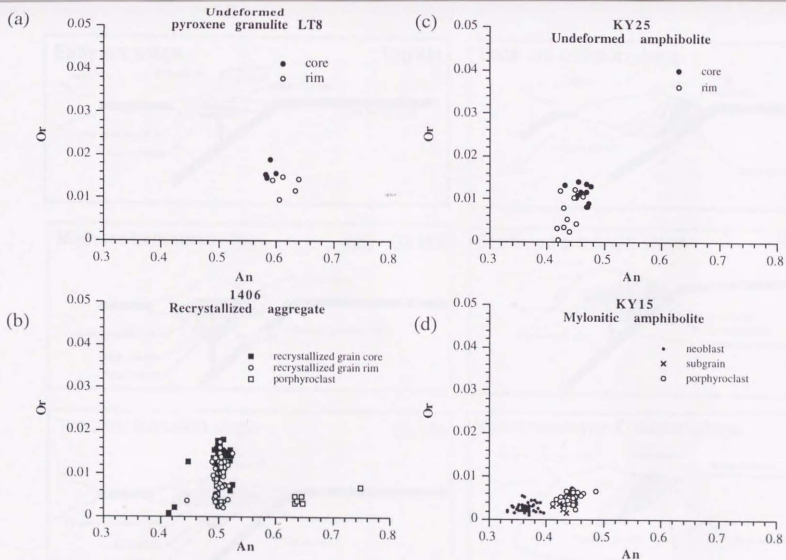
Fig. 6-9. Representative compositional variations of plagioclase in deformed and undeformed rocks from the Kamila amphibolite belt. (a) Undeformed pyroxene granulite in the NKA. (b) Strongly deformed pyroxene granulite in the NKA with S1 structure. (c) Undeformed amphibolite in the SKA. (d) Strongly sheared amphibolite in the SKA with S2 foliation. Note that recrystallized plagioclase is characterized by lower anorthite content. The recrystallized grains with S2 foliation have clearly lower anorthite content than that with S1 foliation. Porphyroclastic grain has similar anorthite content of plagioclase grains in surrounding undeformed rock.
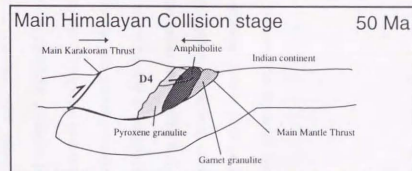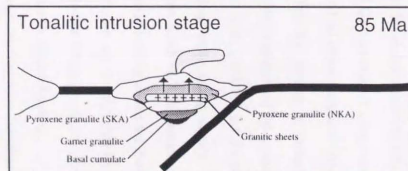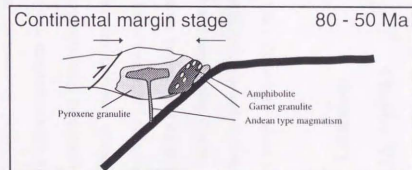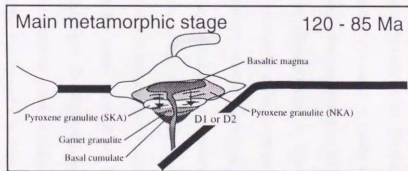
Early arc stage — 120 Ma
Asian Plate — Kohistan arc — Basaltic magma
Pyroxene granulite (SKA) — Tethys oceanic plate
Basal cumulate

Main metamorphic stage — 120 - 85 Ma
Basaltic magma
Pyroxene granulite (SKA) — Pyroxene granulite (NKA)
Garnet granulite — D1 or D2
Basal cumulate

Tonalitic intrusion stage — 85 Ma
Pyroxene granulite (SKA) — Pyroxene granulite (NKA)
Garnet granulite — Granitic sheets
Basal cumulate

Back arc collision stage — 80 Ma
D3 — Amphibolite
Pyroxene granulite — Garnet granulite

Continental margin stage — 80 - 50 Ma
Amphibolite
Pyroxene granulite — Garnet granulite — Andean type magmatism

Main Himalayan Collision stage — 50 Ma
Main Karakoram Thrust — Amphibolite — Indian continent
D4
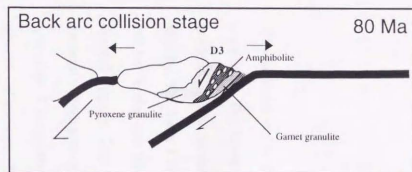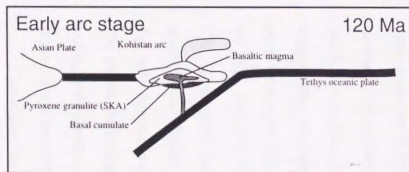Pyroxene granulite — Main Mantle Thrust
Garnet granulite

Fig. 6-10. Schematic model of evolution and exhumation of the lower crust of the Kohistan arc from Cretaceous to Eocene.

Chapter VII

Summary

The Kohistan arc is the Early Cretaceous island arc between the Eurasian and Indian continents. The lower crustal rocks consist of mainly metabasic rocks such as pyroxene granulite, garnet granulite and amphibolite derived from gabbronorite with calc-alkaline affinity. The Early Cretaceous metamorphic event of the lower crust in the Kohistan arc can be divided into three major events: (1) intrusions of the basaltic to intermediate arc-derived magma; (2) a subsequent formation of the pyroxene and garnet granulites under medium to high pressure granulite facies metamorphism; and (3) regional hydration of the granulites. Clinopyroxene with magmatic texture from the pyroxene granulite preserves distinct Al-zoning. Zonal structure of plagioclase in contact with clinopyroxene corresponds the Al-zoning in clinopyroxene. Plagioclase breakdown reaction introduce an increase of Al solubility in clinopyroxene as jadeite and Ca-tschermakite components with quartz as a product. Zoning relations between CaTs and Jd component and An-contents suggest that Al-zoning in clinopyroxene is controlled by zoning of mainly CaTs component in the NKA, whereas it reflects compositional variation of Jd component in the SKA. Peak P-T conditions inferred from these reactions are 0.8-1.2 GPa at around 800 °C. Regional mineral chemistry and geothermobarometry using several methods generally show higher pressure and temperature condition southward. Estimated prograde P-T paths represent a crustal thickening process suggesting loading above the lower crust. The crustal thickening in the lower crust of the Kohistan arc is triggered by magma loading at the middle crustal depth. The highest grade ductile deformation characterized by flattening was probably facilitated by gravity collapse due to magma loading.

Garnet granulites in the Jijal complex and the garnet reaction zone developed within

187

pyroxene granulite pods in the Kamila amphibolite belt overprinted the pre-existing pyroxene granulites by consumption of hornblende, orthopyroxene and calcic plagioclase. Vein-like occurrence of the garnet reaction zone is triggered by channelized infiltration of low $f H_2O$ fluid. In the lower pressure area, the garnet reaction zone developed along quartzo-feldspathic vein, and was formed by dehydration of hornblende near the vein due to hydrofracturing. On the other hand, in the higher pressure area, the garnet reaction zone unrelated to hydrofracturing was formed by lowered water activity due to locally connected network of low $f O_2$ fluid. Garnet granulites in the Jijal complex should be regionally formed by lowered activity of water of residual fluid phase due to selective removal of H_2O caused by decrease in dihedral angle. Relatively high a_{CO_2} leads to scapolite-forming reaction of the Kohistan granulites.

Lower crustal sequence of the Kohistan arc underwent exhumation accompanied by development of ductile shear zones and regional retrogressive metamorphism during two collisional events. Early formed foliation (S1) preserved only in pyroxene granulite pods represents flattening deformation accomodated by crustal thickening process. Strain localized high-T shear zone (S2) characterized by kinematical direction of top-to-the-SW developed in the compressive field around garnet granulites in the Jijal complex after formation of garnet granulites. Development of the regional gneissose foliation (S3) with shear direction of top to the northwest took place the exhumation of the high pressure rocks in the extensional field during the back-arc collision. Strain localized low temperature shear zone (S4 & 5) developed under greenschist facies condition after the back-arc collision.

Acknowledgment

REFERENCES

Ai, Y., 1994. A revision of the garnet-clinopyroxene Fe^{2+}/Mg exchange geothermometer. *Contributions to Mineralogy and Petrology,* **115,** 467-473.

Allégre, C.J. & Jauport, C., 1985. Continental tectonics and continental kinetics. *Earth and Planetary Science Letters,* **74,** 171-186.

Andersen, T., Burke, E.A.J. & Neumann, E.-R., 1995. Nitrogen-rich fluid in the upper mantle: fluid inclusions in spinel dunite from Lanzarote, Canary Islands. *Contributions to Mineralogy and Petrology,* **120,** 20-28.

Anderson, D.J. & Lindsley, D.M., 1988. Internally consistent solution models for Fe-Mg-Mn-Ti oxides. *American Mineralogists,* **73,** 714-726.

Anderson, D.J., Bishop, F.C. & Lindsley, D.M., 1991. Internally consistent solution models for Fe-Mg-Ti oxides: Fe-Mg-Ti oxides and olivine. *American Mineralogists,* **76,** 427-444.

Anderson, D.J., Lindsley, D.M. & Davidson, P.M., 1993. QUIIF: A Pascal program to assess equilibria among Fe-Mg-Mn-Ti oxides, pyroxenes, olivine, and quartz. *Computers and Geosciences,* **19,** 1333-1350.

Anovitz, L.M., 1991. Al-zoning in pyroxene and plagioclase: Window on late prograde to early retrograde *P-T* paths in granulite terranes. *American Mineralogists,* **76,** 1328-1343.

Armstrong, R.L., 1981. Radiogenic isotopes: the case for crustal recycling on a near-steady-state no-continental-growth Earth. *Philosophycal Transactions of Royal Society, London,* **301A,** 443-472.

Baker, J. & Nerton, R.C., 1995. Experimentally determined activity-composition relations for Ca-rich scapolite in the system $CaAl_2Si_2O_8-NaAlSi_3O_8-CaCO_3$ at 7 kbar. *American Mineralogists,* **80,** 744-751.

Bard, J.P., 1983. Metamorphism of an obducted island arc: example of the Kohistan sequence (Pakistan) in the Himalayan collided range. *Earth and Planetary Science Letters,* **65,** 133-144.

Beard, J.S. & Lofgren, G.E., 1991. Dehydration melting and water-saturated melting of basaltic and andesitic greenstones and amphibolites at 1, 3, and 6.9 kb. *Journal of Petrology,* **32,** 365-401.

Bence, A.E. & Albee, A.L., 1968. Empirical correction factors for the electron microanalysis of silicates and oxides. *Journal of Geology,* **76,** 382-403.

Blattner, P. & Black, P.M., 1980. Apatite and scapolite as petrogenetic indicators in granolites of Milford Sound,

New Zealand. *Contributions to Mineralogy and Petrology,* **74,** 339-348.

Bohlen, S.R., 1991. On the formation of granulites. *Journal of Metamorphic Geology,* **9,** 223-229.

Bohlen, S.R., 1987. Pressure-temperature-time paths and a tectonic model for the evolution of granulites. *Journal of Geology,* **95,** 617-632.

Bohlen, S.R. & Essene, E.J., 1977. Feldspar and oxide themometry of granulites in the Adirondack Highlands. *Contributions to Mineralogy and Petrology,* **62,** 153-169.

Bohlen, S.R. & Liotta, J.J., 1986. A barometer for garnet amphibolites and garnet granulites. *Journal of Petrology,* **27,** 1025-1034.

Boivin, P. & Camus, G., 1981. Igneous scapolite-bearing associations in the Chaine des Puys, Massif Central (France) and Atakor (Hoggar, Algeria). *Contributions to Mineralogy and Petrology,* **77,** 365-375.

Brace, W.F., 1980. Permiability of crystalline and argillaceous rocks. *International Journal of Rock Mechnical and Mineralogical Sciences,* **17,** 241-251.

Bradshaw, J.Y., 1989a. Origin and metamorphic history of an early Cretaceous polybaric granulite terrain, Fiordland, southwest New Zealand. *Contributions to Mineralogy and Petrology,* **104,** 346-360.

Bradshaw, J.Y., 1989b. Early Cretaceous vein-related garnet granulite in Fiordland, southwest New Zealand: a case for infiltration of mantle-derived CO_2-rich fluids. *Journal of Geology,* **97,** 697-717.

Brodie, K.H., and Rutter, E.H., 1985. On the relationship between deformation and metamorphism, with special reference to the behavior of basic rocks. In: *Metamorphycal Reactions (Kinetics, Textures and Deformation),* (eds. Thompson, A. B. & Rubie, D. C.), Advance in Physics and Geochemistry, pp. 138-179.

Brown, E.H., 1996. High-pressure metamorphism caused by magma loading in Fiorland, New Zealand. *Journal of Metamorphic Geology,* **14,** 441-452.

Brown, E.H. & Walker, N.W., 1993. A magma loading model for Barrovian metamorphism in the southeast Coast Plutonic Complex, British Columbia and Washington. *Geological Society of America Bulletin,* **105,** 479-500.

Buddington, A.F. & Lindsley, D.H., 1964. Iron-titanium oxide minerals and synthetic equivalents. *Journal of Petrology,* **5,** 310-357.

Butler, R.W.H. & Prior, D.J., 1988. Tectonic controls on the uplift of the Nanga Parbat Massif, Pakistan

Himalayas. *Nature*, **333**, 247-250.

Carmichael, I.S.E., 1991. The redox states of basic and silicic magmas: a reflection of their source regions? *Contributions to Mineralogy and Petrology*, **106**, 129-144.

Chacko, T., Ravindra Kumar, G.R., & Newton, R.C., 1987. Metamorphic P-T conitions in the Kerala (south India) Khondalite Belt: a granulite-facies supracrustal terrain. *Journal of Geology*, **95**, 343-358.

Chakraborty, S. & Ganguly, J., 1990. Compositional zoning and cation diffusion in garnets. In: *Diffusion, Atomic Ordering, and Mass Transport, selected Topics in Geochemistry* (ed. Ganguly, J.), *Advances in Physical Geochemistry*, **8**, 120-175.

Coolen, J.J.M.M.M., 1982. Carbonic fluid inclusions in granulites from Tanzania-A comparison of geobarometric methods based on fluid density and mineral chemistry. *Chemical Geology*, **37**, 59-77.

Coward, M.P., Butler, R.W.H., Khan, M.A. & Knipe, R.J., 1987. The tectonic history of Kohistan and its implications for Himalayan structure. *Journal of Geological Society, London*, **144**, 377-391.

Coward, M.P.,. Jan, M.Q., Rex, D.C., Tarney, J., Thirlwall, M. & Windley, B.F., 1982. Geo-tectonic framework of the Himalaya of N. Pakistan. *Journal of Geological Society, London*, **139**, 299-308.

Coward, M.P., Broughton, R.D., Luff, I.W., Petterson, M.G., Pudsey, C.J., Rex, D.C. & Khan, M.A., 1986. Collision tectonics in the NW Himalayas. In: *Collision Tectonics* (eds. Coward, M. P. & Ries, A. C.),. Blackwell Scientific Publications, London, pp. 203-219

Davidson, A., 1984. Identification of ductile shear zones in the southwestern Grenville province of the Canadian Shield. In: *Precambrian Tectonics Illustrated*, Stuttgart., (eds. Kruer, A. & Greiling, R.), pp. 263-279.

De Paolo, D.J., 1983. The mean life of continents: estimates of continent recycling rates from Nd and Hf isotopic data and implications for mantle structure. *Geophysical Research Letters*, **10**, 705-708.

Dubessy, J., Poty, B. & Ramboz, C., 1989. Advances in C-O-H-N-S fluid geochemistry based on micro-Raman spectrometric analysis of fluid inclusions. *European Journal of Mineralogy*, **1**, 517-534.

Eckert, J.O., Newton, R.C. & Kleppa, O.J., 1991. The ΔH of reaction and recalibration of garnet-pyroxene-plagioclase-quartz geobarometers in the CMAS system by solution calorimetry. *American Mineralogists*, **76**, 148-160.

Edwards, A.C., Lovering, J.F. & Furguson, J., 1979. High pressure basic intrusions from the Kayrunnera kimberlitic diatreme in New South Wales, Australia. *Contributions to Mineralogy and Petrology*, **69**, 185-192.

Ellis, D.J., 1987. Origin and evolution of granulites in normal and thickened crust. *Geology*, **15**, 167-170.

Ellis, D.J. & Green, D.H., 1979. An experimental study of the effect of Ca upon garnet-clinopyroxene Fe-Mg exchange equilibria. *Contributions to Mineralogy and Petrology*, **71**, 13-22.

Ellis, D.J. & Green, D.H., 1985. Garnet forming reactions in mafic granulites from Enderby Land, Antarctica - Implications for geothermometry and geobarometry. *Journal of Petrology*, **26**, 633-662.

Elphick, S.C., Ganguly, J. & Loomis, T.P., 1985. Experimental determination of cation diffusivities in aluminosilicate garnets: I. Experimental methods and interdiffusion data. *Contributions to Mineralogy and Petrology*, **90**, 36-44.

England, P.C. & Thompson, A.B., 1984. Pressure-temperature-time paths of regional metamorphism I. Heat transfer during evolution of regions of thickened continental crust. *Journal of Petrology*, **25**, 894-928.

Essene, E.J. & Bohlen, S.R., 1985. New garnet barometers in the system CaO-FeO-Al_2O_3-SiO_2-TiO_2 (CFAST). *Abstract Transactions of American Geophysical Union*, **66**, 386.

Etheridge, M.A., Wall, V.J. & Vernon, R.H., 1983. The role of the fluid phase during regional metamorphism and deformation. *Journal of Metamorphic Geology*, **1**, 205-226.

Etheridge, M.A., Wall, V.J., Cox, S.F. & Vernon, R.H., 1984. High fluid pressures during regional metamorphism and deformation: implications for mass transport and deformation mechanisms. *Journal of Geophysical Research*, **89**, 4344-4358.

Evans, B.W., Shaw, D.M. & Houghton, D.R., 1969. Scapolite stoichiometry. *Contributions to Mineralogy and Petrology*, **24**, 293-305.

Ferry, J.M., 1980. A case study of the amount and distribution of heat and fluid during regional metamorphism. *Contributions to Mineralogy and Petrology*, **71**, 373-385.

Fisher, D.M. & Brantley, S.L., 1992. Models of quartz overgrowth and vein formation: deformation and episodic fluid flow in an ancient subduction zone. *Journal of Geolphysical Research*, **97**, 20043-20061.

Fountain, D. M., 1976. The Ivrea-Verbano and Strona-Ceneri zones, northern Italy: a cross section of the continental crust - new evidence from seismic velocities.

Tectonophysics, 33, 145-166.

Fountain, D. M. and Salisbury, M. H., 1981. Exposed crustal section through the continental crust: Implications for crustal structure, petrology and evolution. *Earth and Planetary Science Letters,* **5,** 263-277.

Frost, B.R. & Chacko, T., 1989. The granulite uncertainty principle: Limitations on thermobarometry in granulites. *Journal of Geology,* **9 7,** 435-450.

Ganguly, J., Cheng, W. & Tirone, M., 1996. Thermodynamics of alumosilicate garnet solid solution: new experimental data, an optimized model, and thermometric applications. *Contributions to Mineralogy and Petrology,* **1 2 6,** 137-151.

Gasparik, T., 1985. Experimental study of subsolidus phase relations and mixing properties of pyroxene and plagioclase in the system $Na_2O-CaO-Al_2O_3-SiO_2$. *Contributions to Mineralogy and Petrology,* **89,** 346-357.

George, M., Reddy, S. & Harris, N., 1995. Isotopic constraints on the cooling history of the Nanga Parbat-Haramosh Massif and Kohistan arc, western Himalaya. *Tectonics,* **1 4,** 237-252.

Gibson, G.M., McDougall, I. & Ireland, T.R., 1988. Age constraints on metamorphism and development of a metamorphic core complex in Fiordland, southern New Zealnd. *Geology,* **1 6,** 405-408.

Glassley, W.E., 1983. Deep crustal carbonates as CO_2 fluid sources: Evidence from metasomatic reaction zones. *Contributions to Mineralogy and Petrology,* **84,** 15-24.

Goleby, B. R., Shaw, R. D., Wright, C., Kenett, B. L. N. & Lambeck, K., 1989. Geophysical evidence for 'thick-skinned' crustal deformation in central Australia. *Nature,* 337, 325-330.

Goldsmith, J.R., 1976. Scapolites, granulites, and volatiles in the lower crust. *Geological Society of America Bulletin,* **87,** 161-168.

Goldsmith, J.R. & Newton, R.C., 1977. Scapolite-plagioclase stability relations at high pressures and temperatures in the system $NaAlSi_3O_8-CaAl_2Si_2O_8-CaCO_3-CaSO_4$. *American Mineralogists,* **62,** 1063-1081.

Graham, C.M. & Powell, R., 1984. A garnet-hornblende geothermometer: calibration, testing, and application to the Perona schist, Southern California. *Journal of Metamorphic Geology,* **2,** 13-21.

Green, D.H. & Ringwood, A.E., 1967. An experimental investigation of the gabbro to eclogite transformation and its petrological applications. *Geochimica et Cosmochimica Acta,* **3 1,** 767-833.

Griffin, W.L. & O'Reiley, S.Y., 1987. The composition of the lower crust and the nature of the continental Moho - xenolith evidence. In: *Mantle Xenoliths,* (ed. Nixon, P.H.), Elsevier, Amsterdam, pp. 413-430.

Gurnis, M. & Davies, G.F., 1985. Simple parametric models of crustal growth. *Journal of Geodynamics,* **3 ,** 105-135.

Gurnis, M. & Davies, G.F., 1986. Apparent episodic crustal growth arising from a smoothly evolving mantle. *Geology,* **1 4,** 396-399.

Hall, D.L. & Bodnar, R.J., 1990. Metane in fluid inclusions from granulites: A product of hydrogen diffusion? *Geochimica et Cosmochimica Acta,* **54,** 641-651.

Handy, M.R., 1990. The exhumation of cross sections of the continental crust: structure, kinematics and rheology. In: *Exposed Cross-Sections of the Continental Crust* (eds. Salisbury, M.H. and Fountain, D.M.), pp. 485-507. Kluwer Academic Publishers, Netherlands.

Hansen, B., 1981. The transition from pyroxene granulite facies to garnet clinopyroxene facies. Experiments in the system $CaO-MgO-Al_2O_3-SiO_2$. *Contributions to Mineralogy and Petrology,* **7 6,** 234-242.

Hansen, E.C., Janardhan, A.S., Newton, R.C., Prame, W.N.B.K. & Ravindra Kumar, G.R., 1987. Arrested charnockiteformation in southern India and Sri Lanka. *Contributions to Mineralogy and Petrology,* **96,** 225-244.

Harley, S.L., 1984. An experimental study of the partitioning Fe and Mg between garnet and orthopyroxene. *Contributions to Mineralogy and Petrology,* **8 6 ,** 359-373.

Harley, S.L., 1985. Garnet-orthopyroxene bearing granulites from Enderby Land, Antarctica: metamorphic pressure-temperature-time evilution of the Archean Napier Complex. *Journal of Petrology,* **2 6 ,** 819-856.

Harley, S.L., 1989. The origin of granulites: a metamorphic perspective. *Geological Magazine,* **1 2 6,** 215-247.

Holdaway, M.J., 1971. Stability of andalusite and the aluminum silicate phase diagram. *American Journal of Science,* **2 7 1 ,** 97-131.

Holland, T.J.B. & Powell, R., 1990. An enlarged and updated internally consistentthermodynamic dataset with uncertainities and correlations: the system $K_2O-Na_2O-CaO-MgO-MnO-FeO-Fe_2O_3-Al_2O_3-TiO_2-SiO_2-C-H_2-O_2$. *Journal of Metamorphic Geology,* **8 ,** 89-124.

Hollister, L.S. & Crawford, M.L., 1986. Melt-enhanced deformation: a major tectonic process. *Geology,* **1 4,**
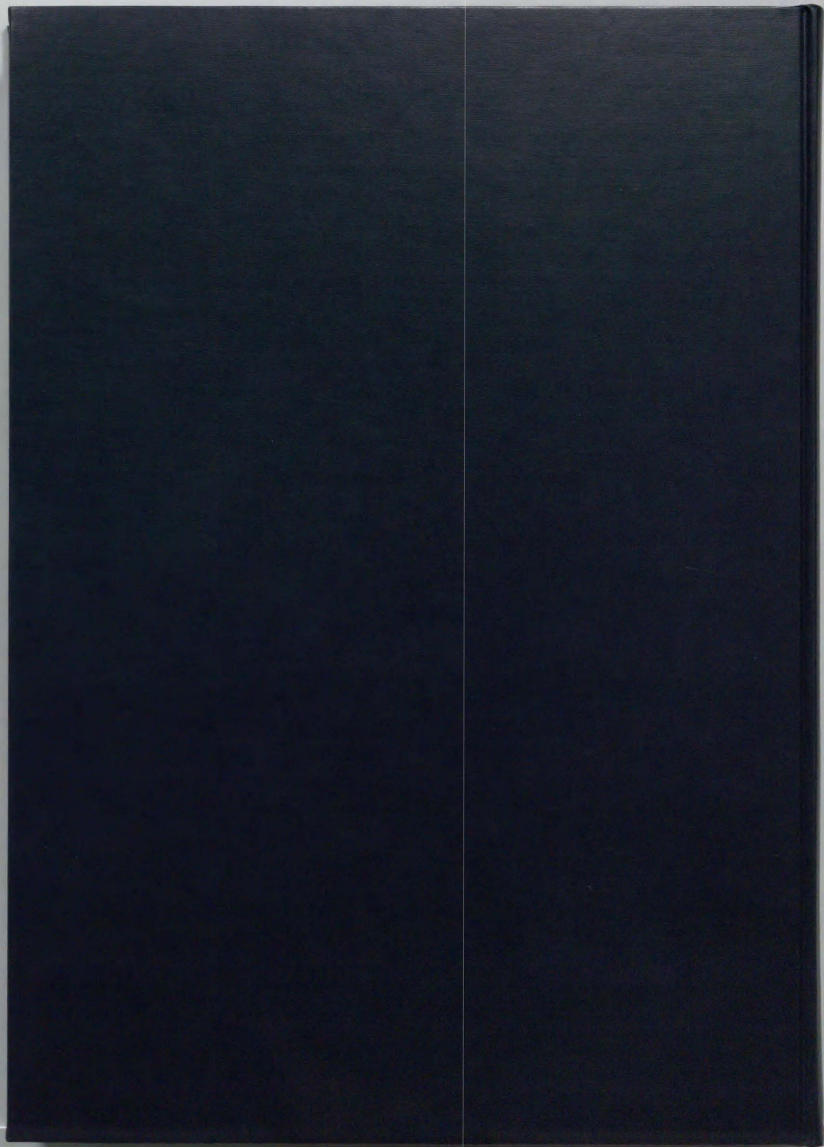
558-561.

Holness, M.B., 1992. Equilibrium dihedral angles in the system quartz-CO_2-H_2O-NaCl at 800 °C and 1-15 kbar: the effects of pressure and fluid composition on the permeability of quartzites. *Earth and Planetary Science Letters*, **114**, 171-184.

Irvine, A.J., 1974. Geochemical and high pressure experimental studies of garnet pyroxenites and pyroxene granulite xenoliths from the Delegate basaltic pipes, Australia. *Journal of Petrology*, **15**, 1-40.

Jan, M.Q., 1988. Geochemistry of amphibolites from the southern part of Kohistan arc, N. Pakistan. *Mineralogical Magazine*, **52**, 147-159.

Jan, M.Q. & Howie, R.A., 1980. Ortho- and clinopyroxenes from the pyroxene granulites of Swat Kohistan, northern Pakistan. *Mineralogical Magazine*, **43**, 715-726.

Jan, M.Q. & Howie, R.A., 1981. The mineralogy and geochemistry of the metamorphosed basic and ultrabasic rocks of the Jijal complex, Kohistan, NW Pakistan. *Journal of Petrology*, **22**, 85-126.

Jan, M.Q., & Karim, A., 1995. Coronas and high-P veins in metagabbros of the Kohistan island arc, northern Pakistan: evidence for crustal thickening during cooling. *Journal of Metamorphic Geology*, **13**, 357-366.

Jones, A.P., Smith, V.J., Dawson, J.B. & Hansen, E.C., 1983. Metamorphism, partial melting and K-metasomatism of garnet-scapolite-kyanite granulite zenoliths from Lashaine, Tanzania. *Journal of Geology*, **91**, 143-165.

Kay, R.W. & Kay, S.M., 1988. Crustal recycling and the Aleutian arc. *Geochimica Cosmochimica et Acta*, **52**, 1351-1359.

Kay, R.W., Kay, S.M. & Arculus, R.J., 1992. Magama genesis and crustal processing. In: *Continental Lower Crust*, (eds. Fountain, D.M., Arculus, R. & Kay, R.W.), Elsevier, Amsterdam, **23**, 423-441.

Khan, M.A. & Coward, M.P., 1990. Entrapment of an island arc in collision tectonics: A review of the structural history of the Kohistan arc complex, N. W. Himalayas. *Physics and Chemistry of Earth*, **17**, 1-18.

Khan, M.A., Jan, M.Q. & Weaver, B.L., 1993. Evolution of the lower arc crust in Kohistan: temporal arc magmatism through early, mature and intra-arc rift stages. In: *Himalayan Tectonics* (eds. Treloar, P. J. & Searle, M. P.) *Geological Society Special Publication, London*, **74**, 123-138.

Kohn, M.J. & Spear, F.S., 1990. Two new geobarometers for garnet amphibolites with applications to southeastern Vermont. *American Mineralogists*, **75**,

89-96.

Khan, M.A., Jan, M.Q., Windley, B.F., Tarney, J. & Thirlwall, M.F., 1989. The Chilas mafic-ultramafic igneous complex; the root of the Kohistan island arc in the Himalaya of northern Pakistan. *Geological Society of America, Special Paper*, **18**, 83-102.

Krogh, E. J., 1988. The garnet-clinopyroxene Fe-Mg geothermometer - a reinterpretation of existing experimental data. *Contributions to Mineralogy and Petrology*, **99**, 44-48.

Lamb, W.M. & Valley, J.W., 1984. Metamorphism of reduced granulites in a low CO_2, vapour-free environment. *Nature*, **312**, 56-58.

Lamb, W.M. & Valley, J.W., 1985. C-O-H fluid calculations and granulite gneiss. In: *The Deep Proterozoic Crust in the North Antrantic Provinces*, (eds. Tobi, A.C. & Touret, J.L.R.), D.Reidel, Dordrecht, Netherland, pp. 119-131.

Lamb, W.M. & Valley, J.W., 1988. Granulite facies amphibole and biotite equilibria, and calculated peak metamorphic water activities. *Contributions to Mineralogy and Petrology*, **100**, 349-360.

Lamb, W.M., Valley, J.W. & Brown, P.E., 1987. Post-metamorphic CO_2-rich fluid inclusions in granulites. *Contributions to Mineralogy and Petrology*, **96**, 485-495.

Lasaga, A.C., 1983. Geospeedmetry: An extension of geothermometry. In: *Kinetics and equilibrium in mineral reactions* (eds. Saxena, S. K.) *Advances in Physical Geochemistry*, Springer-Verlag, pp. 81-114.

Lister, G.S. & Snoke, A.W., 1984. S-C mylonites. *Journal of Structural Geology*, **6**, 617-638.

Liu, J. & Bohlen, S. R., 1995. Mixing properties and stability of jadeite-acmite pyroxene in the presence of albite and quartz. *Contributions to Mineralogy and Petrology*, **119**, 443-440.

Lovering, J.F. & White, A.J.R., 1964. The significance of primary scapolite in granulitic inclusions from deep-seated pipes. *Journal of Petrology*, **5**, 195-218.

Lovering, J.F. & White, A.J.R., 1969. Granulitic and eclogitic inclusions in basic pipes at Delegate, Australia. *Journal of Petrology*, **21**, 9-52.

Lucas, S.B., St-Onge, M.R., Parrish, R.R. & Dunphy, J.M., 1992. Long-lived continent-ocean interaction in the Early Proterozoic Ungava orogen, northern Quebec, Canada. *Geology*, **20**, 113-116.

Lucassen, F. & Franz, G., 1996. Magmatic arc metamorphism: petrology and temperature history of metabasic rocks in the Coastal Cordillera of northern Chile. *Journal of Metamorphic Geology*, **14**, 249-265.

Miller, D.J., Loucks, R.R. & Ashraf, M., 1991. Platinum group elements mineralization in the Jijal layered mafic-ultramafic complex, Pakistani Himalayas. *Economic Geology*, **86**, 1093-1102.

Moecher, D.P. & Essene, E.J., 1990. Phase equilibria for calcic scapolite, and implications of variable Al-Si disorder for P-T, T- X_{CO_2}, and a-X relations. *Journal of Petrology*, **31**, 997-1024.

Moecher, D.P. & Essene, E.J., 1991. Calculation of CO_2 activities using scapolite equilibria: constraints on the presence and composition of a fluid phase during high grade metamorphism. *Contributions to Mineralogy and Petrology*, **108**, 219-240.

Moecher, D. P., Essene, E. J. & Anovitz, L. M., 1988. Calculation and application of clinopyroxene-garnet-plagioclase-quartz geobarometers. *Contributions to Mineralogy and Petrology*, **100**, 92-106.

Moecher, D.P., Valley, J.W. & Essene, E.J., 1994. Extraction and carbon isotope analysis of CO_2 from scapolite in deep crustal granulites and xenoliths. *Geochimica et Cosmochimica Acta*, **58**, 959-967.

Nakashima, Y., 1995. Transport model of buoyant metamorphic fluid by hydrofracturing in leaky rock. *Journal of Metamorphic Geology*, **13**, 727-736.

Newton, R.C., 1983. Geobarometry of high-grade metamorphic rocks. *American Journal of Science*, **283A**, 1-28.

Newton, R.C., 1985. Temperature, pressur, and metamorphic fluid regimes in the amphibolite facies to granulite facies transition zones. In: *The Deep Proterozoic Crust in the North Atrantic Provinces*, (eds. Tobi, A.C. & Touret, J.L.R.), D.Reidel, Dordrecht, Netherland, pp. 75-104.

Newton, R.C., 1989. Metamorphic fluids in the deep crust. *Annual Reviews of Earth and Planetary Science*, **17**, 385-412.

Newton, R.C. and Perkins, D.III., 1982. Thermodynamic calibration of geobarometers based on the assemblages garnet-plagioclase-orthopyroxene (clinopyroxene)-quartz. *American Mineralogist*, **67**, 203-222.

Newton, R.C., Smith, J.V. & Windley, B.F., 1980. Carbonic metamorphism, granulites and crustal growth. *Nature*, **292**, 144-146.

Oliver, G. J. H. & Coggon, J. H., 1979. Crustal structure of Fiordland, New Zealand. *Tectonophysics*, **54**, 253-292.

Orville, P.M., 1975. Stability of scapolite in the system Ab-An-NaCl-CaCO₃ at 4 kb and 750 °C. *Geochimica et Cosmochimica Acta*, **39**, 1091-1105.

Oterdoom, H. & Gunter, W.D., 1983. Activity models for plagioclase and CO_3-scapolites: na analysis of field and laboratory data. *American Journal of Science*, **283A**, 255-282.

Otten, M.T., 1984. The origin of brown hornblende in the Artfjället gabbro and dolerites. *Contributions to Mineralogy and Petrology*, **86**, 189-199.

Pasteris, J.D., Wopenka, B. & Seitz, J.C., 1988. Practical aspects of quantitative laser Raman microprobe spectroscopy for the study of fluid inclusions. *Geochimica et Cosmochimica Acta*, **52**, 979-988.

Pasteris, J.D., Seitz, J.C., Wopenka, B. & Chou, I.M., 1990. Recent advances in the analysis and interpretation of C-O-H-N fluids by application of laser Raman microspectroscopy. In: *Microbeam analysis-1990*, (eds. Micheal, J.R. & Ingram, P.), pp. 228-234.

Patriat, P. & Attache, J., 1984. India-Eurasia collision chronology and its implications for crustal shortening and driving mechanism of plates. *Nature*, **311**, 615-621.

Pattison, D.R.M. & Newton, R.C., 1989. Reversed experimental calibration of the garnet-clinopyroxene Fe-Mg exchange thermometer. *Contributions to Mineralogy and Petrology*, **101**, 87-103.

Percival, J.A., Fountain, D.M. & Salisbury, M.H., 1992. Exposed crustal sections as windows on the lower crust. In: *Continental Lower Crust*, (eds. Fountain, D.M., Arculus, R. & Kay, R.W.), Elsevier, Amsterdam, **23**, 317-362.

Percival, J. A. & McGrath, P. H., 1986. Deep crustal structure and tectonic history of the northern Kapskasing uplift of Ontario: An integrated petrological-geophysiacl study. *Tectonics*, 5, 553-572.

Percival, J. E., Green, A. G., Milkereit, B., Cook, F. A., Geis, W. & West, G. F., 1989. Seismic reflection profiles across deep continental crust exposed in the Kapskasing uplift structure. *Nature*, 342, 416-420.

Perkins, D. & Newton, R. C., 1981. Charnockite geobarometers based on coexisting garnet-pyroxene-plagioclase-quartz. *Nature*, **292**, 144-146.

Petterson, M.G. & Windley, B.F., 1985. Rb-Sr dating of the Kohistan arc-batholith in the Trans-Himalaya of N. Pakistan and tectonic implications. *Earth and Planetary Science Letters*, **74**, 54-75.

Petterson, M.G. & Windley, B.F., 1992. Field relations, geochemical and petrogenesis of the Cretaceous basaltic Jutal dykes, Kohistan, northern Pakistan. *Journal of Geological Society, London*, **149**, 107-114.

Pudsey, C.J., 1986. The Northern Suture, Pakistan: margin of a Cretaceous island arc. *Geological Magazine*, **123**, 405-423.

Pudsey, C.J., Coward, M.P., Luff, I.W., Shackleton, R.M., Windley, B.F. & Jan, M.Q., 1985. The collision zone between the Kohistan arc and the Asian Plate in the Trans-Himalaya of NW Pakistan. *Transactions Royal Society of Edinburgh, Earth Sciences,* **76**, 45-57.

Robinson, P., Spear, F.S., Schumacher, J.C., Laird, J., Klein, C., Evans, B.W. & Doolan, B.L., 1982. Phase relations of metamorphic amphiboles: natural occurrence and theory. *Mineralogical Society of America, Reviews in Mineralogy,* **9B**, 1-227.

Rudnick, R.L., 1992. Xenoliths-Samples of the lower continental crust. In: *Continental Lower Crust,* (eds. Fountain, D.M., Arculus, R. & Kay, R.W.), Elsevier, Amsterdam, **23**, 269-316.

Rudnick, R.L. & Presper, T., 1990. Geochemistry of intermediate- to high-pressure granulites. In: *Granulites and Crustal Evolution,* (eds. Vielzeuf, D. & Vidal, P), Kruwel, Dordecht, pp. 523-530.

Rudnick, R.L. & Taylor, S.R., 1987. The comilation and petrogenesis of the lower crust: a xenolith study. *Journal of Geophysical Research,* **94**, 13981-14005.

Rutter, E.H. & Brodie, K.H., 1992. Rheology of the lower crust, in Continental Lower crust, eds. Fountain, D.M., Arculus, R. & Kay, R.W.), Elsevier, Amsterdam, **23**, 201-258.

Sautter, V., Jaoul, O. & Abel, F., 1988. Aluminum diffusion in diopside using the 27Al(p, g)28Si nuclear reaction: preliminary results. *Earth and Planetary Science Letters,* **89**, 109-114.

Schmid, R. & Wood, B. J., 1976. Phase relationships in granulitic metapelites from the Ivrea-Valbeno zone (Northern Italy). *Contribution to Mineralogy and Petrology,* 54, 255-279.

Schmid, S.M., Zingg, A. & Handy, M.R., 1987. The kinematics of movements along the Insubric line and the emplacement of the Ivrea-Vervano zone, *Tectonophysics,* **135**, 47-66.

Spencer, K.J. & Lindsley, D.M., 1981. A solution model for coexisting iron-titanium oxides. *American Mineralogists,* **66**, 1189-1201.

Stoltz, A.J., 1987. Fluid activity in the lower crust and upper mantle: mineralogical evidence bearing on the origin of amphibole and scapolite in ultramafic and mafic granulite zenoliths. *Mineralogical Magazine,* **51**, 719-732.

Tahirkheli, R.A.K., Mattauer, M., Proust, F. & Tapponnier, P., 1979. The India Eurasia suture zone in northern Pakistan: synthesis and interpretation of recent data at plate scale. In: *Geodynamics of Pakistan* (eds. Farah, A. and DeJong, K. A.) *Geological Survey of Pakistan, Quetta,* 125-130.

Taylor, S.R., 1977. Island arc models and the composition of the continental crust. In *Island arcs, Deep Sea Trenches, and Back Arc Basins,* (eds. Talwani, M. and Pitman, W.C.), American Geophysical Union, Washington, D.C., pp. 325-335.

Thompson, A.B. & Connolly, J.A.D., 1992. Migration of metamorphic fluid: some aspects of mass and heat transfer. *Earth-Science Reviews,* **32**, 107-121.

Touret, J.L.R., 1971. Le facies granulite en Norvège Méridionale. II. Les inclusions fluides. *Lithos,* **4**, 423-426.

Touret, J.L.R., 1981. Fluid inclusions in high-grade metamorphic rocks. In: *Fluid inclusions: applications to petrology,* (eds. Hollister, L.S. & Crawford, M.L.), *Mineralogical Association of Canada Shortcoarce Handbook,* **6**, 182-207.

Treloar, P.J., Rex, D.C., Guise, P.G., Coward, M.P., Searle, M.P., Windley, B.F., Petterson, M.G., Jan, M.Q. & Luff, I.W., 1989. K-Ar and Ar-Ar geochronology of the Himalayan collision in NW Pakistan: Constraints on the timing of suturing, deformation, metamorphism and uplift. *Tectonics,* **8**, 881-909.

Treloar, P.J., Brodie, K.H., Coward, M.P., Jan, M.Q., Khan, M.A., Knipe, R.J., Rex, D.C. & Williams, M.P., 1990. The evolution of the Kamila shear zone, Kohistan, Pakistan. In: *Exposed Cross-Sections of the Continental Crust* (eds. Salisbury, M.H. and Fountain, D.M.), pp. 175-214. Kluwer Academic Publishers, Netherlands.

Treloar, P.J., Petterson, M.G., Jan, M.Q. & Sullivan, M.A., 1996. A re-evaluation of the stratigraphy and evolution of the Kohistan arc sequence, Pakistan Himalaya: implications for magmatic and tectonic arc-building processes. *Journal of Geological Society, London,* **153**, 681-693.

Tullis, J., 1990. Experimental studies of deformation mechanisms and microstructure in quartzo-feldspathic rocks. In: *Deformation Processes in Minerals, Ceramics and Rocks,* (eds. Barber, D. J. & Meredith, P.G.), Unwin Hyman, London., 190-227.

Turcotte, D.L. & Schubert, G., 1982. In: *Geodynamics,* (eds. Turcotte, D. L., and Schubert, G.), John Wiley and Sons, New York. p. 450.

Wartho, J., Rex, D.C. & Guise, P.G., 1996. Excess argon in amphiboles linked to greenschist facies alteration in the Kamila Amphibolite Belt, Kohistan island arc system, northern Pakistan: insights from $^{40}Ar/^{39}Ar$ step-heating and acid leaching experiments. *Geological*

Magazine, **133**, 595-609.

Watson, E.B. & Brenan, J.M., 1987. Fluids in the lithosphere, 1. Experimentally-determined wetting characteristics of CO_2-H_2O fluids and their implications for fluid transport, host-rock physical properties, and fluid inclusion formation. *Earth and Planetary Science Letters*, **85**, 497-515.

Wells, P.R.A., 1980. Thermal models for the magmatic accretion and subsequent metamorphism of continental crust. *Earth and Planetary Science Letters*, **46**, 253-265.

Wood, B.J., 1978. Relation involving anorthite and $CaAl_2SiO_6$ pyroxene at high pressures and temperatures. *American Journal of Science*, **278**, 930-942.

Wood, B.J., 1979. Activity-composition relationships in $Ca(Mg,Fe)Si_2O_6$-$CaAl_2SiO_6$ clinopyroxene solid solutions. *American Journal of Science*, **279**, 854-875.

Wood, B.J., Holland, T., Newton, R.C. & Kleppa, O.J., 1980. Thermochemistry of jadeite-diopside pyroxenes. *Geochimica et Cosmochimica Acta*, **44**, 1363-1371.

Yamamoto, H., 1993. Contrasting metamorphic *P-T*-time paths of the Kohistan granulites and tectonics of the western Himalayas. *Journal of Geological Society, London*, **150**, 843-856.

Yamamoto, H. & Nakamura, E., 1996. Sm-Nd dating of garnet granulites from the Kohistan complex, northern Pakistan. *Journal of Geological Society, London*, **153**, 965-969.

You, Z., Han, Y., Suo, S., Chen, N. & Zhong, Z., 1993. Metamorphic history and tectonic evolution of the Qinling Complex, eastern Qinling Mountains, China. *Journal of Metamorphic Geology*, **11**, 549-560.

Zeitler, P.K., 1985. Cooling history of the N. W. Himalaya, Pakistan. *Tectonics*, **4**, 127-151.

Zeitler, P.K., Sutter, J.F., Williams, I.S., Zartman, R. & Tahirkheli, R.A.K., 1989. Geochronology and temperature history of the Nanga-Parbat-Haramosh massif, Pakistan. In: *Tectonics of the Western Himalayas*, (eds. Malinconico, L. L. and Lillie, R. J.), *Geological Society of America, Special Paper*, **232**, 1-22.

Zeitler, P.K., Tahirkheli, R.A.K., Naesser, C., Johnson, N. & Lyons, J., 1981. Preliminary fission track ages from the Swat Valley, northern Pakistan. *Geological Bulletin of the University of Peshawar*, **13**, 63-65.